7-1-1988

Use of Image Processing Techniques for the Analysis of Echocardiographic Images

Enrique Garcia-Melendo
Purdue University

Edward J. Delp
Purdue University

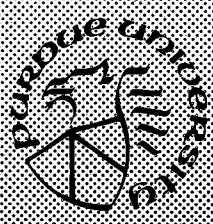

The Use of Image Processing Techniques for the Analysis of Echocardiographic Images

Enrique Garcia-Melendo
Edward J. Delp

TR-EE 88-29
July 1988

School of Electrical Engineering
Purdue University
West Lafayette, Indiana 47907

THE USE OF IMAGE PROCESSING TECHNIQUES FOR THE ANALYSIS OF ECHOCARDIOGRAPHIC IMAGES

Enrique Garcia-Melendo

Edward J. Delp

Purdue University

School of Electrical Engineering

West Lafayette, Indiana 47907

TR-EE-88-29

July 1988

This page is intentionally blank.

ACKNOWLEDGMENTS

The authors would like to thank Henry C. Chu for his help and suggestions in the preparation of this report.

This work was partially supported by the "La Caixa" Program, Barcelona, Spain.

TABLE OF CONTENTS

Page

LIST OF TABLES

LIST OF FIGURES

Figure Page

Figure Page

Figure Page

Figure Page

ABSTRACT

Echocardiography is a medical imaging modality that uses ultrasound in order to obtain cross sectional views of the heart. The basic problem in the use of echocardiography is the ability to obtain a reliable set of physical parameters related to cardiac status, so that assessment of heart disease can be performed automatically. This work overviews different image processing techniques used in the analysis of two dimensional echocardiographic images.

After reviewing how the echocardiographic image formation process works, an outline of the general processing steps from image acquisition to automatic detection of important features is presented. Special emphasis on cardiac image segmentation is presented. In particular, a relaxation algorithm for image segmentation is discussed. Also, echocardiographic image segmentation using temporal analysis and a new algorithm for boundary detection is described. Measurements of left ventricular area, wall thickness, and ejection fraction is also presented.

Shape analysis is introduced as a tool for echocardiographic image analysis. A high level description of the left ventricular boundaries using curvature is proposed. Curvature analysis attempts to identify stable landmarks during the beating process. muscles. Tracking these landmarks aids in the detection of abnormal heart contractions. Finally the use of expert systems is proposed in the

analysis of echocardiographic images.

CHAPTER 1
BASICS OF HEART ANATOMY, PHYSIOLOGY, AND ECHOCARDIOGRAPHY

1.1 Introduction to Cardiac Anatomy and Physiology

1.1.1 Cardiac Anatomy

The heart is a four-chambered hollow muscle within the thorax whose task is to pump the blood to the lungs so that it can be oxygenated, and then pumped to the rest of the body. The front of the heart is known as the Anterior aspect (see Figure 1.1) while the back is known as the Posterior aspect (see Figure 1.2). If we assume that the heart's shape is close to that of a cone, then the vertex is called the apex, whereas the top portion is the heart's base (see Figures 1.1 and 1.2).

An excellent description of the heart was provided by Jacob and Francone [1]:

> The structures of the heart include the *pericardium*; the wall enclosing the chambers, separated by valves; and the *arteries*, which supply blood to the heart muscle.
>
> **Pericardium.** The pericardium is an invaginated sac consisting of two layers, an external fibrous and an internal layer (the serous membrane). The external fibrous layer, which has an inner surface of serous membrane, is the parietal pericardium. The internal serous layer, which adheres to the heart and becomes the outermost layer of the heart, the epicardium, is the visceral pericardium.
>
> **Wall of the heart.** The wall of the heart consists of three distinct layers: the *epicardium* (external layer), the *myocardium* (middle layer), and the *endocardium* (inner layer). The epicardium has mesothelial and subserous layers of connective tissue and is frequently infiltrated with fat. Coronary vessels supplying arterial blood to the heart traverse the epicardium before entering the myocardium. The myocardium consists of interlacing bundles of striated muscle fibers. This layer is responsible for the ability of the heart to contract. The endocardium lines the cavities of the heart, covers the valves, and is continuous with the

lining membrane of the large blood vessels.

Chambers of the heart. The heart is divided into right and left halves, with each half subdivided into two chambers. The upper chambers, the *atria*, are separated by the *interatrial septum*; the lower chambers, the *ventricles*, are separated by the *interventricular septum*.

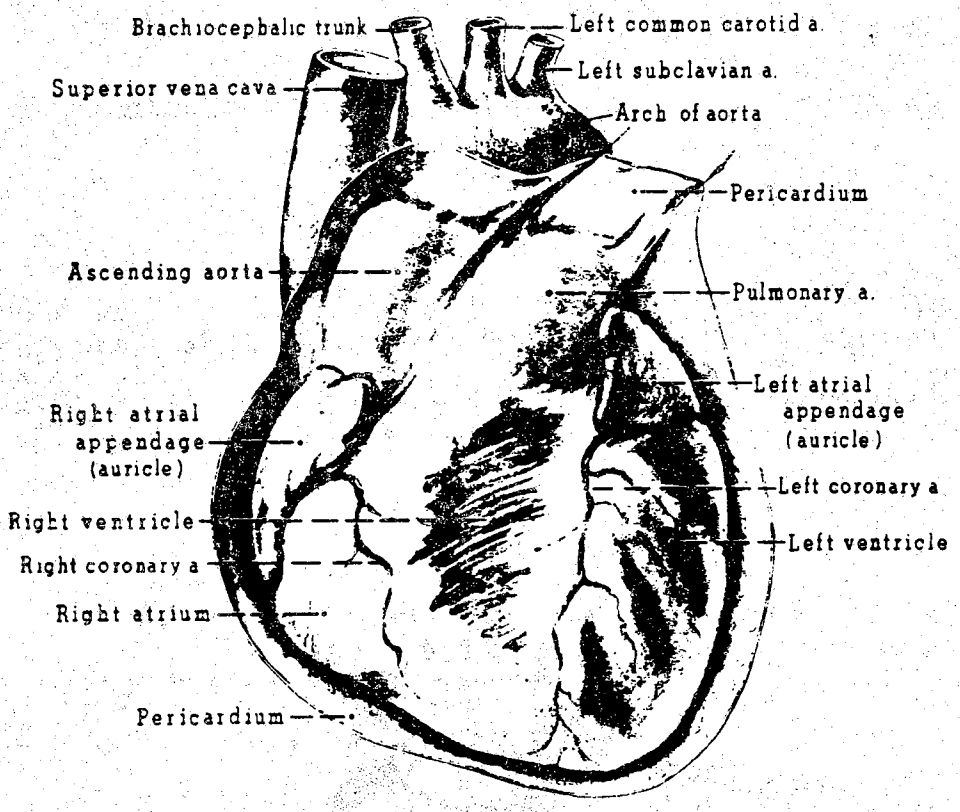

Figure 1.1 Anterior aspect of the heart [1].

The *right atrium* constitutes the right superior portion of the heart. It is a thin-walled chamber receiving blood from all tissues except the lungs. Three veins empty into the right atrium: the superior and inferior venae cavae, bringing blood from the upper and lower portions of the body; and the coronary sinus, draining blood from the heart itself. Blood flows from the atrium to the right ventricle.

The *right ventricle* constitutes the right inferior portion of the heart's apex. The pulmonary artery carrying blood to the lungs leaves from the superior surface of the right ventricle.

The *left atrium* constitutes the left superior portion of the heart. It is slightly smaller than the right atrium, with a thick wall. The left atrium receives the four pulmonary veins draining oxygenated blood from the lungs. Blood flows from the left atrium into the left ventricle.

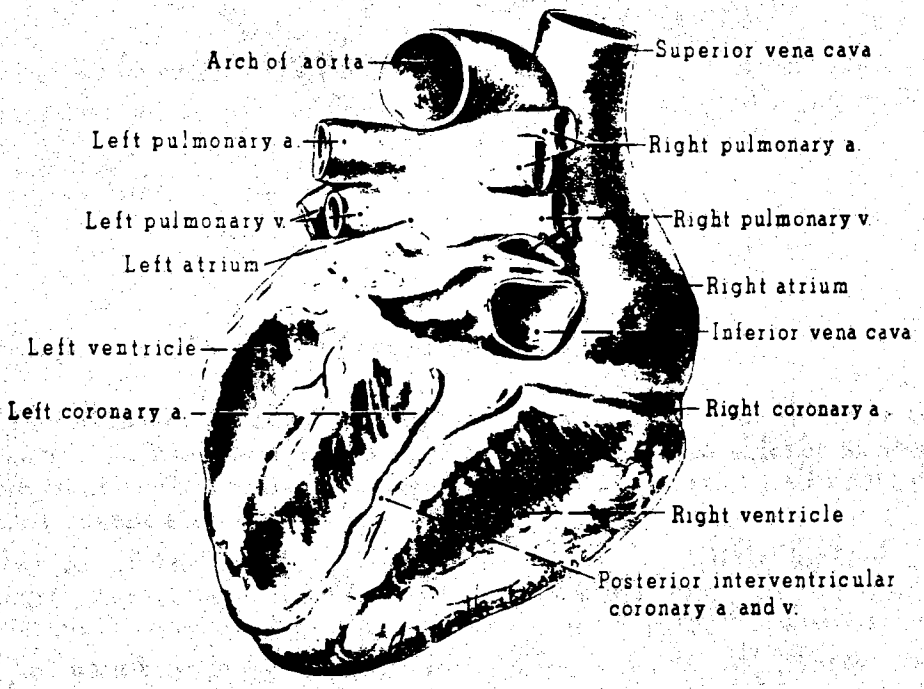

Figure 1.2 Posterior aspect of the heart [1].

The *left ventricle* constitutes the left inferior portion of the apex of the heart. The walls of this chamber are three times as thicker as those of the right ventricle. Blood is forced through the aorta to all parts of the body except the lungs.

Valves of the heart. There are two types of valves located in the heart: the *atrioventricular valves* (*tricuspid* and *mitral*) and the *semilunar valves* (*pulmonary* and *aortic*) (see Figures 1.3 and 1.4).

The atrioventricular valves are thin, leaf-like structures located between the atria and ventricles. The right atrioventricular opening is

guarded by the tricuspid valve, so called because it consists of three irregularly shaped flaps (or cusps) formed mainly of fibrous tissue and covered by endocardium. These flaps are continuous with each other at their bases, creating a ring-shaped membrane surrounding the margin of the atrial opening. Their pointed ends project into the ventricle, and attached by cords called the *chordae tendineae* to small muscular pillars, the *papillary muscles*, within the interior of the ventricles. The left atrioventricular opening is guarded by the mitral or bicuspid valve, so named because it consists of two flaps. The mitral valve is attached in the same manner as the tricuspid, but it is stronger and thicker since the left ventricle is a more powerful pump.

Blood is propelled through the tricuspid and mitral valves as the atria contract. When the ventricle contracts, blood is forced backward, passing between the flaps and walls of the ventricles. The flaps are thus pushed upward until they meet and unit, forming a complete partition between the atria and the ventricles. The expanded flaps of the valves resist any preassure of the blood which might force them to open into the atria, since they are restrained by the cordae tendineae and papillary muscles.

The semilunar valves are pocket-like structures attached at the point at which the pulmonary artery and aorta leave the ventricles. The pulmonary valve guards the orifice between the right ventricle and the pulmonary artery. The aortic valve guards the orifice between the left ventricle and the aorta.

An important aspect of heart anatomy and physiology is the coronary system of arteries and veins that supply blood to the heart. According to Jacob and Francone [1]:

Blood supply to the heart. The heart is supplyed by the *right* and *left coronary arteries* (see Figures 1.5). These vessels are the first branches of the aorta. They encircle the heart and supply blood to all portions of the myocardium. The blood in the coronary arteries returns to the heart, either by way of the coronary veins or by special sinusoids in the myocardium. The coronary arteries and their branches are as follows.

Left coronary artery. The anterior descending branch supplies blood to the left and right ventricles. The circumflex branch supplies blood to the left atrium and left ventricle. *Right coronary artery.* The posterior descending branch supplies blood to the left and right ventricles. The marginal branch supplies blood to the right atrium and right ventricle.

1.1.2 Cardiac Physiology and Ischemic Heart Disease

The heart, as a muscle, needs oxygen to perform its task. This oxygen is supplied by the coronary artery system. Thus, there must be a balance between the oxygen demand of the heart and the oxygen supply.

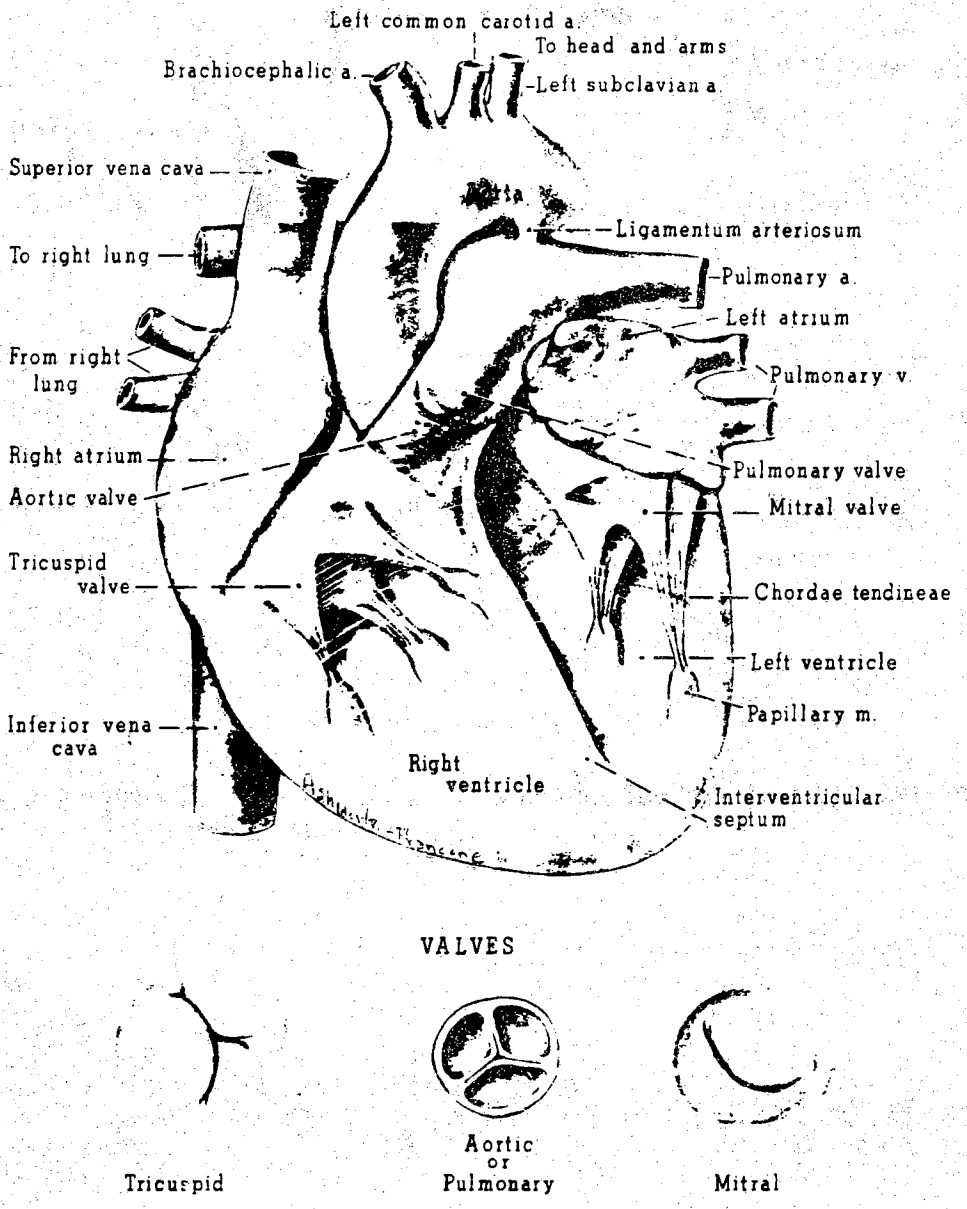

Figure 1.3 Interior view of the heart showing the relationships between the cavities and the valves [1].

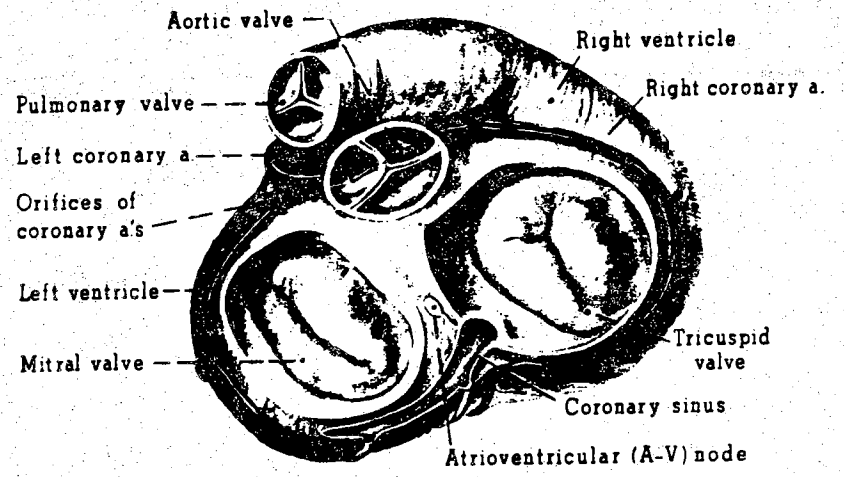

Figure 1.4 View of the heart's valve system through the base of the heart [1].

The oxygen demand is not constant, it depends on many factors, basically it can be stated that oxygen consumption is closely related to the work performed by the heart. In other words, the greater the work, the greater the oxygen demand, and vice versa. Since oxygen is brought to any point of the body by blood flow, it is brought to the cardiac muscle by coronary circulation. Thus, an increase in oxygen demand must be answered with an increase in coronary artery blood flow. Figure 1.6 describes the factors which determine oxygen demand and supply to the heart.

Ischemic heart disease is one of the most common heart diseases and results from insufficient coronary blood flow, or generally speaking, from an insufficient

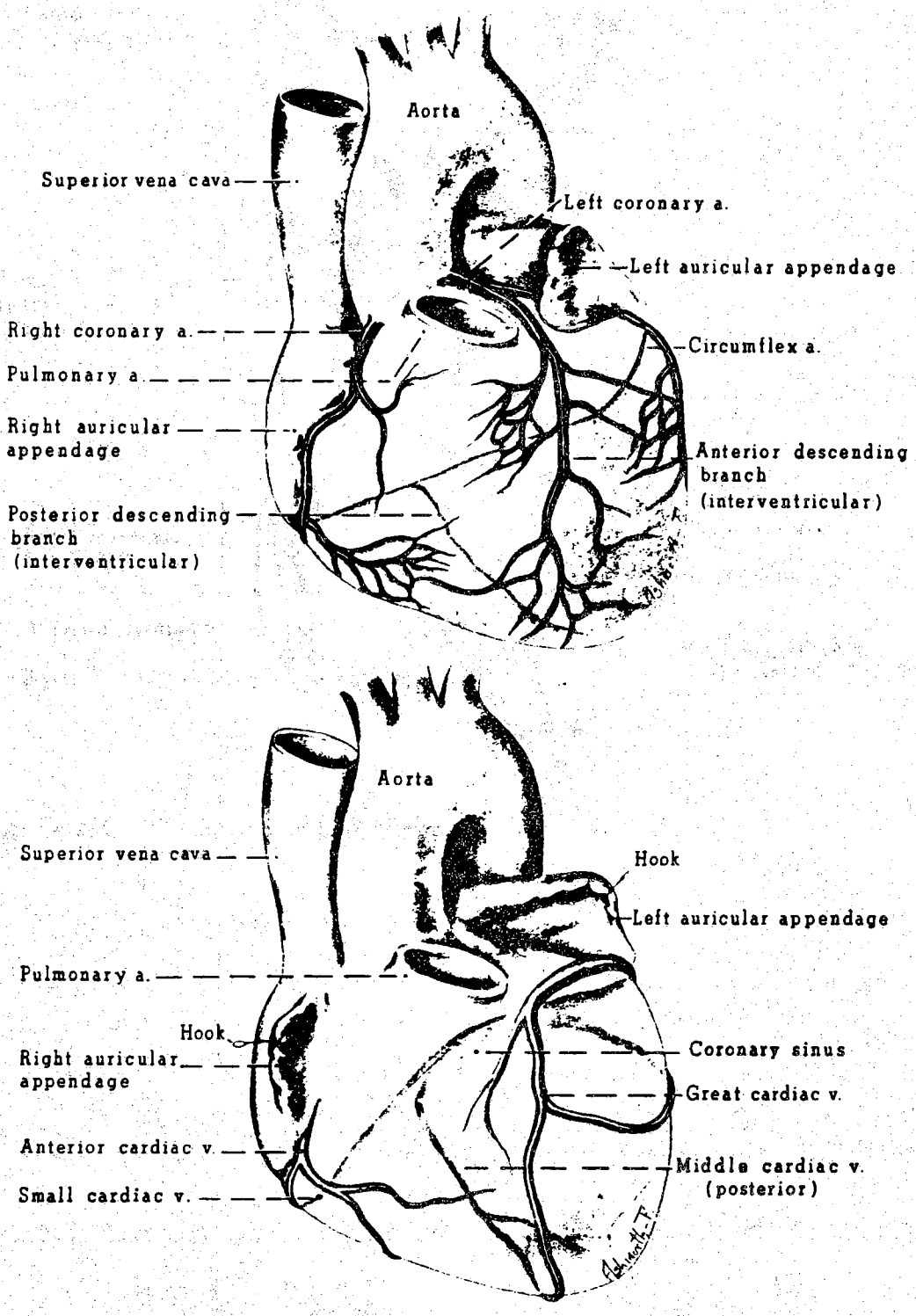

Figure 1.5 The coronary artery system of the heart [1].

oxygen supply to the cardiac muscle. One of the factors that produces insufficient blood flow is acute coronary occlusion, which means a total lack of blood circulation through part of the coronary artery system. Immediately after acute coronary occlusion, the area of muscle that is no longer irrigated by blood is said to be *infarcted.* The overall process is called *myocardial infarction,* commonly known as heart attack.

Acute coronary occlusion is not the only determinant of ischemic heart disease, it can also be produced by a diminished capacity of the coronary system to supply a greater blood flow for higher oxygen demand. *Angina Pectoris,* for instance, appears when increased heart effort can not be matched with an increased blood flow. When the muscle cells do not obtain the oxygen they need, they die. Besides heart failure, abnormal cardiac status can produce alterations in the beating process and in the general behavior of the organ.

1.2 Echocardiography: An Overview

1.2.1 Viewing Modalities of Echocardiography

Widespread use of ultrasound in the study of the heart is due to its real time capabilities and noninvasiveness. In addition, it is quite inexpensive when compared with other imaging modalities. It is also relatively easy to perform on a patient since the equipment is portable.

Ultrasound is used in order to visualize tissue and organs. One or an array of ultrasound beams are directed at the organ under examination. When the ultrasonic wavefront propagates into a transition surface between two tissues of different density, part of the wavefront is reflected. A sensor at the receiver collects the reflected energy. Assuming that the speed of the ultrasonic wave is known, and that the receiver knows the time when the wave was sent, an image can be constructed from the returned signal, (the time delay and attenuation must be known). These concepts are shown in Figure 1.7.

There are several aspects in the interaction between ultrasound and tissue which must be discussed to understand what an ultrasonic image looks like [2]. The first is *attenuation.* Ultrasound is a longitudinal pressure wave, if we express the value of the wave amplitude as a function of position, we have:

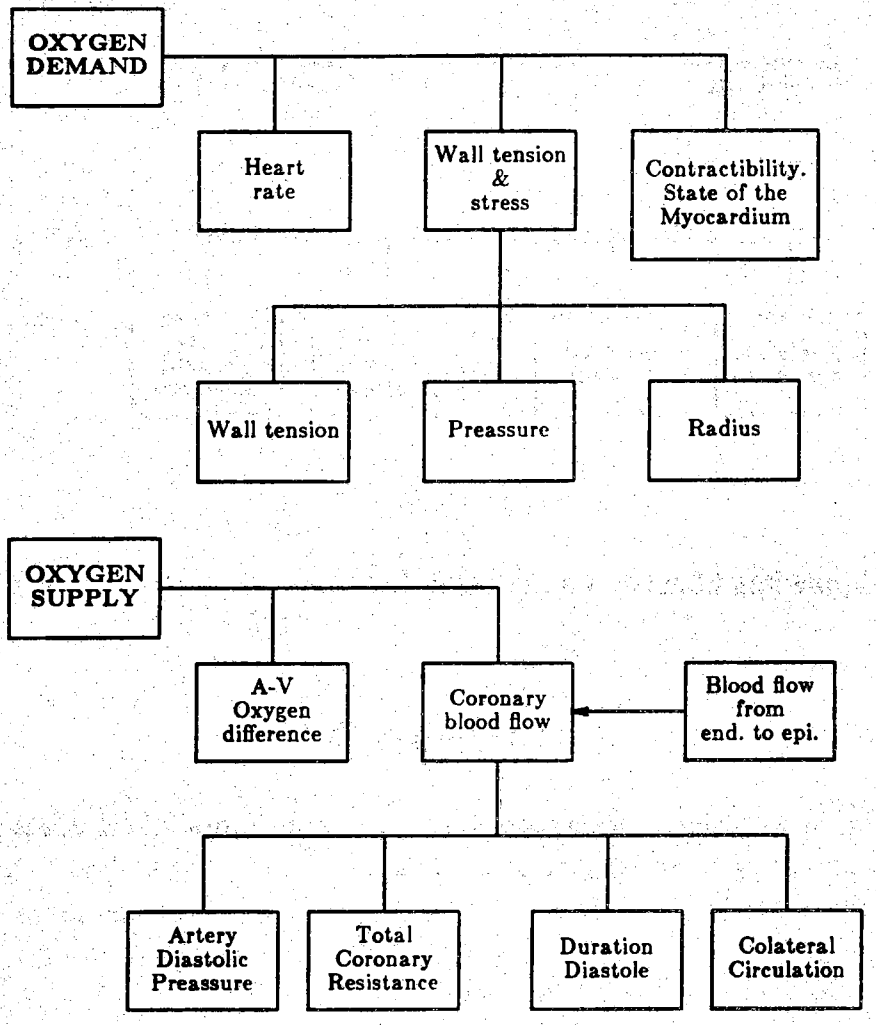

Figure 1.6 Factors which determine oxygen demand and supply to the heart.

$$A = A_0 \sin[\frac{2\pi}{\lambda}(vt - x)]$$

Where A is the amplitude, v is the propagation velocity, x is the position, t is the time, and A_0 is a real constant. The amplitude of the propagating wave would remain constant if there were no friction forces, and the medium through which the wave propagates were homogeneous.

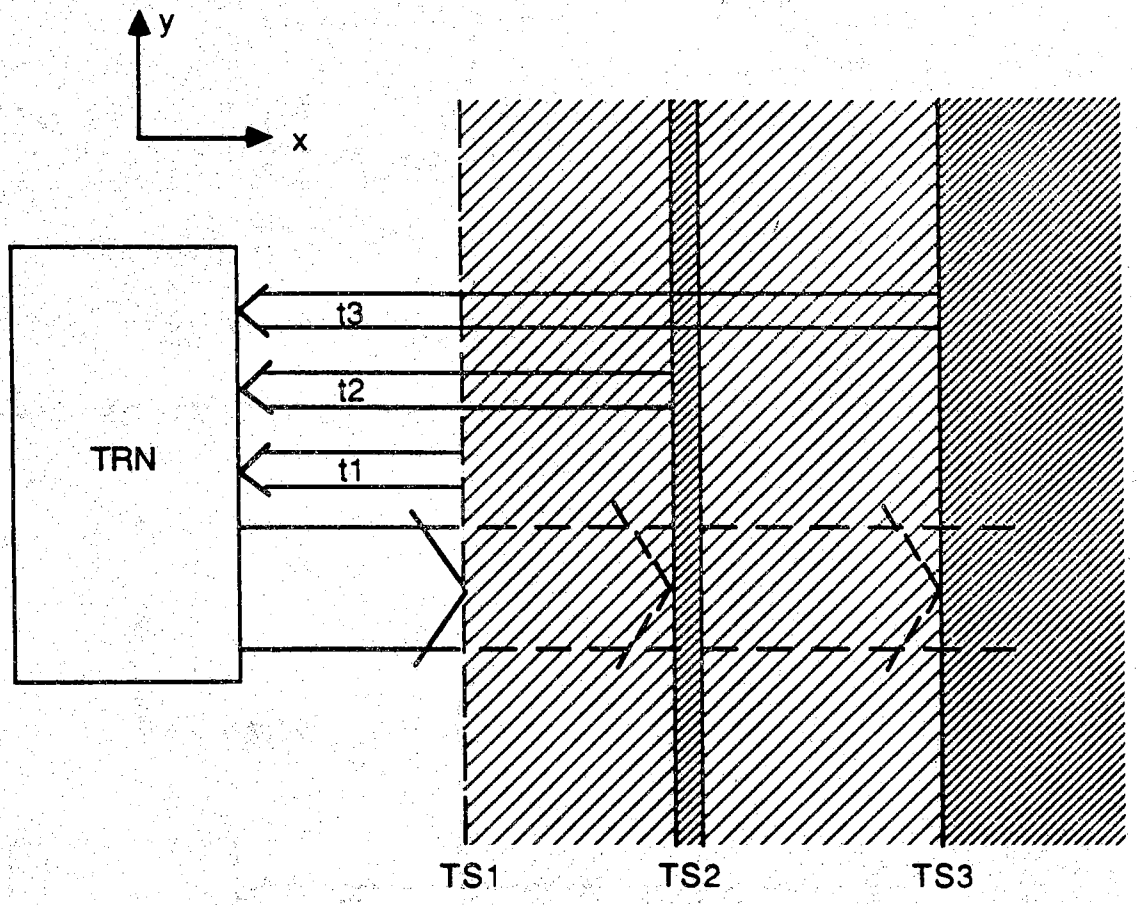

Figure 1.7 This figure shows the basics of ultrasound imaging. A transducer (TRN) directs an ultrasound beam at the tissue structure that is to be visualized. When the ultrasound wave arrives at TS1, the transition surface between the two superficial layers of tissue, part of the wave is reflected back to the transducer; t1 is the time it takes for the ultrasound to travel from TRN to TS1 and for the reflected portion of the wave to reach TR again. Part of the ultrasound signal penetrates the tissue beyond TS1 and encounters TS2. Again, part of this wave is reflected back to TRN, with a total traveling time t2. The same happens at TS3 with returning time t3. Since we can measure t1, t2, and t3, and the speed at which ultrasound travels through the different tissues, we can compute how far away TS1, TS2, and TS3 are from the transducer. If we further assume that the tissue distribution does not change along the y axis, and that all the tissue layers are homogeneous, then it is possible to draw a map of tissue thickness and distribution (distance between the different layers and the transducer) from the echoes received at TRN.

Actually, human tissue is very heterogeneous and there are other phenomena involved, such as scatter due to the cellular structure, absorption, and reflection/refraction. Usually attenuation can be modeled by a decreasing exponential:

$$B=B_0 e^{-\alpha z}$$

Where B_0 is a real constant which is the amplitude of the incident wave on the surface of the tissue through which ultrasound is propagating, α is the attenuation coefficient that characterizes the propagation medium, and z is the distance traveled by ultrasound through the tissue. B describes the ultrasound amplitude at the given point z. The coordinate origin is located on the tissue surface.

Reflection takes place whenever the ultrasound wave encounters the boundaries of two tissues. The reflected wave depends on the characteristic impedance of both tissues, and it is given by :

$$I_r=I_i(\frac{z_2-z_1}{z_2+z_1})^2$$

Where I_r is the intensity of the reflected wave, and I_i refers to the intensity on the incident wave. z_1 and z_2 are the characteristic impedances of the tissue on either side of the interface. The characteristic impedance is defined by:

$$z = \rho v$$

where ρ is tissue density and v is propagation velocity.

The reflected angle is equal to the incident angle and the direction of the transmitted beam depends on the ratio of the velocities of propagation in both media. Figure 1.8 shows the general situation when reflection and refraction occur. Because the receiver is placed at the same location as the transmitter, the receiver only detects the reflected waves coming from almost perpendicular surface to the propagating direction.

When objects encountered by the ultrasonic wave are much smaller than the wavelength, then the interaction between ultrasound and tissue is very different. Energy is reflected in all directions, this phenomenon is known as *scattering*.

When ultrasound is scattered by the cellular structure, the scattered waves interfere either constructively or in a destructive manner at all points of the space where they propagate. When the interference is constructive the intensity

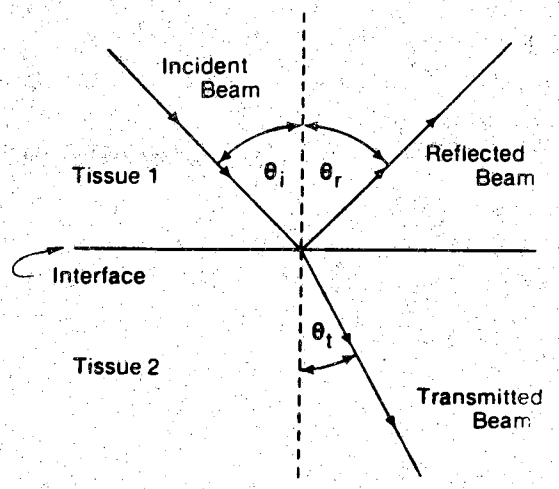

Figure 1.8 Reflection and refraction phenomena [2].

of the ultrasound signal is reinforced whereas when the interference is destructive the intensity diminishes significatively or even vanishes. The effect of such a process is known as *speckle* and in echocardiography it produces a "grainy" looking image. The points where the brightness is low, due to the interference, are known as drop-outs. As stated above, the primary source of scattering in biological tissue is cells or groups of cells, and it is quite important in echocardiography, since it affects image quality.

A final phenomenon to be taken into account is the Doppler effect, due to moving objects, that produces a shift of the frequency of the ultrasonic wave detected by the transducer. Although it is not important in echocardiography, it is used as a tool in other cardiac imaging modalities.

1.2.2 The Echocardiographic System and Display Modes

Figure 1.9 is a block diagram of a typical echocardiographic system. The source of the ultrasound waves is a transducer usually made of a crystal that uses the piezoelectric effect. When a crystal is excited electrically, it transforms part of the electrical energy into mechanical energy by vibrating. The frequency at which the crystal vibrates depends on the geometry of the crystal. The mechanical energy is reflected back by the tissue structure under analysis and is detected by the same crystal. This is possible since the piezoelectric effect works in the opposite way, i.e., the returning mechanical energy is converted into electrical energy.

The electrical signal, corresponding to the reflected ultrasound signal, is amplified and time-gain compensated. Time-gain compensation minimizes the attenuation of the ultrasonic wave as it travels through the tissue. Since the distance traveled by ultrasound reflected back from deeper tissue structures is longer it reaches the transducer more attenuated, hence the signal must be amplified to compensate for this "depth" attenuation.

There are different ways of displaying the information received from the transducer. These are known as A-mode, B-mode, M-mode, and 2-D echocardiography (see Figure 1.10).

In A-mode, the intensity of the returning ray is plotted against time. In other words, we obtain a plot where amplitude peaks correspond to energy reflections of the incident beam, and time is the time it takes for the reflected amplitude to reach the transducer.

In B-mode, the amplitude of the returning energy is represented in the form of brightness, so it can be displayed on a CRT screen. For instance, assume that the object is vibrating; in this case B-mode display would contain an oscillating chain of bright spots. If the brightness is plotted against time onto a strip of photographic paper which moves at a constant rate then we obtain a M-mode display.

If many B-mode lines are generated very quickly, either parallel to each other or from a single point in a fan shape, then a two-dimensional display of a cross section of the object is obtained. This essentially is a tomographic view of the region under study. This can be performed by either mechanically steering the transducer or by phased array techniques. The data collected along each line of sight (each B-mode line) is known as *scan line data.* Figure 1.11 shows how two dimensional displays are obtained.

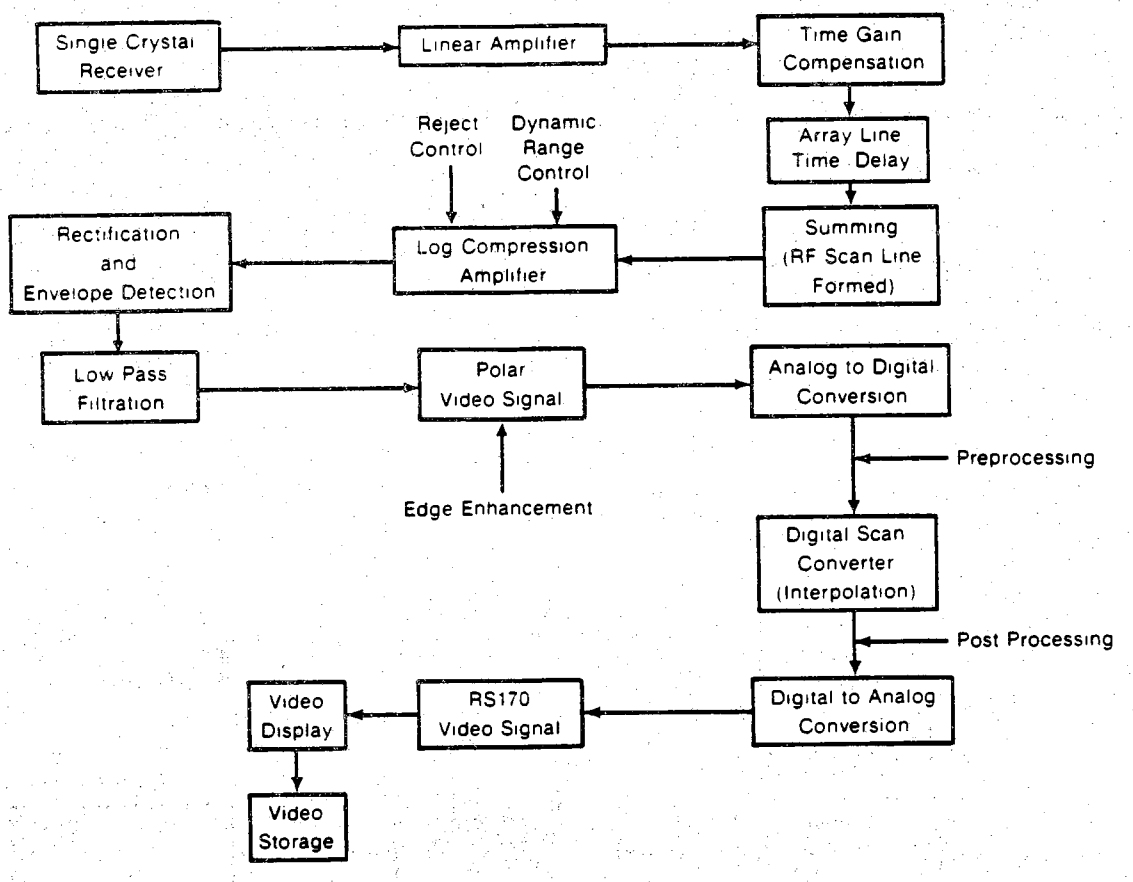

Figure 1.9 Block diagram of an echocardiographic system (suggested by [2]).

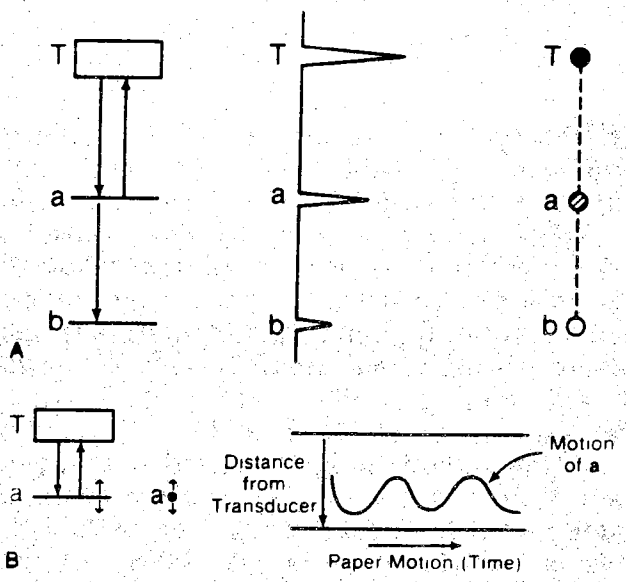

Figure 1.10 Display modes of ultrasound signal. **A:** on the left, a transducer (T), two reflecting interfaces (a and b) and ultrasound waves (arrows) traveling from the transducer to the interfaces and returning to the transducer. In the middle, the A-mode (amplitude versus time) display format is shown, where a and b are indicated by two different amplitude peaks. On the right the B mode (brightness versus time) display format is shown, where the brightness spots a and b mark the position of the two reflecting interfaces. **B:** on the left, a transducer (T) and interface (a) are shown, along with ultrasound beams (large arrows); interface exhibits a periodic motion (small arrows). In the middle, B mode representation is that of a moving dot (dot a with two small vertical arrows). On the right the M-mode display is shown, produced by inscribing the position of the B-mode dot on a strip chart.

Since the dynamic ultrasound signal is very large (between 80 and 100 dB [2]), and since the human eye is able to perceive only a 25 to 30 dB range, a log compression amplifier is used in the system (see Figure 1.9). Further signal processing has to be performed so that a displayble signal can be obtained. This signal processing is represented by the *Rectification and Envelope Detection* block (the original signal is a radio frequency signal, between 2 and 10MHz), the

Low Pass Filter block, and the *Polar Video Signal* block. The Polar Video Signal is digitized and converted to a rectangular format so that it is compatible with a standard television signal. The digitized signal is also interpolated to fill the gaps between the digitized scan line data. The digitization process allows storage of the image and also allows further processing of the image.

1.3 Digital Image Processing of Two Dimensional Echocardiograms

One of the goals of computer processing of two-dimensional echocardiograms is automatic detection of features of the heart. These features are then useful for cardiac status assessment. Because of its importance in the detection of myocardial ischemia, the analysis of the left ventricle has received the most attention, although other parts of the heart have also been studied[3].

The steps generally used for automatic left ventricular analysis are image acquisition (digitization and storage), preprocessing, segmentation and boundary detection, feature extraction and interpretation of cardiac status.

1.3.1 Image Acquisition

In the early attempts to digitally process echocardiographic images there was a lack of adequate interfacing between the computer used to analyze the image data and the image source.

For instance, according to Garcia, et al. [4], initial attempts used video cameras aimed at a still frame from an echocardiographic sequence displayed on a CRT, others devices such as flying spot scanners, contour digitizers, and video disk recorders have also been utilized.

Buda, et al. [5] proposed direct digitization of the envelope detected RF signal. Digitized scan line data is known as *line mode data*. Line mode data is obtained in polar format. Figure 1.12 shows the processing in a typical echo machine versus direct digital computer acquisition and processing using line mode data.

The superior quality of this direct digitization of the signal display is shown in Figure 1.13. This superior quality is possible since the envelope-detected signal is independent of all control settings of the the echo system except gain control. Also the envelope detected signal has a larger dynamic range than the output signal of the digital scan converter for video data acquisition. The line

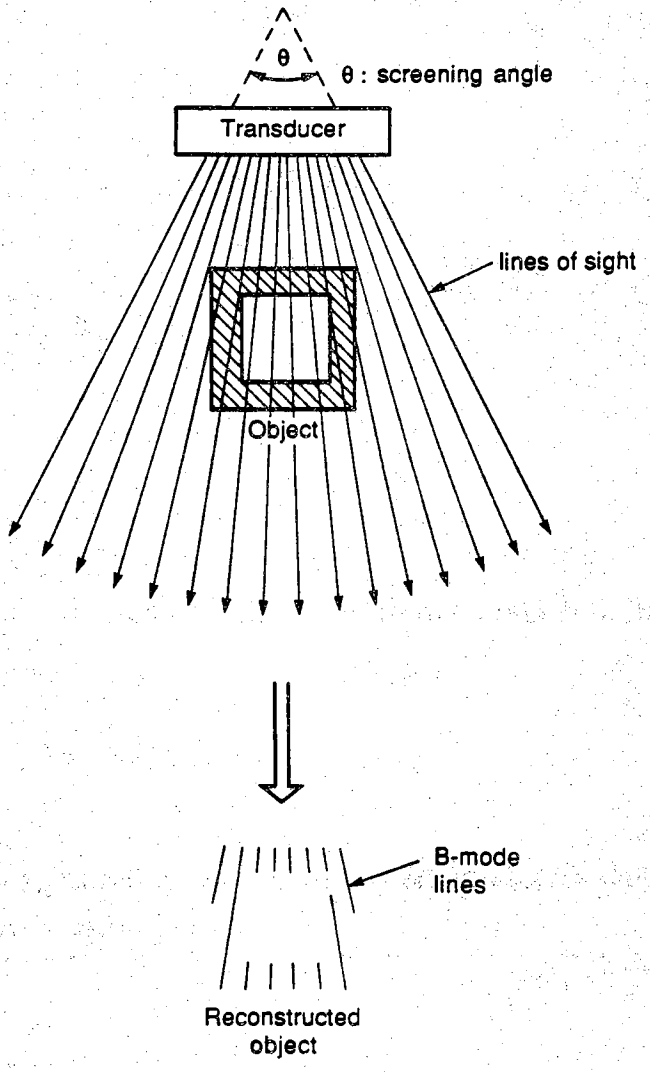

Figure 1.11 Construction of a two dimensional image from line mode data.

mode data can be digitized in real time at 30 images/second, hence image sequences of the entire cardiac cycle can be obtained.

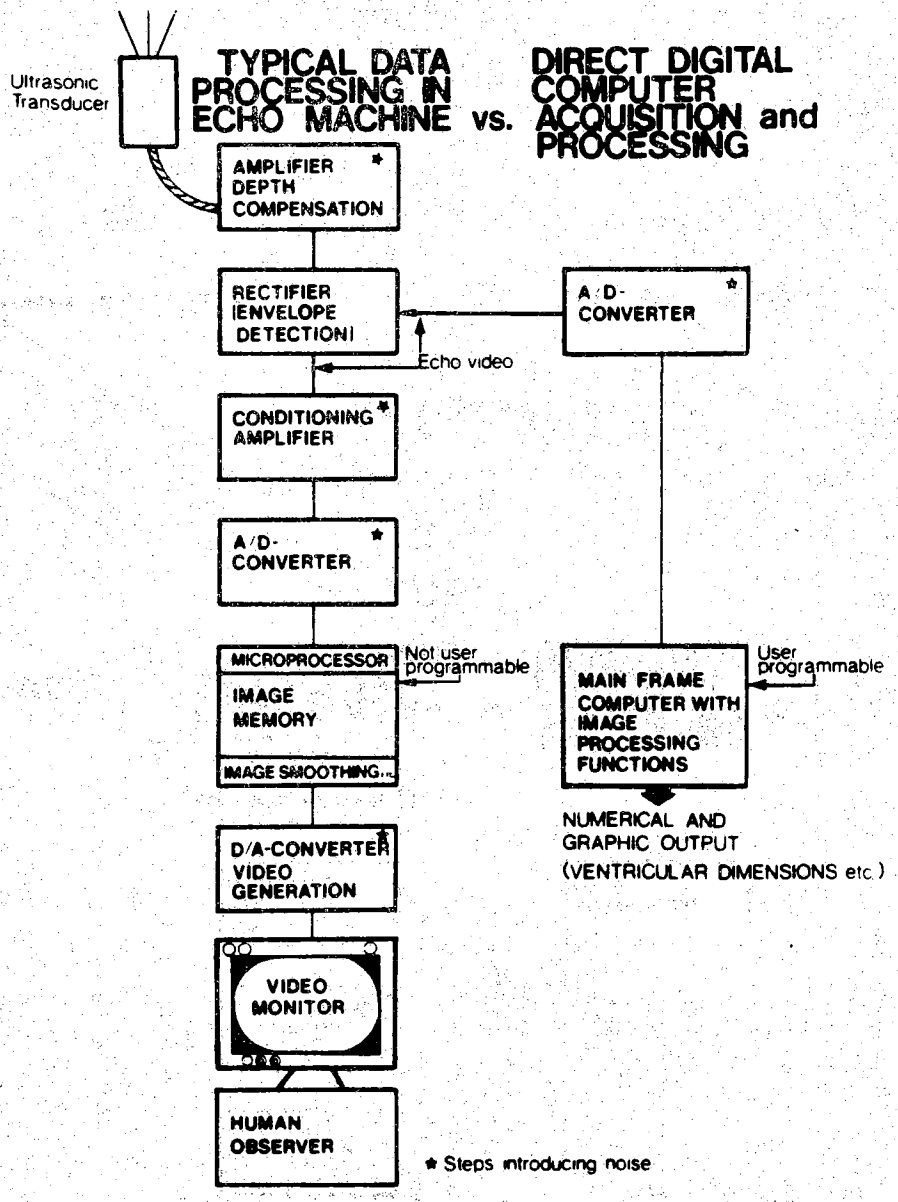

Figure 1.12 Typical signal processing in an echocardiographic system versus direct digital computer acquisition.

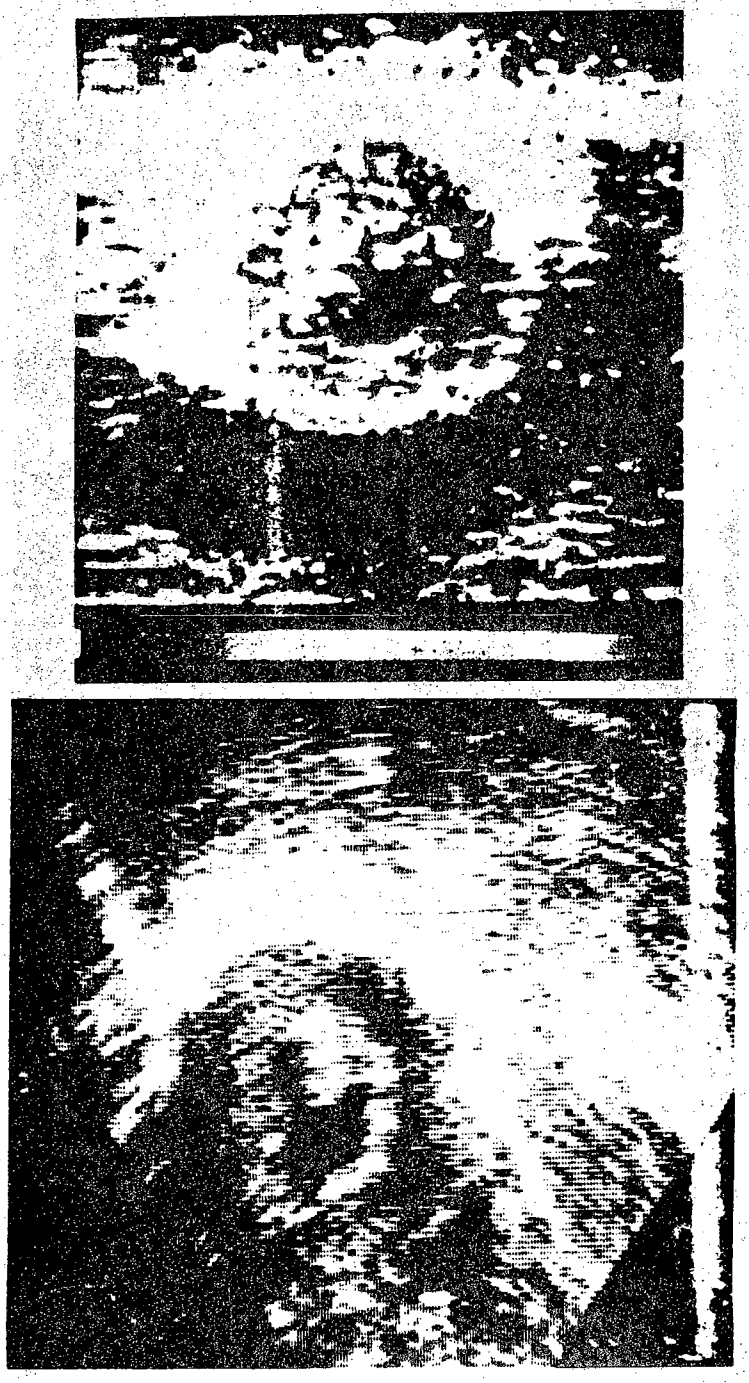

Figure 1.13 Top image: image acquired from video screen. Bottom image: image acquired using a direct computer acquisition system [5].

1.3.2 Preprocessing

Before endocardial left ventricular boundaries can be obtained, the image is processed in order to remove noise. Garcia, et al. [4] smoothed the image sequence in the spatial and temporal domains. The time domain smoothing consisted of the weighed average of the pixel under consideration, and the pixels with the same coordinates the frames before and after the frame under consideration. The weighting factors are two to one (one for the frames before and after).

The spatial domain smoothing consisted of a simple 3x3 window operation. In this case the weighting factors were 4 for the central pixel (to be replaced by the average), 2 for the adjacent pixels, and one for the diagonally-aligned pixels. The smoothing process, according to the authors: "increases the statistical accuracy of each pixel and also helps reduce the effect of drop-outs".

Others have used similar preprocessing techniques [7-11]. According to Delp et al. [12], temporal smoothing blurs edge locations since the heart is not exactly at the same position at the beginning of each cardiac cycle due to the fact that the heart rotates and translates, and it is difficult to assume that it reaches the same position after each cardiac cycle. The results are "the edges of the temporally smoothed image exhibit the phenomena of very small radius of curvature and have large spurious edge locations". Furthermore smoothing data in the spatial domain may change edge locations.

Other types of preprocessing are gray scale equalization [11], and gray scale equalization by using different gain settings of the ultrasound scanner [13].

1.3.3 Boundary Detection and Segmentation

Because the left ventricular chamber usually appears as a dark region surrounded by the much brighter cardiac muscle, edge detection techniques have been employed. Edge detection is used to identify the regions in the image where a substantial gray level difference exists between adjacent pixels. Garcia et al. [4] used a combination of thresholding and second derivative techniques commonly used in nuclear cardiology.

Other edge detection methods have also been used. The Sobel operator, for example, uses a 3x3 pixel window mask to compute estimates of the magnitude of the gradient. A threshold is used to discriminate between those pixels

considered as boundary pixels and those which are not.

Zwehl, et al. [8] used a Laplacian operator which computes the second derivative of an image in the X and Y directions. Since the second derivative is zero at points of inflection, zero crossings of the output of the Laplacian indicate possible edge locations.

The continuous Laplacian is given by the following:

$$\nabla^2 = \frac{\partial^2}{\partial x^2} + \frac{\partial^2}{\partial y^2}$$

In the simple digital version, a 3x3 pixel window operator is usually used as a kernel. The expression for the digital version is [14]:

$$\nabla^2 f(i,j) = [f(i+1,j)+f(i-1,j)+f(i,j+1)+f(i,j-1)]-4f(i,j)$$

Where i and j are the pixel coordinates. Collins, et al. [9] experimented with the Sobel operator, the Laplacian operator, and global gray level thresholding. They reported that no significant differences were found among these simple methods.

Another procedure, gray-level thresholding, is based on the assumption that the blood in the chamber and noise have low gray level values, whereas the myocardium and in general the muscular tissue have high gray level values. Edges are obtained at the boundaries between two different areas of the thresholded image. According to Collins, et al [9], the threshold was manually selected by an operator.

Other more advanced techniques for left ventricular detection will be discussed in Chapter 2.

1.3.4 The Left Ventricular Detection Process

All of the techniques reviewed above attempt to obtain automatically the location of the left ventricular endocardium.

In clinical practices a human operator selects a frame or a sequence of frames and manually traces the boundaries of the left ventricular inner chamber. This process is a time consuming task, since the operator often has to watch a whole sequence of frames in motion so that he or she gets a "feeling" where the

"real" boundaries are located. Trained human operators are also not objective. All these reasons motivate the computerization of the detection process.

Most of the previously reported work requires that a human operator pick a point somewhere within the left ventricular chamber after preprocessing the image [4, 7-13]. Most of the algorithms perform a radial search from this starting point after an edge enhancement algorithm is used on the preprocessed image. The search is stopped when a pixel indicating the presence of an edge is encountered.

The detected edges may not be "well located" or thin, therefore some sort of postprocessing is in order to obtain a final useful estimation of the edge locations. This postprocessing generally includes filling in the gaps due to dropouts in the original image, edge thining, etc. Figure 1.14 outlines the general procedure.

The strength of this method is that it may be possibile to carry out further detection in successive frames once the process has been successfully applied to the first frame. The basic assumption is that the general characteristics of the heart do not change substantially from frame to frame. In actual echocardiographic sequences this will probably not be true.

1.3.5 New Trends in Feature Detection in Echocardiography

The use of intelligent algorithms for feature detection and tracking are becoming more attractive in the analysis of echocardiographic images. Emphasis is on the use of apriori knowledge has largerly been ignored in previous work. Ezekiel, et al. [10] proposed the use of a cost function which serves as a knowledge acquisition tool. The use of cost functions allows a quantitative assessment of the found edge. In addition, such a cost function allows further comparison between successive detected edges.

Chu and Delp have proposed the use of various new algorithms developed in the computer vision area and have developed a paradigm for the use of apriori knowledge [6].

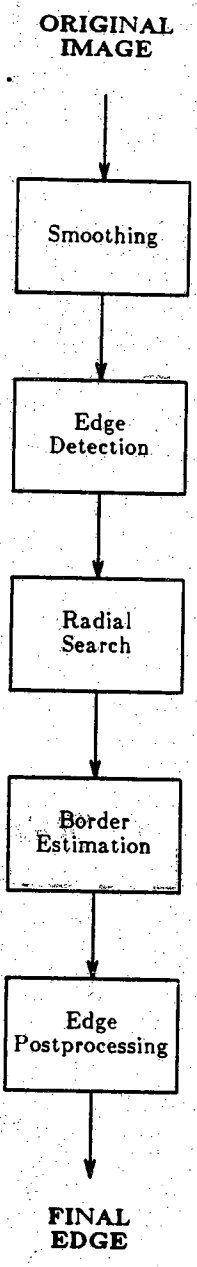

Figure 1.14 Block diagram of boundary estimation in echocardiographic images.

1.4 Summary

We have reviewed in this chapter the basic concepts of heart anatomy. In addition the basic principles of two-dimensional echocardiography were also presented. At the end of this chapter the basic trends in two-dimensional echocardiography processing was also reviewed.

As far as data acquisition quality is concerned, it seems obvious that the acquisition problem should be addressed by digitizing the envelope detected signal. The ability to deal with the original signal also allows a more flexible and reliable treatment of the digitized image.

CHAPTER 2
SEGMENTATION

2.1 Introduction

Image segmentation is the process of reducing processing complexity by examining only those regions in the image that are of interest. In other words, we try to separate useful information from the "background" (the "background" is made of those parts of the image which do not convey information for our purposes).

Segmentation implies a higher level description of the image than that provided by the original gray level pixels. It separates the "raw" image into different areas which can be represented by parameters others than the gray levels. These parameters are known as features.

For instance, if our image is a scene with strong lighting where bright objects cast dark shadows, and our goal is to extract the shadow locations, then a simple thresholding operation may be used. We might proceed by choosing a threshold, i.e. a fixed gray level to which all the gray levels in the picture would be compared. Then, after performing the comparison for every pixel, a value of "1" would be assigned to all of the pixels whose gray levels were lower than that of the threshold, and "0" otherwise. If the threshold value is smaller than the average gray value of the bright objects in the scene, but not smaller than the average value of the shadow pixels, then we obtain a second image, where blobs with value "1" indicate the presence of shadows.

Although simplistic, the previous example illustrates a typical segmentation strategy. In echocardiography, the segmentation step is very important since we need to accurately determine the left ventricular boundaries. Most segmentation techniques used in echocardiography are usually forms of edge detection [6].

2.2 Segmentation in Echocardiography

Skorton, et al. [7] reported the use of various image segmentation algorithms that have been used to identify the endocardium boundaries. One method obtained the boundary locations by thresholding. The threshold is set by examining the histogram of the pixels. If the histogram contains a deep valley between two significative peaks, the minimum in the valley is chosen as threshold. If the histogram is not clearly bimodal, then several thresholds are chosen in the neighborhood of the probable histogram minimum.

Although segmentation by thresholding seems to be an attractive tool for the identification of the darker inner left ventricular chamber region from the brighter surrounding tissue, there are many problems with this simple approach. Zhang and Geiser [15] pointed out the problems with global thresholding:

> In view of the large contrast variation and echo dropout in echocardiographic images, a global threshold is not suitable for segmenting the echocardiographic information from the image background. It is well known that portions of short axis echocardiographic views will have a large amount of noise or an excessive amount of dropout if rib-shadowing is present. Thus, if the threshold is too high, much of the information in a shadowed region will be lost. On the other hand, if the threshold is low, a great deal of noise will be included. It is also obvious that the region involved with shadowing in each image changes because of the rotational and swinging motion of the heart during the cardiac cycle.

2.2.1 Segmentation of Echocardiographic Images Using Relaxation

Rosenfeld and Kak [14] divide segmentation methods into parallel and sequential techniques. Parallel methods perform pixel classification at each point without examining the other pixels in the image. For example, thresholding is a parallel segmentation technique. We classify every pixel without taking into account the value of any other pixel. This is a very fast method if parallel processing is utilized since the final result can be obtained after performing only one operation per pixel.

Sequential methods make use of other information and the values of neighboring pixels to decide how a pixel will be classified. Sequential methods are slower than parallel methods, but they are pontentially more powerful.

Relaxation methods are a hybrid between parallel and sequential methods. Relaxation methods used in segmentation are iterative processes where the segmentation of the image is "improved" in some sense at each iteration.

In order to illustrate what relaxation is and how it works, we will use the example discussed by Rosenfeld and Kak [14]. Suppose that we want to detect smooth curves in a picture. For a point P, using a parallel method, we compute the curvature at that point and it is compared to a threshold to decide whether a curve at point P is smooth enough or not. In the relaxation approach, let us assume that we can assign an initial probability a_i to P with slope θ_i. For another point Q, we compute the probability b_j with a slope θ_j. Instead of thresholding these probability values, the relaxation approach uses b_j to modify a_i according to some criterion. For instance, a criterion that depends on the degree of smoothness by which slope θ_j at Q merges to slope θ_i.

This modification process is carried out in such a way that for a single point in the image, its set of probabilities and the way it is affected by the set of probabilities of other points is computed simultaneously. These probabilities are then modified, and the process iterated until significant changes no longer exist. After a few iterations, the probabilities of the points where smooth curves are located should increase and the other probabilities should decrease.

The relaxation method can be stated in a more rigorous fashion. Suppose that we have a set of objects $A_1, \ldots, A_n$ that must be classified into m different classes $C_1, \ldots, C_m$. However, the classification of an object A_i into the class C_j is not independent of other classifications such as that of the object A_h into the class C_k. In order to measure the idea of "dependency", a function $c(i,C_j;h,C_k)$ called *compatibility* is defined. Large values of $c(i,C_j;h,C_k)$ will represent "high compatibility" between both classifications. Small values of $c(i,C_j;h,C_k)$ (which can be either close to zero or negative, depending on the definition of the compatibility function) will represent "low compatibility" or "incompatibility".

This compatibility function can be used for modifying the probabilities of assigning the object C_i to the class C_j, denoted by p_{ij}. Of course p_{ij} :

$$0 \leqq p_{ij} \leqq 1$$

$$\sum_{j=1}^{m} p_{ij}^{(r)} = 1$$

$$1 \leqq i \leqq n$$

Now we make use of the probabilities $p_{ij}^{(r)}$, where r denotes the current estimate, and the compatibility function $c(i,C_j;h,C_k)$ in order to address the thresholding problem.

2.2.2 Relaxation and Thresholding

Bhanu and Faugeras [17], and Rosenfeld and Smith [18] used relaxation methods to perform image segmentation. The approach of Bhanu and Faugeras was utilized to segment echocardiographic images. Ordinary parallel techniques used in echocardiography threshold gray level values, without taking advantage of a priori information in the image. The result of such thresholding is a poorly segmented image due to drop-outs and speckle noise.

Bhanu and Faugeras [17] defined a criterion function as follows:

$$C(p_1,p_2, \ldots, p_N) = \sum_{i=1}^{N} p_i q_i \tag{2.1}$$

Where $p_i q_j$ is the inner product of the probability vector p_i and the compatibility vector q_i. This function is maximized by means of the gradient projection approach. N is the total number of pixels.

Since we want to produce a binary image that indicates where the relevant boundaries are located we assume we have two classes λ_1 and λ_2 corresponding to white and black (gray level values 0 and 255 respectively). Now we define an eight pixel neighborhood V_i around the pixel under consideration and a cost function:

$$c(i,\lambda_k;j,\lambda_l)=0 \quad k \neq l \quad j \in V_i \ \forall \ i$$

$$c(i,\lambda_k;j,\lambda_k)=1 \quad k=1,2 \quad j \in V_i \ \forall \ i$$

Next the compatibility vector q_i is defined as:

$$q_i(\lambda_k) = \frac{1}{8} \sum_{j \in V_i} \sum_{l=1}^{2} c(i,\lambda_k;j,\lambda_l) p_i(\lambda_l) \tag{2.2}$$

$k=1,2 \quad i=1,\ldots,N$

In other words, $q_i(\lambda_k)$ is the mean neighborhood probability of the i-th pixel for the class under consideration.

$$q_i(\lambda_k) = \frac{1}{8} \sum_{j \in V_i} p_j(\lambda_k) \tag{2.3}$$

Intuitively, when we try to maximize C, we are trying to minimize the discrepancy between the pixel under consideration and its surrounding neighbors. This is a good strategy, since in noisy images such as echocardiographic images, this will minimize the effects of drop-outs.

Another important issue is the way the initial probabilities $p_i(\lambda_k)$ are computed. The simpliest choice is:

$$p_i(\lambda_1) = \frac{I(i)}{G-1} \tag{2.4}$$

Where I(i) is the gray level of the i-th pixel and G is the total number of gray levels. Here we are ignoring the actual gray level values of the image and are assuming an equally likely pixel distribution. Another way that uses the information in the gray level values is the ratio between white and black pixels. Thus we obtain:

$$r = \frac{n_{white}}{n_{black}} = \frac{E(\lambda_1)}{E(\lambda_2)}$$

$$= \frac{\frac{1}{N}\sum_i p_i(\lambda_1)}{\frac{1}{N}\sum_i p_i(\lambda_2)} = \frac{\sum_{i=1}^{n} \frac{I(i)}{G-1}}{\sum_i (1-p_i(\lambda_1))}$$

$$= \frac{\frac{1}{G-1}\frac{1}{N}\sum_{i=1}^{n} I(i)}{\frac{1}{N}\sum_{i=1}^{n}(1-\frac{I(i)}{G-1})} = \frac{\bar{I}}{G-1-\bar{I}} \tag{2.5}$$

Where $\bar{I}$ is the mean gray level value, and E is the expectation operator.

The ratio r can be used to modify the probabilities $p_i(\lambda_1)$ if we want to modify the distribution of gray levels. Let us assume that $\bar{I}_0$ is the desired mean for the image under consideration, then we can assign the initial probabilities as:

$$p_i(\lambda_1) = F * \left[\frac{I(i) - \bar{I}}{255} \right] + \frac{\bar{I}_0}{255} \tag{2.6}$$

Where $\bar{I}_0$ is the desired mean gray level. F is a factor which is 1 if $I > \bar{I}$ and less than one if $I < \bar{I}$. We can see that $p_i(\lambda_1)$ is modified by $\bar{I}_0$ according to the actual values of I(i) and $\bar{I}$. F modulates how much we want this discrepancy to be.

We can then address the iterative process utilizing a gradient projection technique:

$$p_i^{(n+1)}(\lambda_1) = p_i^{(n)}(\lambda_1) + \rho^{(n)} P_i^{(n)} \left[\frac{\partial C}{\partial p_i(\lambda_1)} \right] \tag{2.7.a}$$

$$p_i^{(n+1)}(\lambda_2) = p_i^{(n)}(\lambda_2) + \rho^{(n)} P_i^{(n)} \left[\frac{\partial C}{\partial p_i(\lambda_2)} \right] \tag{2.7.b}$$

Where $\rho^{(n)}$ is a positive step size, $P_i^{(n)}$ is a projection operator, and the superscript n is the iteration number. Since we require $p_i^{(n+1)}(\lambda_1) + p_i^{(n+1)}(\lambda_2) = 1$ then the projection of the gradient (the projection operator) should be:

$$P_i^{(n)} \left[\frac{\partial C}{\partial p_i(\lambda_k)} \right] = 2q_i(\lambda_k) - \frac{1}{2} \left[\frac{\partial C}{\partial p_i(\lambda_1)} + \frac{\partial C}{\partial p_i(\lambda_2)} \right]$$

In addition:

$$\frac{\partial C}{\partial p_i(\lambda_1)} = 2q_i(\lambda_1) \quad \text{and} \quad \frac{\partial C}{\partial p_i(\lambda_2)} = 2q_i(\lambda_2)$$

then the projection operator turns out to be:

$$P_i^{(n)}\left[\frac{\partial C}{\partial p_i(\lambda_k)}\right] = 2q_i(\lambda_k) - 1 \tag{2.8}$$

and

$$p_i^{(n+1)}(\lambda_1)=p_i^{(n)}(\lambda_1)+\rho^{(n)}[2q_i(\lambda_1)-1] \tag{2.9.a}$$

$$p_i^{(n+1)}(\lambda_2)=p_i^{(n)}+\rho^{(n)}[1-2q_i(\lambda_1)] \tag{2.9.b}$$

The fastest convergence rate is achieved when $\rho^{(n)}$ is such that $p_i^{(n+1)}(\lambda_1)=1$ or 0 when $2q_i(\lambda_1)-1$ is >0 and $2q_i(\lambda_1)-1<0$ respectively. This can be obtained when:

$$\rho_{i_{max}}^{(n)} = \begin{cases} \dfrac{1-p_i^{(n)}(\lambda_1)}{2q_i(\lambda_1)-1} & \text{if } 2q_i(\lambda_1)-1>0 \\ \dfrac{p_i(\lambda_1)}{1-2q_i(\lambda_1)} & \text{if } 2q_i(\lambda_1)-1<0 \end{cases} \tag{2.10}$$

If the convergence rate is desired to be controlled then a factor α can be used such that:

$$\rho_i^{(n)} = \begin{matrix} \alpha_1\rho_{i_{max}}^{(n)} & \text{if } 2q_i-1>0 \quad 0 \leqq \alpha \leqq 1 \\ \alpha_2\rho_{i_{max}}^{(n)} & \text{if } 2q_i-1<0 \quad 0 \leqq \alpha \leqq 1 \end{matrix} \tag{2.11}$$

2.2.3 Implementation and Results

Since echocardiographic images are strongly unimodal (see Figure 2.1) the above relaxation algorithm is a candidate segmentation technique. In our implementation, we experimented with different values of α_1, α_2, F, and $\bar{I}_0$, and found that for a fixed F and $\bar{I}_0$ the segmented areas did not change appreciably after the first iteration (see Figures 2.2, 2.3, and 2.4). Therefore the values of α_1 and α_2 were set to one in order to obtain a totally segmented binary image after the first iteration, where pixels with $p_i(\lambda_1)=0$ were set to black and pixels with $p_i(\lambda_1)=1$ were set to white.

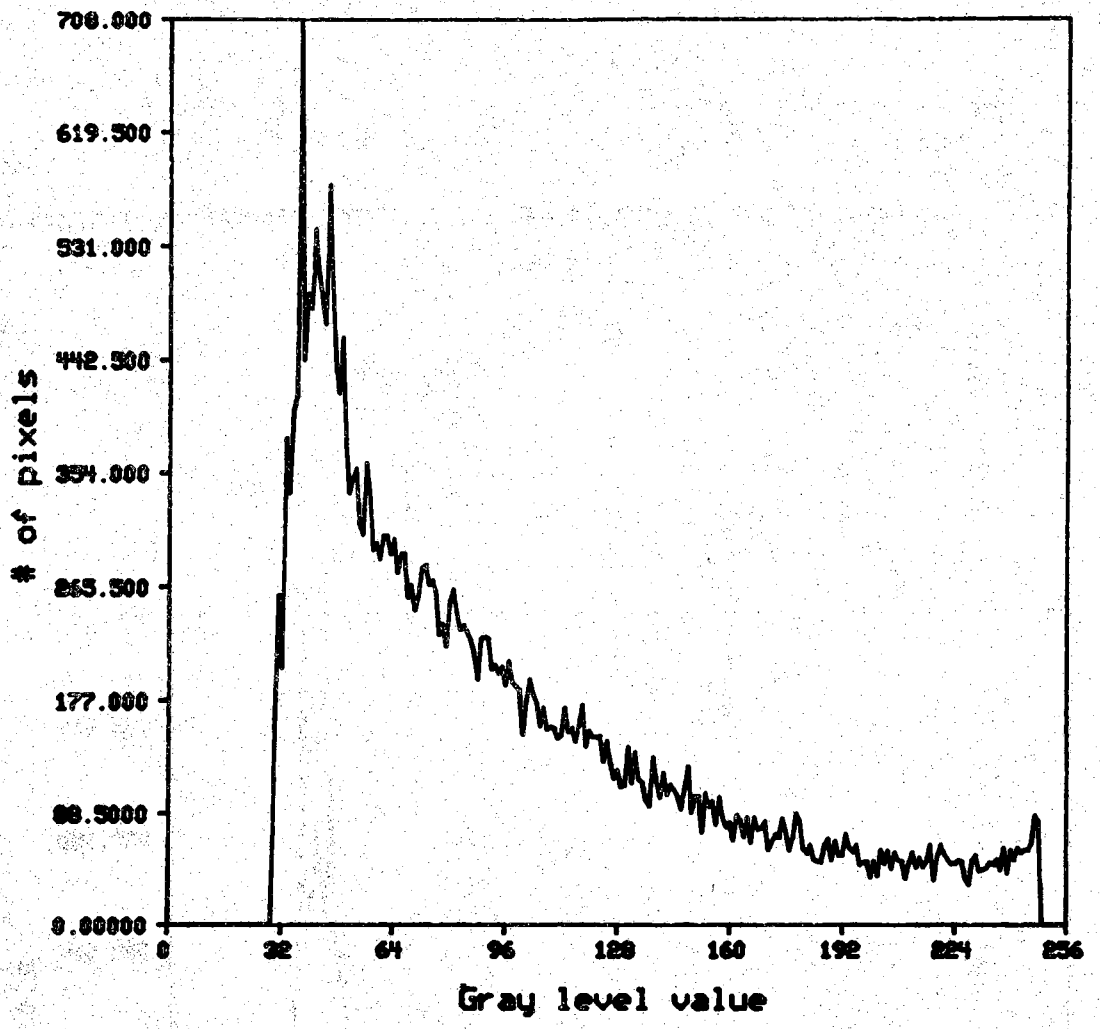

Figure 2.1 Typical histogram of an echocardiographic image

The segmented regions were very sensitive to the values of F and $\bar{I}_0$ (see Figure 2.5).

One conclusion that can be drawn is that this method does not allow an optimum threshold to be selected.

The images were first smoothed in the original line mode format using a 5x5 square window, then the pixels in the original image were interpolated into Cartesian coordinates. Smoothing first and then performing coordinate conversion results in a more effective smoothing of the image, since in the original line mode format, noise is homogeneous over the image.

After smoothing, segmentation is performed using the relaxation algorithm described in the previous section. The resulting binary images show that segmentation using relaxation provides a "cleaner" segmented image than that achieved by simple thresholding. A "cleaner" segmented image, where the drop-out and speckle effects are not as severe as in the original image, may aid in the reduction of the complexity of postprocessing algorithms used to obtain the endocardial and epicardial boundaries. In many cases these boundaries turn out to be ragged because of image dropouts. Relaxation might help to obtain "smoother" boundaries (see Figure 2.6).

2.3 Segmentation of Echocardiographic Images Using Temporal Analysis

It seems reasonable to take advantage of the temporal redundancy available in consecutive frames of the cardiac cycle.

One of the early techniques is averaging several image frames in order to reduce the noise [10]. One of the main drawbacks of this approach is edge smoothing or blurring. When two consecutive images are averaged, the cardiac muscle moves from one frame to the next hence producing blurred edges. A possible solution is to align images corresponding to the same points in the cardiac cycle, but since the heart moves in a three dimensional space, and it is not possible to view the same cross section from one frame to the next.

In order to segment echocardiographic images making use of temporal analysis, Zhang and Geiser [16] proposed a segmentation algorithm based on the dynamic characteristics of the heart. Zhang and Geiser define a bistable function $B^L(i,j)$ as follows :

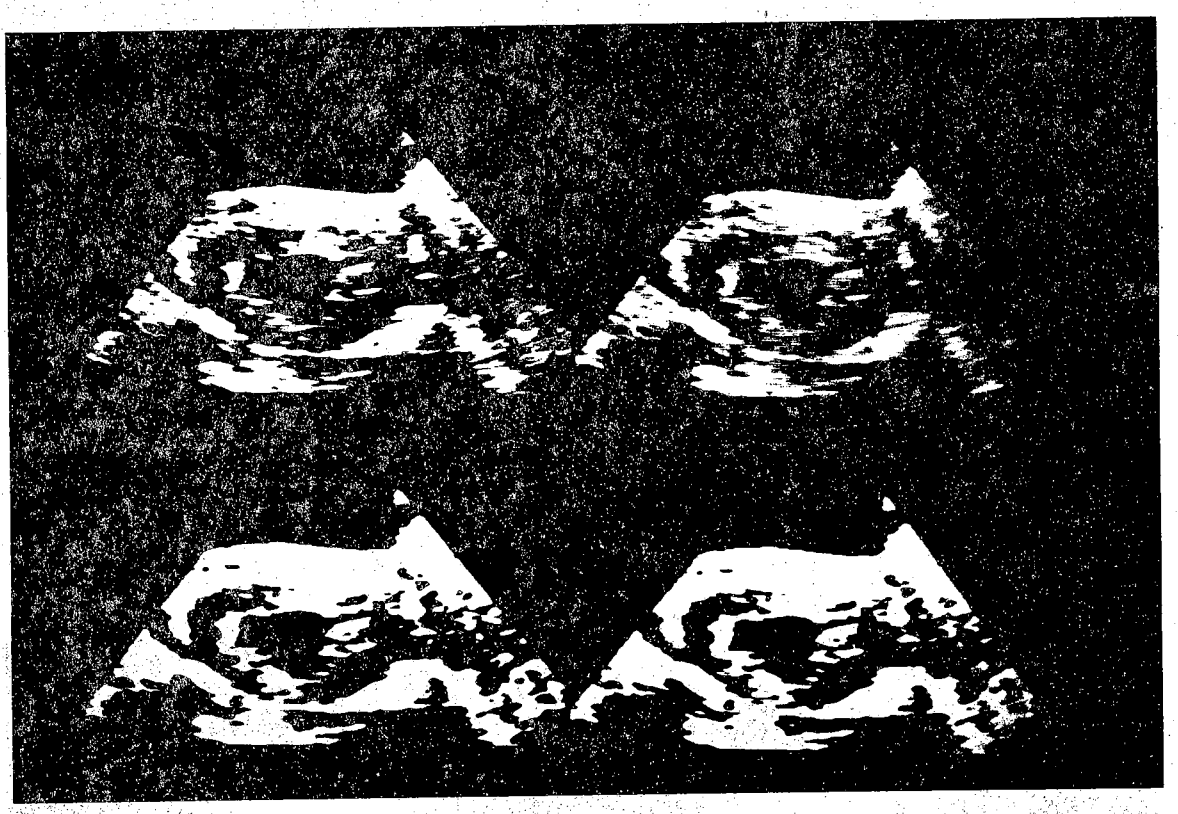

Figure 2.2 Original image (upper left) and thresholded image after one (upper right), five (lower left), and ten iterations for $\alpha_1=\alpha_2=0.1$, $F=0.5$, and $I_0=0.0$.

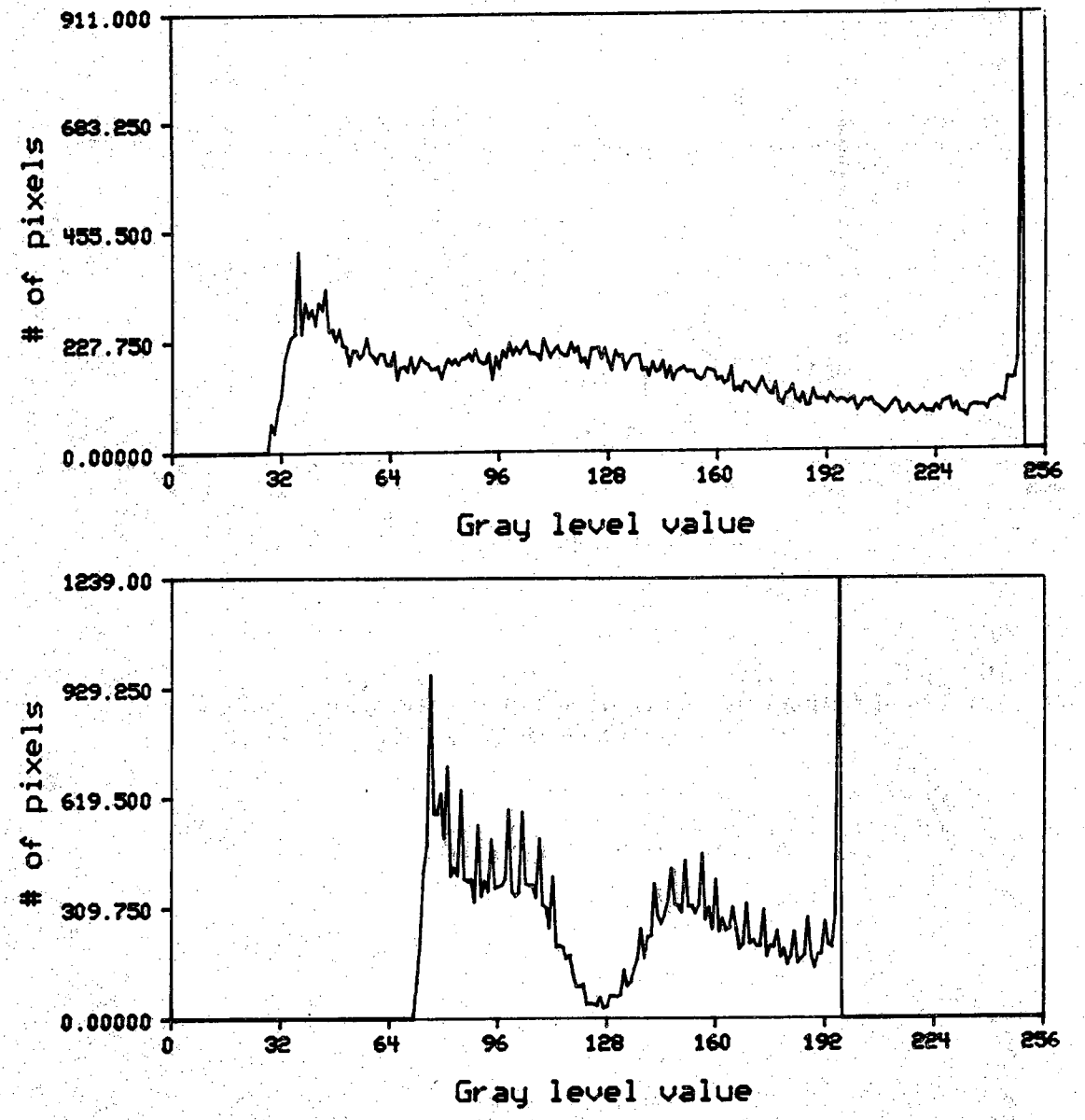

Figure 2.3 Histograms of original image (top) and segmented image after one iteration (bottom) as shown in Figure 2.2

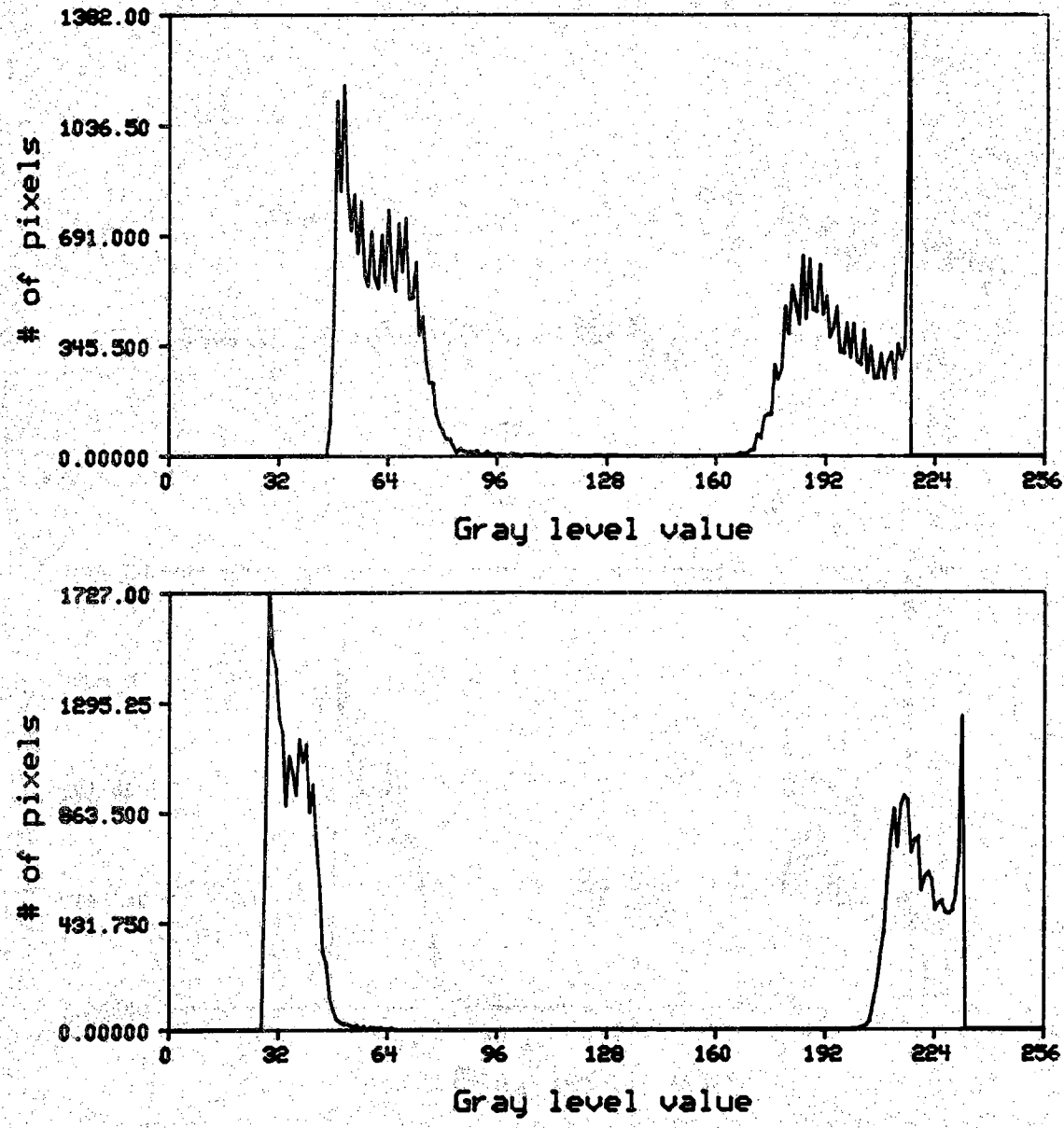

Figure 2.4 Histograms of segmented images after five (top) and ten iterations (bottom) as shown in Figure 2.2

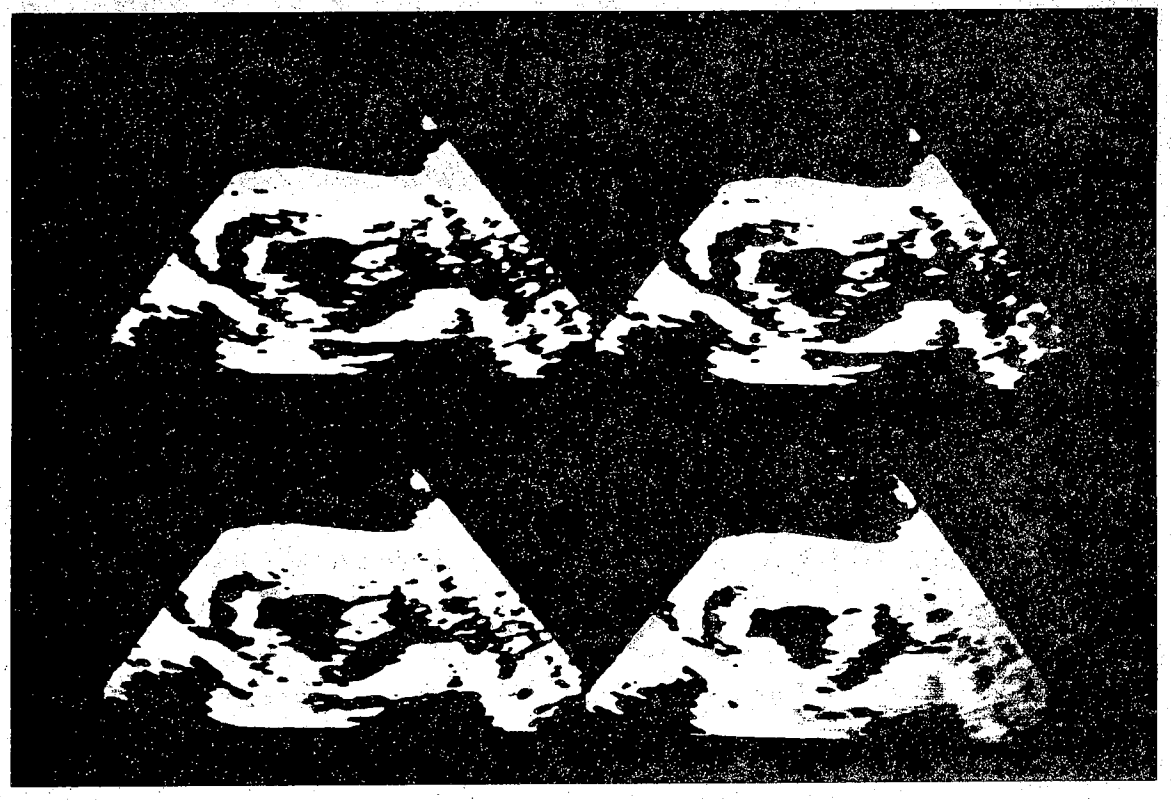

Figure 2.5 Segmented images for $\bar{I}_0$ fixed and F variable (top), and F fixed and $\bar{I}_0$ variable (bottom). F=0.3 (top left) and F=0.8 (top right), in both cases $\bar{I}_0$=0.0. And $\bar{I}_0$=0.03 (bottom left), and $\bar{I}_0$=0.04 (bottom right), in both cases F=0.5. In all cases the number of iterations was 5 and $\alpha_1=\alpha_2=0.1$.

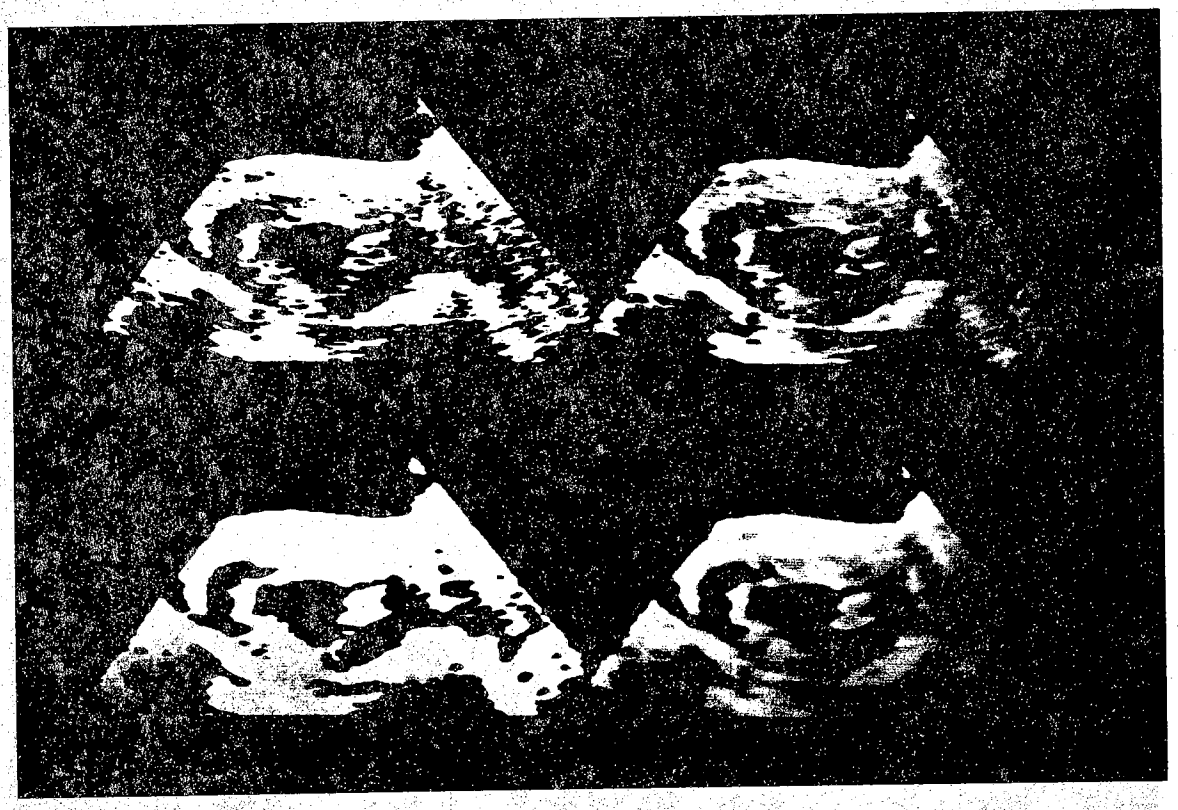

Figure 2.6 Top: Image in Figure 2.3 segmented using a "row" threshold (no smoothing) (left) and the relaxation algorithm (right). Bottom: Same image segmented by means of a threshold and the relaxation algorithm (left and right) after smoothing.

$$B^L(i,j) = \begin{cases} 0 & \text{if } G^L(i,j) \leqq G_T \\ 1 & \text{if } G^L(i,j) > G_T \end{cases} \qquad (2.12)$$

Where $G^L(i,j)$ is the gray level of the pixel at the position (i,j) in the image frame L and G_T is the threshold value. If B changes from 0 in frame L to 1 in frame L+1 or vice versa, then the pixel at (i,j) is said to be a moving pixel. The moving points represent gray value variation from frame to frame. $B^L(i,j)$ is the function that permits quantitative definition of this gray level variation.

The temporal coocurrence matrix M is a square matrix such that the entry M_{ij} is the relative frequency of two temporally corresponding pixels, one with gray level i in the first frame and the other with gray level j in the second one. Hence, M_{ij} will take the value m if there are m points such that their gray value changes from the value i in the current frame to the value j in following frame. The size of the matrix M is $k \times k$ where k is the number of quantization levels.

It is assumed that the heart beating process will produce large changes in gray level from frame to frame on and near the endocardial boundary. Following this reasoning, it is further assumed that a "good" threshold value should highlight the endocardial boundary and maximize the number of moving points in the image.

The moving points in the image are given by P:

$$P = \sum_{i=1}^{G_T} \sum_{j>G_T}^{k} M_{ij} + \sum_{i>G_T}^{k} \sum_{j=1}^{G_T} M_{ij} \qquad (2.13)$$

The first term of the right hand side of the equality is the number of pixels whose gray levels are less than or equal to the threshold in frame L, but greater than the threshold on frame L+1, and vice versa for the second term. Then choosing the optimum threshold G_T is equivalent to maximizing P. This approach, on the other hand, does not take into account two dimensional spatial information, so it is quite sensitive to drop-outs and spurious noise.

Herman and Liu [19] proposed an enhancement operator that looks for time varying edges (edges that move from frame to frame). Herman and Liu use a three-dimensional edge detector as a time varying edge detector by treating the temporal axis as the third dimension. The most important drawback of this technique is the multiple responses obtained when the intensity jump across time frames is larger than the jump in the spatial coordinates.

High level techniques have also been explored. Some of these techniques are *token-based methods.* Tokens are spatial features found in images, such as important structures that remain "essentially" unchanged throughout the cardiac cycle (e.g., the papilary muscles, various heart wall segments, etc). Tracking these important features allow more efficient image segmentation to be obtained, since it overcomes drop-outs and noise. Unfortunately this approach is not totally successful due to the gross temporal undersampling in a typical echocardiographic sequence.

Optical flow estimation is another important method for temporal analysis of echocradiographic images. Optical flow is used to obtain estimates of the velocity of each pixel. Here the important assumption is that the movement of the heart wall is different from the background. Mailloux, et al. [29], used optical flow to examine echocardiographic sequences. For instance, points in the image with radial movement can be considered as points belonging to the endocardial borders of the left ventricle. Again, this technique is limited by temporal undersampling and a low signal-to-noise ratio, which make velocity estimation very difficult.

2.4 A New Algorithm for Boundary Detection

Chu, et. al. [6] described a new algorithm for endocardial and epicardial boundary detection. This algorithm can be summarized in the following way: edge enhancement is performed using a general edge operator, then a radial search is performed for initial edge estimation; finally, nonlinear processing of edge estimates provides the final edge estimation.

After interpolating the echocardiographic images into cartesian coordinates from the line mode data, the image is enhanced using a linear window with Gaussian weighting. Since cardiac images have relatively few features, and the signal to noise ratio is small, large windows are utilized. In this particular case a 41x41 pixel window. Since features that are to be detected (endocardial and epicardials borders) are far larger, and echo images are not very complex, hence large windows are justified as a way of reducing the perturbing effects of noise as much as possible.

The next operation is the application of a digital Laplacian operator. The zero crossings at the output of the Laplacian operator are considered to be

potential edge points. The combined steps of Gaussian smoothing and Laplacian enhancement is commonly known as the $\nabla^2 G$ operator. Endocardial and epicardial edge detection is started after picking a point within the limits of the left ventricular chamber and performing a radial search.

In order to make sure that only boundary points are detected, a search limit is imposed when looking for edge points, so the search stops beyond a fixed distance from the center. Further processing is carried out to remove noise and fill the gaps produced by dropouts and false detections. Missing edge points are interpolated out of the neighbouring points by means of linear interpolation.

The authors point out that this method is not flawless, since the presence of the papilary muscles or other structures may occlude part of the boundary from the point of view of the starting search point chosen by the operator. If such a thing happens, then a secondary search is performed to complete the original border. Figure 2.7 shows the detected boundaries obtained by this new algorithm along with the original images.

2.5 Summary

One of the main problems in automatic processing of echocardiographic images is segmentation. The simple approach to echocardiographic image segmentation, thresholding, will not work due to speckle noise and drop-outs. Some algorithms have tried to overcome these problem by using the dynamic characteristics of echocardiographic images as well as the spatial information provided by neighbouring pixels.

The first approach considered in this chapter is thresholding via relaxation. The drawbacks of this technique is the lack of a criteria for choosing a threshold. A number of other techniques which make use of the temporal information, all of them attempting to make use of temporal redundancy in the echocardiographic image sequence, were discussed.

Finally a new algorithm for endocardial and epicardial boundary detection and segmentation is described. This algorithm uses a priori knowledge and produces edge boundaries that are smooth.

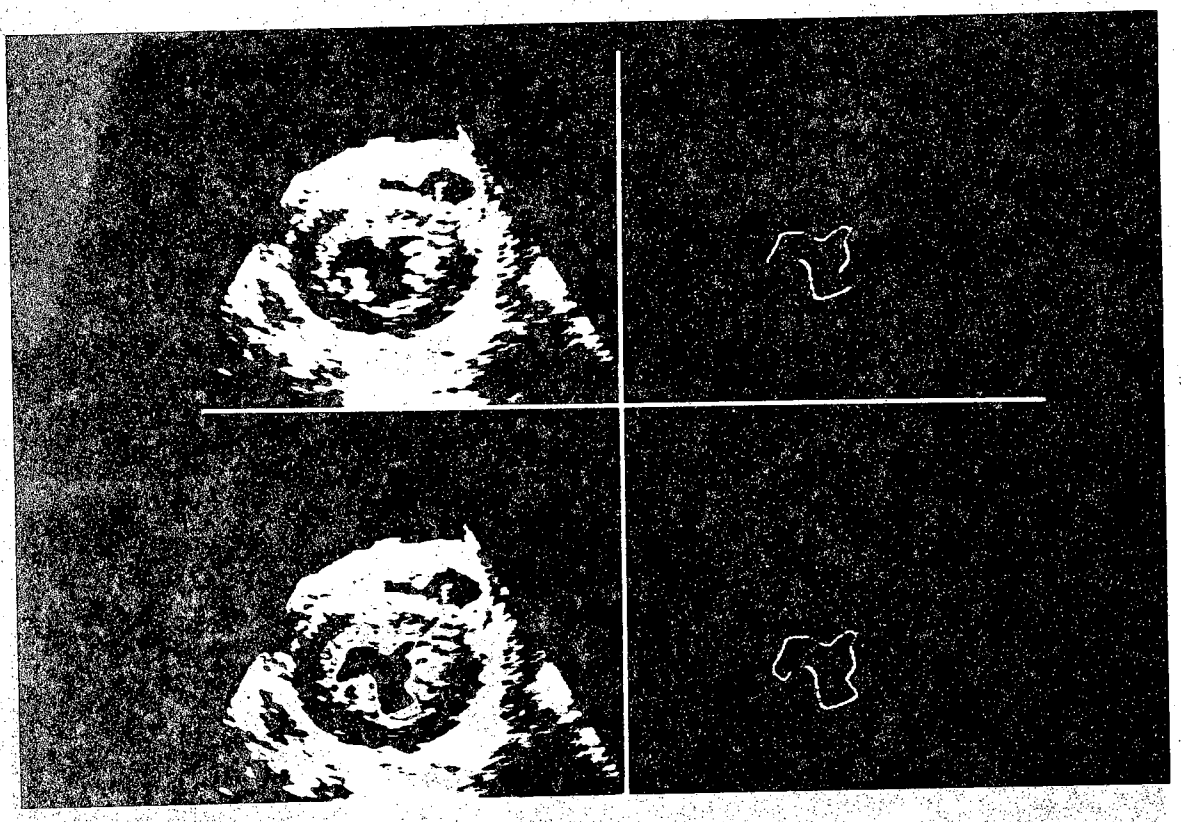

Figure 2.7 Detected boundaries in dog study. *Upper left:* Original image. *Upper Right:* Detected raw edge points. *Lower left:* Edge boundaries after processing. *Lower Right:* Detected boundaries in the original image.

CHAPTER 3
ASSESSMENT OF CARDIAC STATUS

3.1 The Importance of Two Dimensional Echocardiography in the Assessment of Cardiac Status

3.1.1 Introduction

Since the advent of two dimensional echocardiography, new possibilities in the detection and analysis of abnormal motion of the heart have opened new diagnostic horizons to physicians. It is well known that cardiac problems due to coronary occlusion, such as ischemic heart disease, produce abnormal wall motion.

Sasayama, et al. [20] showed, using coronary occlusion studies performed on canine hearts, that there are significant changes in the cardiac muscle and in the way it moves due to cardiac disease. As shown in Figure 3.1, they placed two pairs of ultrasonic crystals in the myocardium in order to monitor the wall thickness in an area to be rendered ischemic and in a normally perfused region. After blocking blood flow through the left circumflex coronary artery, changes of the myocardial wall were studied. For normal areas the authors stated [20]:

> In the normal zone, an increase in end-diastolic length has been reported as a result of acute coronary occlusion and increased systolic shortening suggested early use of the Frank-Starling mechanism as a fundamental adaptation to loss of function in ischemic myocardium. In previous experiments we observed a progressive increase in diastolic subendocardial segment lengths in normal regions associated with enhanced shortening beginning one week after chronic coronary occlusion, a change attributed to the development of hypertrophy in noninfarcted areas. Similar changes in end-diastolic segment lengths were observed in the present study, but no significant changes in

systolic shortening were detected until three week after coronary occlusion. We also measured wall thickness simultaneously with subendocardial segment lengths and observed concomitant changes in end-diastolic wallthickness and wall-thickening dynamics. End-diastolic segment

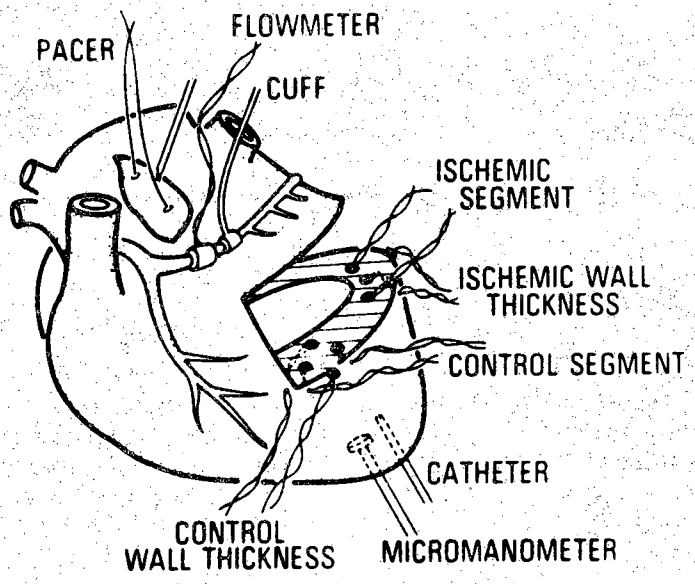

Figure 3.1 In each dog, 2 pairs of ultrasonic crystals were inserted at two sites: in normally perfused area and in area to be rendered ischemic by inflation of a cuff around the left circumflex coronary artery. One crystal pair at each site was implanted subendocardially in the left ventricular wall in the circumferential plane for measurement of segment length, and the other pair was positioned across myocardium for measurement of wall thickness. The left ventricular pressure was measured by implanted micromanometer (from [20]).

lengths elongated and end-diastolic wallthickness decreased in the weeks after coronary occlusion; consequently it was not possible to document increased muscle mass over the time span studied in this approach. Longer studies in one dog, however, clearly showed progressive hypertrophy, with wall thickening. This change in normal myocardium during healing after myocardial infarction may resemble the response to chronic volume overloading, which is characterized by an immediate increase in diastolic volume and early increase in stroke volume, followed by progressive dilation and later development of moderate left ventricular hypertrophy over 8-10 weeks.

In the ischemic region, changes involved important variations in the wall dimensions. Because of these and other results, the possibility of using two dimensional echocardiography to detect physical changes has been extensively studied.

3.1.2 Detecting Myocardial Ischemia and Infarction Using Two Dimensional Echocardiography

Two dimensional echocardiography of the left ventricle has advantages over other imaging techniques because of the excellent spatial and temporal resolution, direct measurement of some of the physical parameters of the heart (e.g. wall thickness, area, and ejection fraction), monitoring of heart dynamics in real time, quick data acquisition, and nonivasiveness [21]. Nevertheless, there are still some problems which need to be addressed in order to evaluate what is the role of two dimensional echocardiography when compared with other imaging techniques. According to Falsetti, et al. [22] there are two basic phenomena that limit the effectiveness of two dimensional echocardiography: biological and technical.

To begin with, during the cardiac cycle the heart rotates and translates within the thorax. In the case of a sick heart with localized contraction abnormalities, such a behavior may be of considerable more importance, increasing the distortion or asymmetric appearance of the ventricle. Along with these biophysical problems, the translation of the whole cardiac body because of respiration should also be considered, although it is possible to record a few cardiac cycles keeping the patient from breathing.

There are more subtle biological phenomena which account for these limitations. It has been observed that the whole cardiac muscle moves inwards during systole and vice versa during diastole. Thus, any absence of either motion in any portion of the left ventricular wall is a sign of coronary disease. The problem arises when defining the limits between normal and abnormal contraction[20]:

> Normal myocardium demonstrates systolic thickening and inward movement of the endocardium. Thus, absence of systolic thickening/endocardial inward motion (akinesis), or systolic thining/endocardial expansion (dyskinesis), is clearly abnormal when

seen on echocardiographic examination. The difficulty arises when one attempts to define the lower limit of normal, so that myocardial segments that retain some, but only minimal, thickening or motion (hypokinesis) can be identified. This lower limit has not been well delineated, and there appears to be marked variability of the degree of thickening and endocardial motion of closely adjacent segments.

This marked spatial heterogeneity of thickening and motion may in part be explained by intrathoracic cardial rotational and translational motion and in part by temporal asynergy.

One of the conclusions that can be drawn from this is that unusual or apparently abnormal contractions do not always mean that an abnormality is present.

The second problem: technical limitations, refers in part to the lack of landmarks for the analysis of tomographic sections of the heart. For instance, the region between the tip of the papilary muscle and the true apex lacks landmarks, therefore the tomographic sections visualized in this zone can not be compared with images from other studies.

In addition, the accuracy of M-mode echocardiography in identifying cardiac borders has been documented, whereas reproducibility and accuracy of two dimensional echocardiography has not been documented. Despite these problems, several studies have tryed to assess cardiac status through the use of two dimensional echocardiography.

3.1.3 Indicies of Cardiac Status

Lieberman, et al. [23] examined the regional percentage of systolic wall thickening (%Th) and percentage of endocardial motion (%EM) in infarcted canine hearts, where %Th is defined as:

$$\%Th = \frac{Th_{ES} - Th_{ED}}{Th_{ED}} \times 100 \tag{3.1}$$

Where Th_{ES} is the thickness of a myocardial segment at end-systole and Th_{ED} is the thickness of a segment at end-diastole. Positive values of %Th show a wall thickening process while negative values indicate wall thining.

The regional percentage of radial endocardial motion toward the center of an area fixed at end-diastole (%EM) is defined as:

$$\%EM = \frac{R_{ED} - R_{ES}}{R_{ED}} \times 100 \tag{3.2}$$

Where R_{ED} is the end-diastolic segmental endocardial radius and R_{ES} is the end-systolic segment endocardial radius. As with the regional percentage of systolic thining, positive values of %EM indicate an increase of the radius at diastole whereas negative values indicate a shortening of the radius at systole.

Figure 3.2 shows %EM and Figure 3.3 shows %Th for data obtained from fifteen dogs to which the left circumflex artery had been occluded acutely and permanently.

As can be seen from both figures, %EM and %Th can distinguish between normal, adjacent, and infarcted tissue. However, %Th was more significant in separating normal tissue from infarcted one. In addition, the variability from subject to subject is greater for %EM than for %Th [23].

Monyhan [24] also evaluated cardiac status using geometric measurements. After obtaining two dimensional echocardiographic images of the left ventricle, the left ventricular chamber was divided into halves, quadrants, and octants. Area, hemiaxis, and perimeter measurements was obtained to describe contraction abnormalities. The reproductibility of these measurements was also studied.

In order to obtain these measurements, a landmark in the left ventricular wall was chosen. In this case the landmark was the interventricular septum on the LV endocardial surface in diastole. From this point, an initial axis was constructed to the opposite lateral LV wall so as to divide the image into equal anterior and posterior areas (Figure 3.4). Further subdivision into quadrants and octants was performed.

Figure 3.5 shows the three kinds of measurements used, the regional area change (ΔA), hemiaxis shortening (ΔH), and endocardial perimeter contraction (ΔP). Where ΔA, ΔH, and ΔP are defined as:

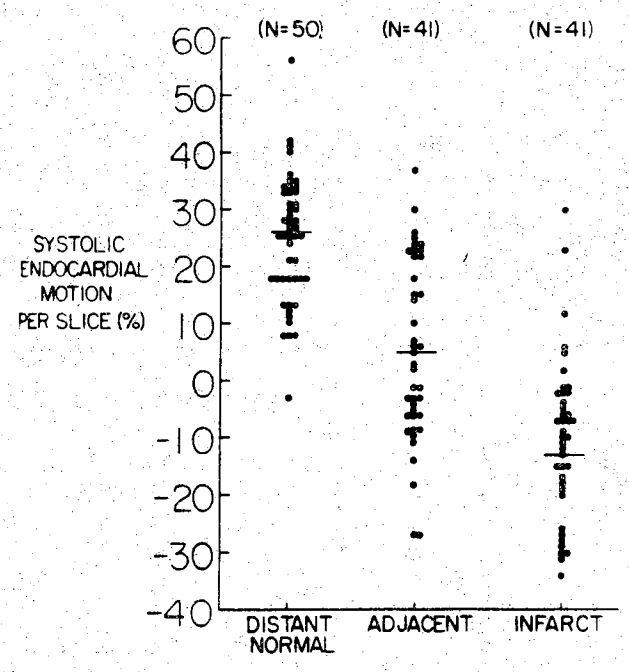

Figure 3.2 Echocardiographic percentage of regional endocardial wall motion as a function of tissue histology and location. The horizontal line in each group indicates the mean, adjusted for dog-to-dog variability. Data for each point were obtained by combining echocardiographic data from all segments of each anatomic type within each ventricular ring, grouped according to anatomic location. The overall standard deviation was 11.5%. From Lieberman [23].

$$\Delta A = \frac{D_A - S_A}{D_A} \times 100 \tag{3.3}$$

Where D_A is the diastolic area and S_A the systolic area,

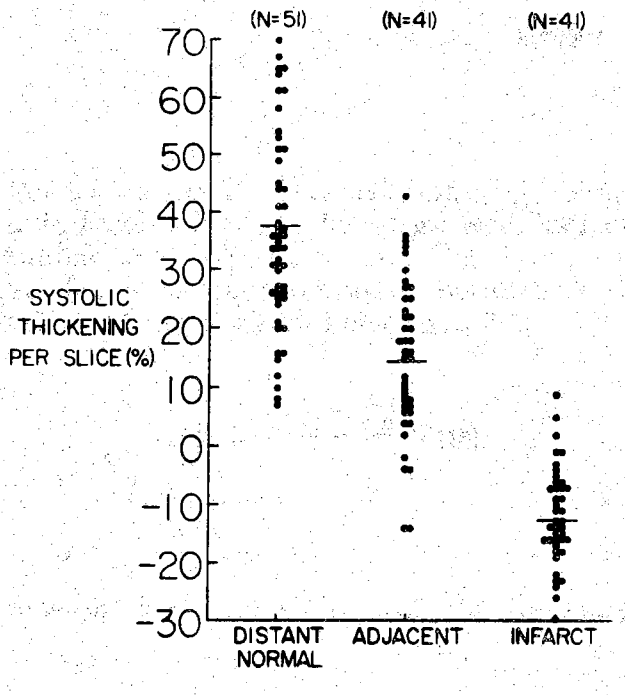

Figure 3.3 Echocardiographic regional percentage change in thickening as a function of tissue histology and location. The analysis is similar to that in Figure 3.2. Percentage change in thickening yielded a clearer separation between normal, adjacent, and infarcted zones. From Lieberman [23].

$$\Delta H = \frac{D_H - S_H}{D_H} \times 100 \tag{3.4}$$

where D_H is the diastolic hemiaxis length and S_H the sytolic hemiaxis length, and

$$\Delta P = \frac{D_P - S_P}{D_P} \times 100 \tag{3.5}$$

Where D_P is the segmented perimeter length and S_P is the systolic segment perimeter length.

As stated before, the heart rotates and translates within the thorax throughout the cardiac cycle. Thus, the same measurement obtained at different points of the cardiac cycle might correspond to different physical portions of the cardiac body.

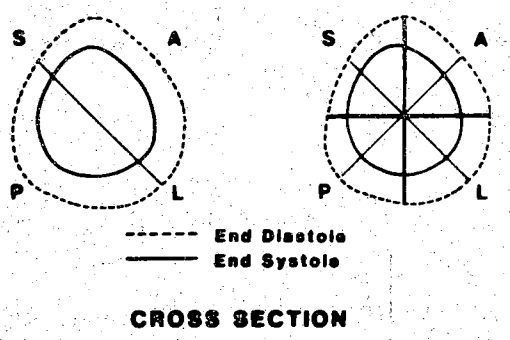

Figure 3.4 Convention used for different degrees of subdivision of cross section images. *Left*: The initial septolateral (S,L) axis, constructed to divide the diastolic outline into anterior (A) and posterior (P) halves of equal area. This axis was used for regional analysis of anterior and posterior halves. *Right*: Further subdivision of the left ventricle outlines into octants is demonstrated. The four bolder hemiaxes indicate the regions used for quadrant analysis. From Moynihan [24].

To assess how this phenomenon affects the measurement process, Moyniham, et al. used a fixed coordinate system and a floating one (see Figure 3.6). In the case of a fixed coordinate system, the division of the LV chamber is performed automatically at diastole, and the same division is used for the systolic phase.

When a floating coordinate system is used the axis is plotted at both diastole and systole, according to the landmark procedure, and then they are translated and rotated so that both are superimposed.

The results indicates that there is no significant difference between a fixed or floating axis strategy, and that the area-based methods were superior in the evaluation of regional LV function using two dimensional echocardiography. The degree of subdivision of the image did not affect the reproducibility and variability of the experiments.

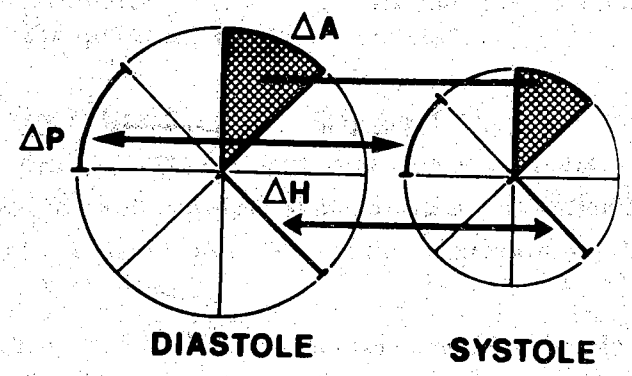

Figure 3.5 Schematic of diastolic and systolic left ventricular outlines subdivided into octants showing different approaches to measuring regional contraction. Δ A = regional area change; Δ H = hemiaxis shortening; Δ P = segmental endocardial perimeter contraction. Similar measurements were made for the quadrant and halves analysis.

In a later paper Parisi, et al. [25] used the area method for studying coronary artery disease via octant-based measurements. Their results were certainly encouraging, and showed that, at least statistically, it is possible to distinguish between normal and abnormal contractions due to an ischemic process.

In spite of these results, more research needs to be done since there have been almost no systematic studies dealing with variability of left ventricle wall motion, either in normal subjects or subjects with coronary disease. For example, Pandian, et al. [26] found a great variability among normal subjects so that qualitative assessments of the symmetry of contraction as a method for identifying segmental ventricular dysfunction was not possible.

3.2 Left Ventricular Area, Wall Thickness, and Ejection Fraction

After estimating the boundaries of the left ventricular inner chamber using the algorithm discused in [6], we computed the cardiac indices related to the area, wall thickness, and ejection fraction throughout a cardiac cycle for normal canine hearts and hearts suffering from ischemic heart disease (after occlusion).

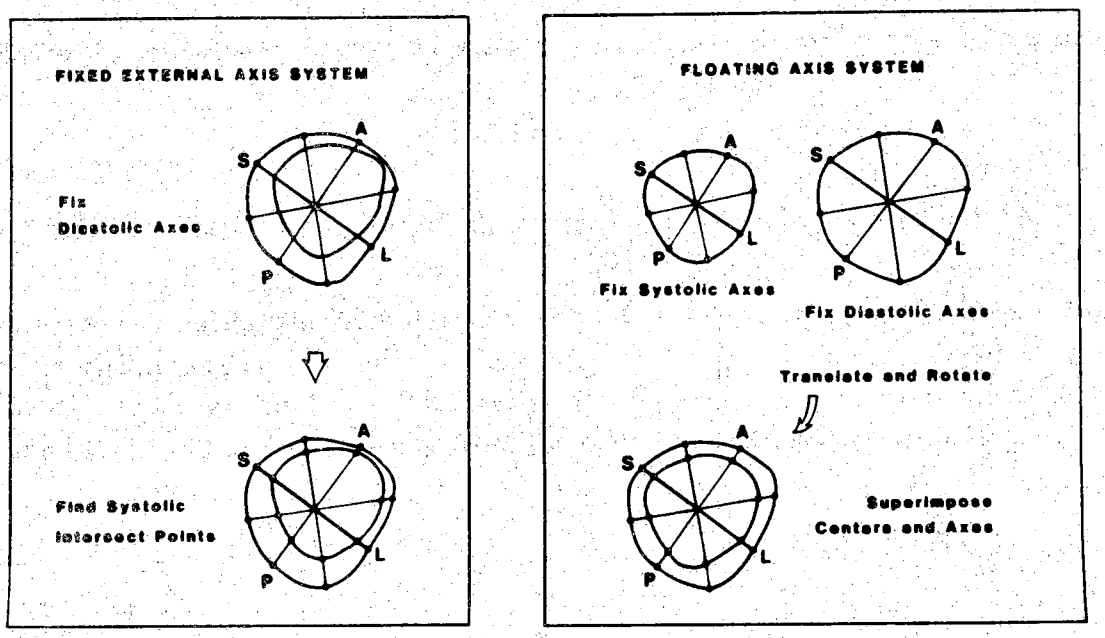

Figure 3.6 Fixed and floating axis system conventions for analyzing the regional function [24].

3.2.1 Left Ventricular Area and Wall Thickness

The left ventricular area was computed by counting the number of pixels inside the left ventricular contour. In computing the wall thickness the inner and outer boundary of the left ventricular area (endocardium and epicardium) were obtained. As previously discused in Section 3.1 a floating coordinate system was used for every frame.

In order to compute the center of coordinates, the left ventricle contour was fitted with a rectangle whose edges were parallel to the picture edges, in such a way that the left and right points and the top and bottom points are tangent to the rectangle. The coordinate center was chosen as the intersection of the lines spanning between the middle points of opposite rectangle edges. Figure 3.7 shows how the center of the coordinates is obtained.

The next step was computing the wall thickness. First, the number of wall thickness points is chosen, then we construct from the coordinate center to the outer boundary the number of radii chosen. Since the exact value of wall thickness is meaningless, all the distances between the center and the left ventricular contour within the adjacent radii were computed and averaged. The outer boundary was handled in a similar manner. The difference between the averaged outer radius and inner one was defined as the wall thickness. Figure 3.8 shows this in detail.

Finally the ejection fraction (EF) is computed as:

$$EF = \frac{D_A - S_A}{D_A} \times 100$$

Where the ejection fraction indicates how efficiently the heart pumps blood. A low EF value may mean an abnormal behavor of the heart. Table 3.1 shows ejection fractions computed for the different studies.

3.3 Results

Figures 3.10 to 3.17 show the left ventricular area as a function of time for four cardiac cycles. Solid line plots show the area change of normal hearts whereas dashed line plots show the area change of dog hearts after coronary occlusion.

The titles of the figures are the names of the studies. The x axis represents the frame number which corresponds to a single image in the image sequence from which information related to the left ventricle is extracted. The y axis is the estimated left ventricular area given in pixel units. Every study was performed on a dog's heart after undergoing open chest surgery.

Given the small number of studies, no specific conclusions can be drawn. However, it can be seen that all the plots show a strong periodicity due to the cardiac cycle, and that the shape of these periodic waves is quite different from study to study, but rather similar from cycle to cycle if a specific study is considered.

It suggests the possibility of using this information to help the boundary detection process. For example, from the area computed in previous cycles it may be possible to predict what the next area has to be. If after detecting the endocardial boundary the computed area is very different from the expected area, the detection system may trigger further actions in order to obtain a more realistic estimation of the endocardial boundary.

Figures 3.18 to 3.33 show wall thickness computed for two studies corresponding to a healthy dog's heart (d259_bl1) and a sick dog's heart (d254_oc1). The x axis represents the frame number, and the y axis represents wall thickness in pixel units. The wall thickness values were computed between the estimated endocardial and epicardial boundaries, as shown in Figure 3.8. Wall thickness values were computed every 45 degrees as shown in Figure 3.9. For every figure, the last two digits of the title represent the angle of the line of sight along which wall thickness is computed.

Again, no global conclusions can be drawn from these studies. Although a periodic pattern can also be seen, it is nearly missing for some lines of sight. Since area computation is an integration process, fine errors are filtered out (area plots are "smoother"), wall thickness computation is very sensitive to estimation errors in the inner or outer boundaries. Perhaps statistical studies performed on a large number of studies would give different wall thickness values for infarcted and noninfarcted areas of the heart wall muscle.

3.4 Summary

Since ischemic heart disease can cause contraction abnormalities; the possibility of detecting the presence of an abnormal heart by measuring geometric parameters such as left ventricular area, wallthickness, left ventricular radius, and ejection fraction was discussed. For instance, studies carried out over several days on canine hearts after coronary occlusion showed that heartwall motion undergoes changes. In addition, it has been reported that it is possible to

distinguish statistically between normal and abnormal contractions, and between normal and infarcted tissue using geometric measurements [25].

There are several problems that need to be addressed when using these measures. First, the normal human heart presents an enormous variability, and apparently abnormal contractions do not always mean that an abnormality is present. Furthermore, this variability and the lack of landmarks makes it difficult to standardize studies among different patients.

We have examined the use of several classical geometric features and have shown that the variability in a normal heart can indeed cause these features to provide inconsistent interpretation of cardiac status.

Table 3.1 Ejection Fraction as computed for 8 studies.

Study	EF%
d252_as2	20.4
d254_as2	29.7
d254_bl2	36.5
d254_oc1	22.2
d259_as1	43.2
d259_as2	77.0
d259_bl1	54.0
d259_bl2	58.8

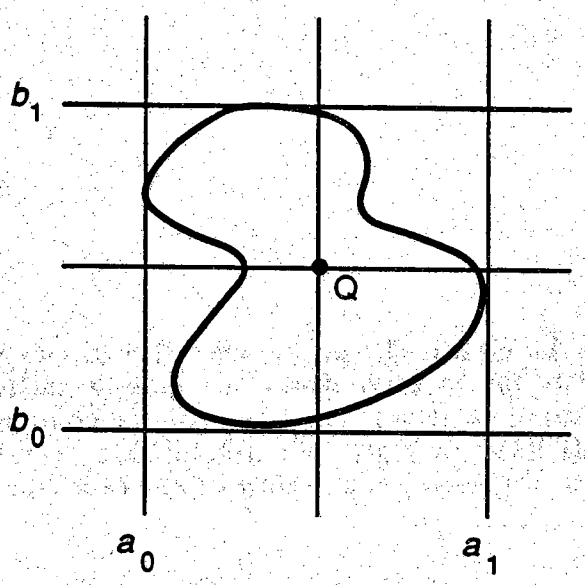

Figure 3.7 Procedure for computing the center of coordinates is shown. After finding the coordinates of the delimiting lines for the boundary: a_0 and a_1 (vertical limits), and b_0 and b_1 (horizontal limits), the origin for wall thickness estimation is chosen as Q(x,y) where $x = (a_0+a_1)/2$ and $y = (b_0+b_1)/2$.

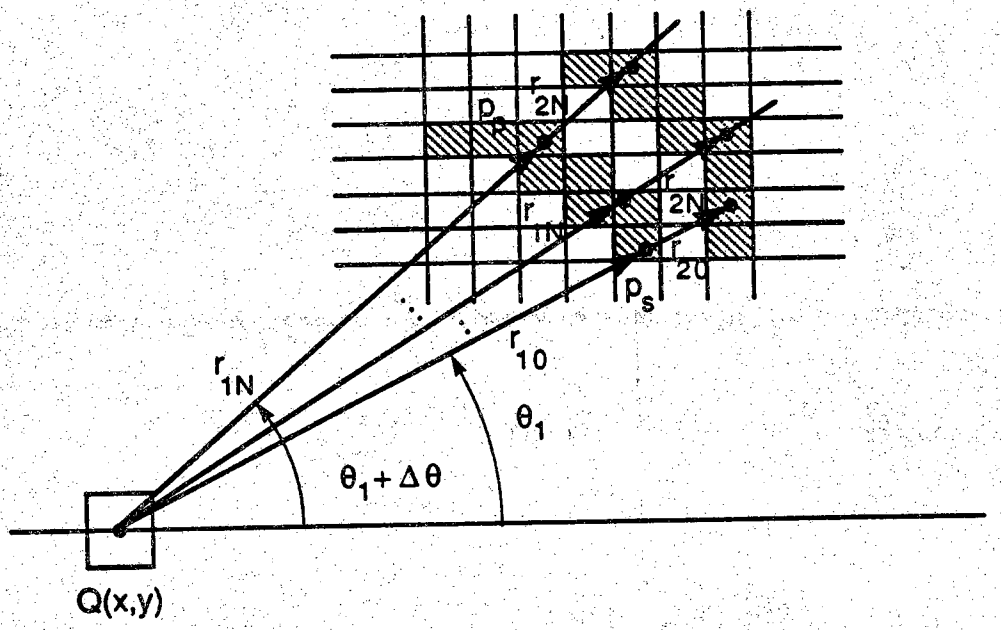

Figure 3.8 Wall thickness is computed as follows. The initial radii r_{10} and r_{20} are determined after computing Q(x,y) and angle θ_1 (which depends on the number of wall thickness estimates and the chosen origin of angles which consists of the horizontal line that originates at Q and runs to the right). According to $\theta_1 + \Delta\theta$ where $\Delta\theta = 360^\circ / (\textit{number of wall thickness estimates})$. Then from pixel p_s to pixel p_p radii r_{1i} are computed for every inner boundary pixel, and following the direction given by r_{1i}, the first outer boundary pixel hit by the line determined by such a radius, provides the coordinates to compute r_{2i}. Wall thickness is computed as:

$$W(\theta) = \frac{1}{N-1} \sum_{i=0}^{N-1} (r_{2i} - r_{1i})$$

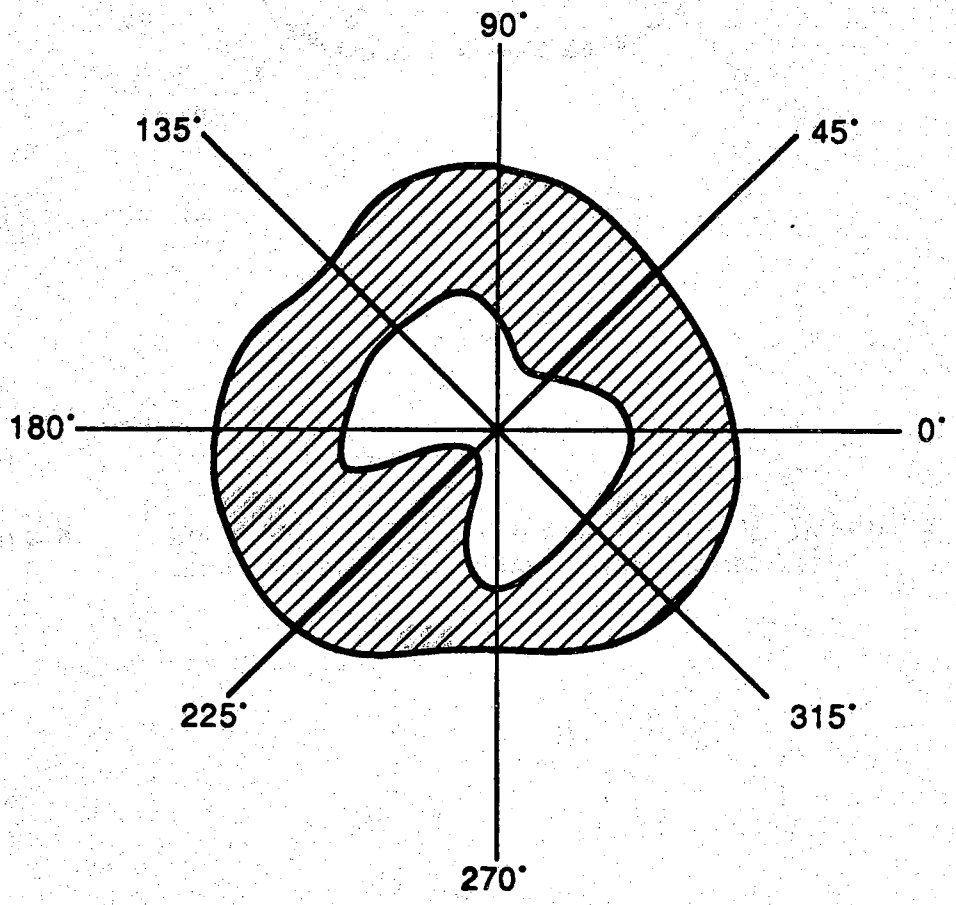

Figure 3.9 Lines of sight along which wall thickness is computed given the endocardial and epicardial boundary estimations.

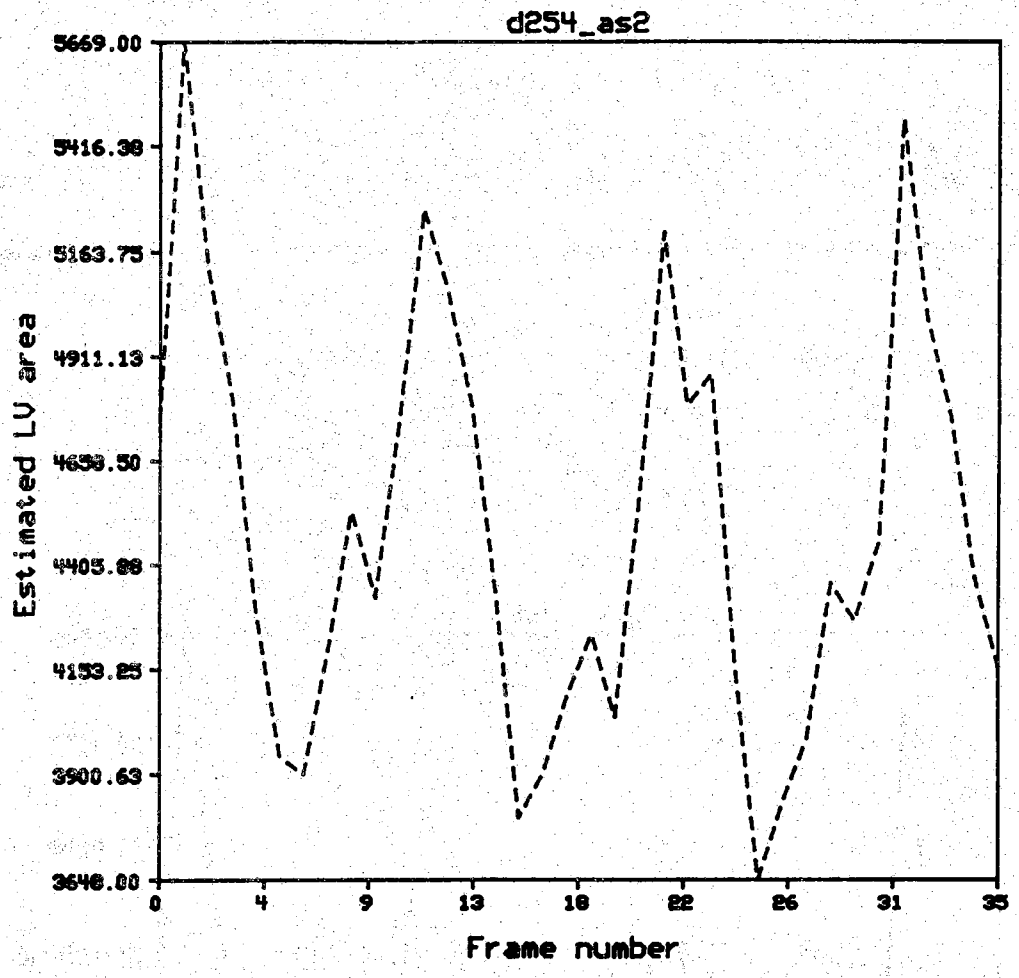

Figure 3.11 Estimate of the left ventricular area in pixel units for a healthy canine heart (open chest study) for d254_as2.

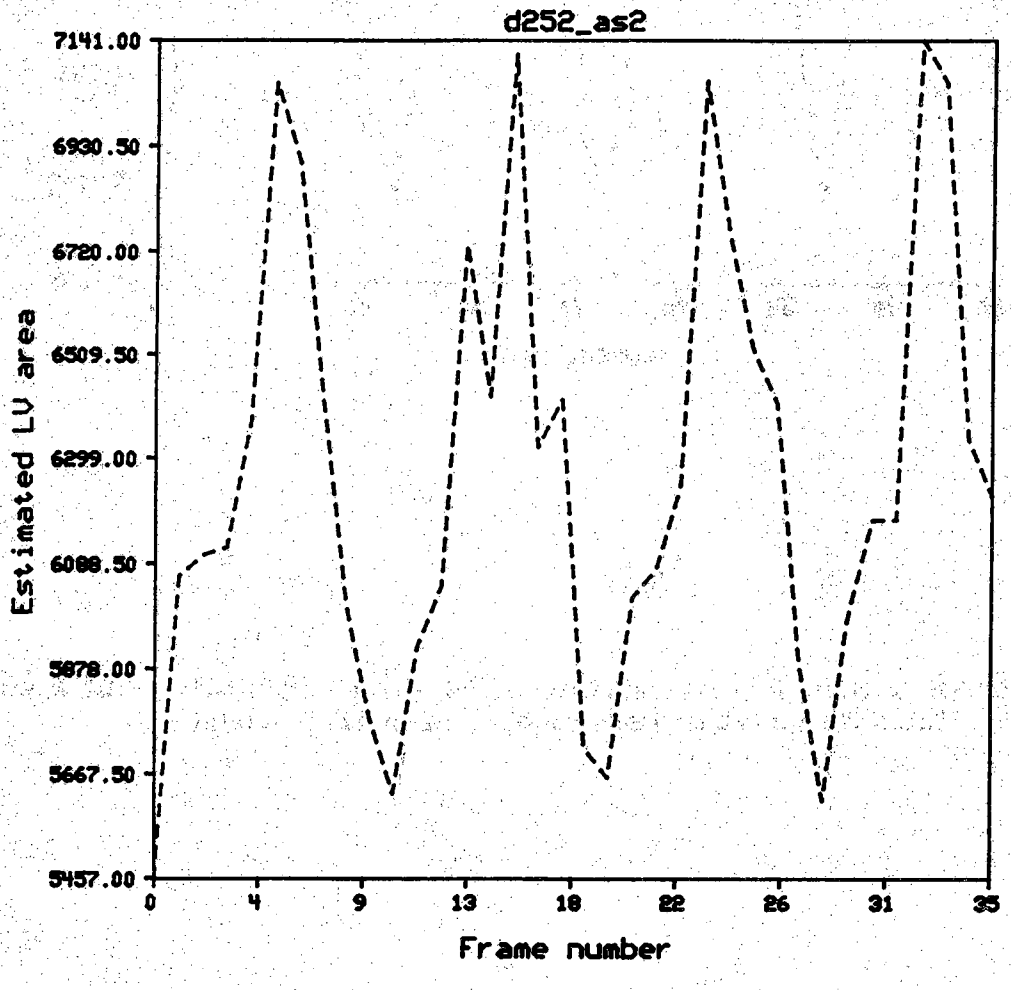

Figure 3.10 Estimate of the left ventricular area in pixel units for an infarcted canine heart (open chest study) for d252_as2.

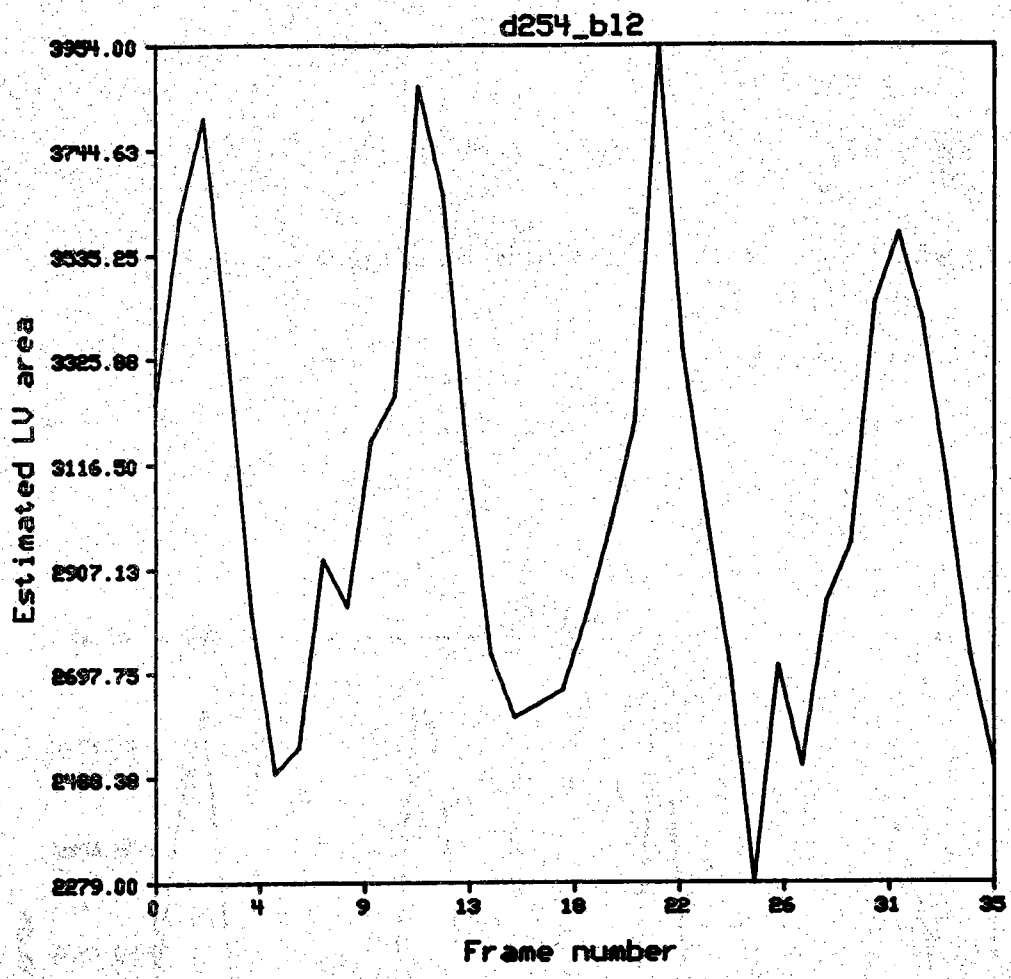

Figure 3.12 Estimate of the left ventricular area in pixel units for an infarcted canine heart (open chest study) for d254_bl2.

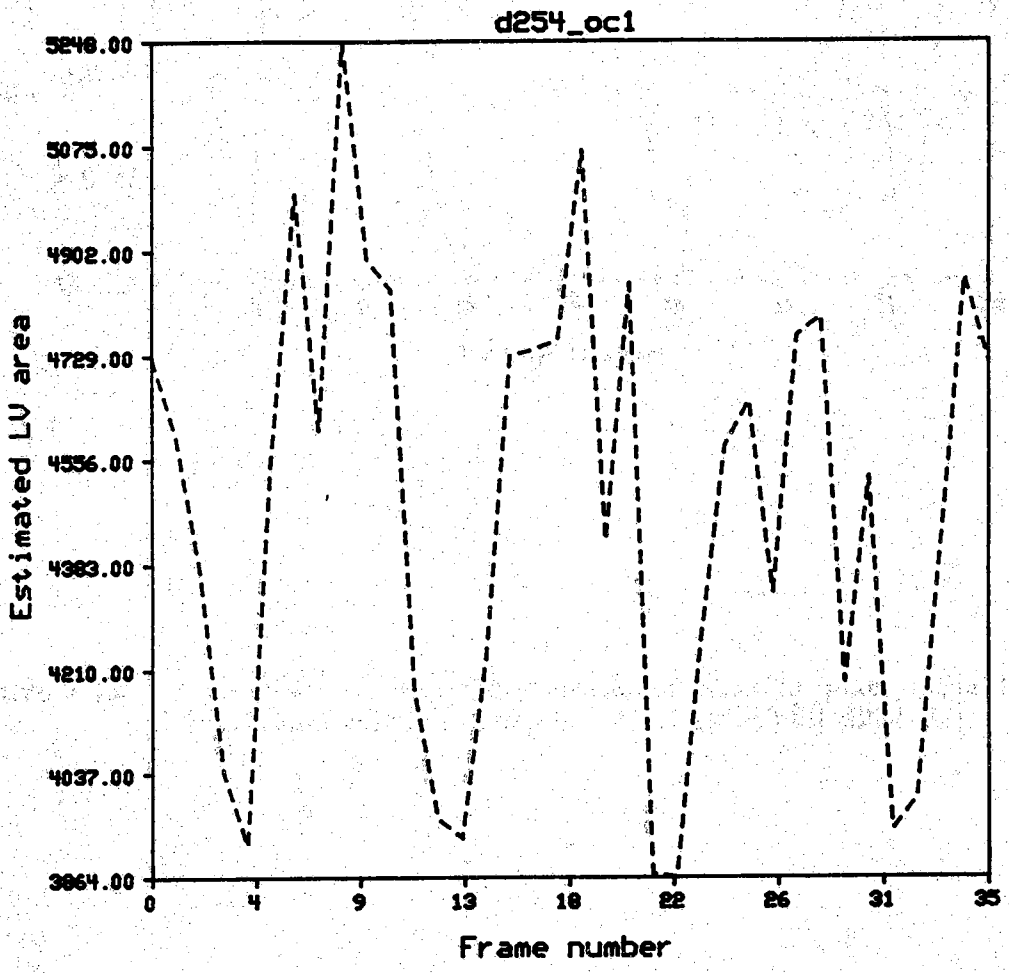

Figure 3.13 Estimate of the left ventricular area in pixel units for an infarcted canine heart (open chest study) for d254_oc1.

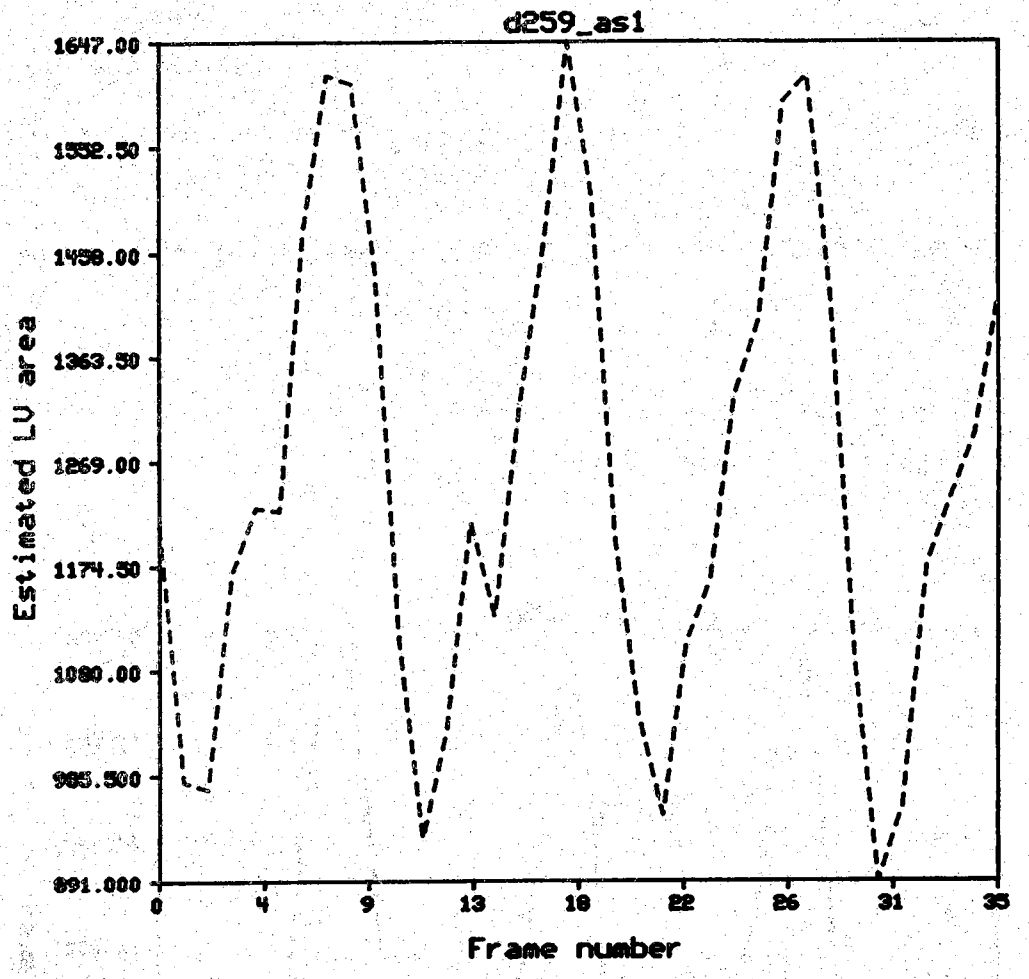

Figure 3.14 Estimate of the left ventricular area in pixel units for an infarcted canine heart (open chest study) for d259_as1.

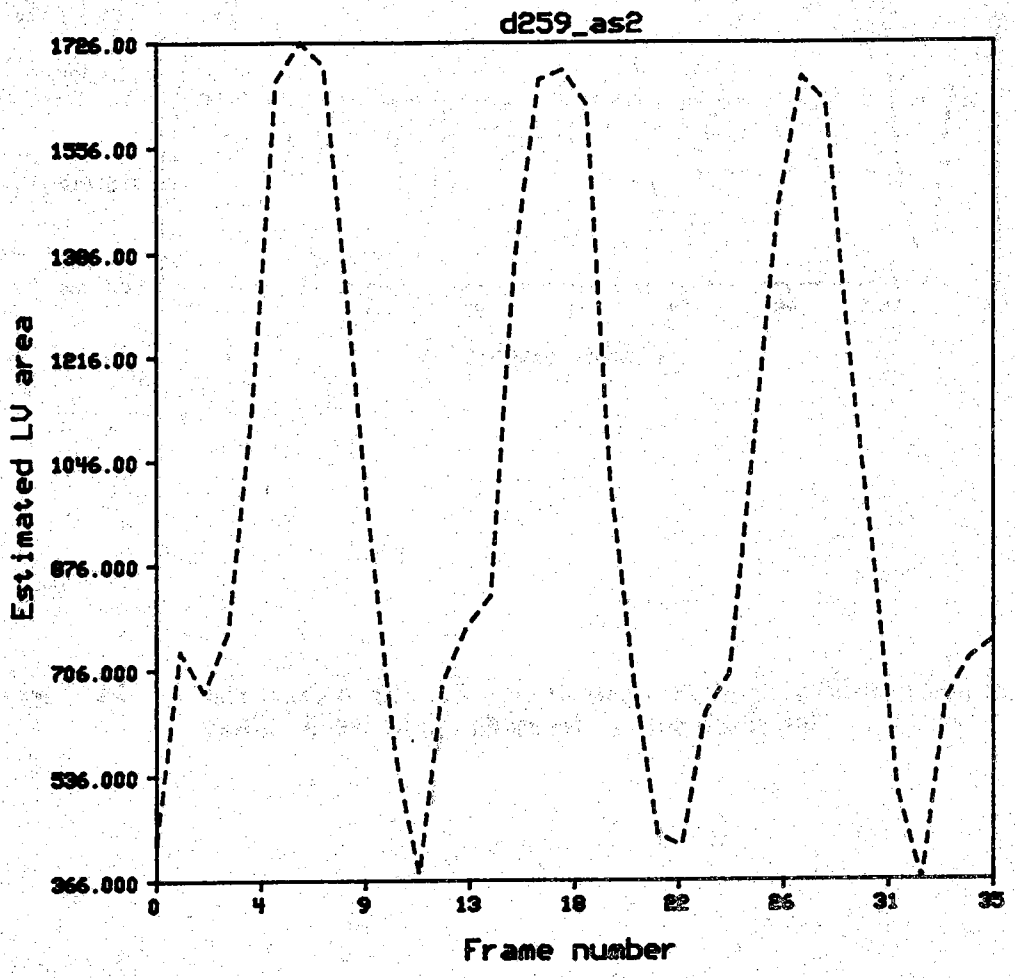

Figure 3.15 Estimate of the left ventricular area in pixel units for a healthy canine heart (open chest study) for d259_as2.

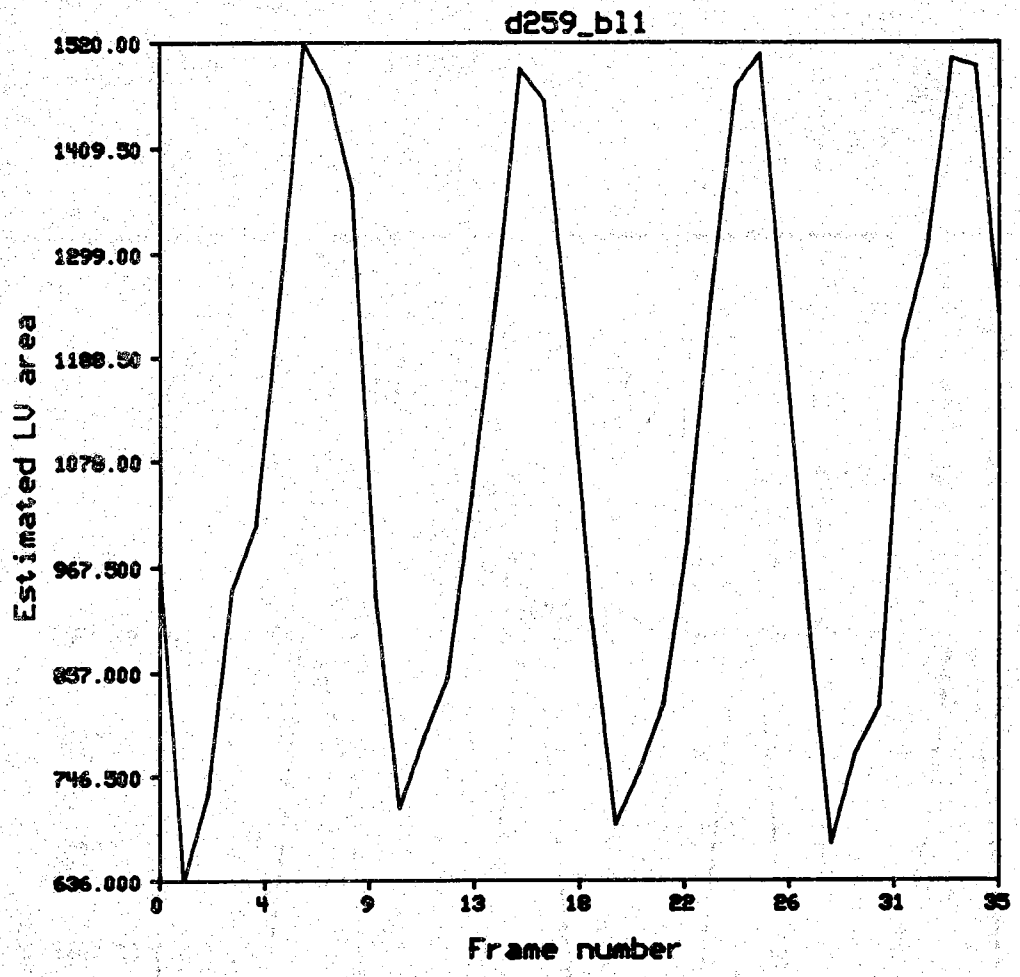

Figure 3.16 Estimate of the left ventricular area in pixel units for a healthy canine heart (open chest study) for d259_bl1.

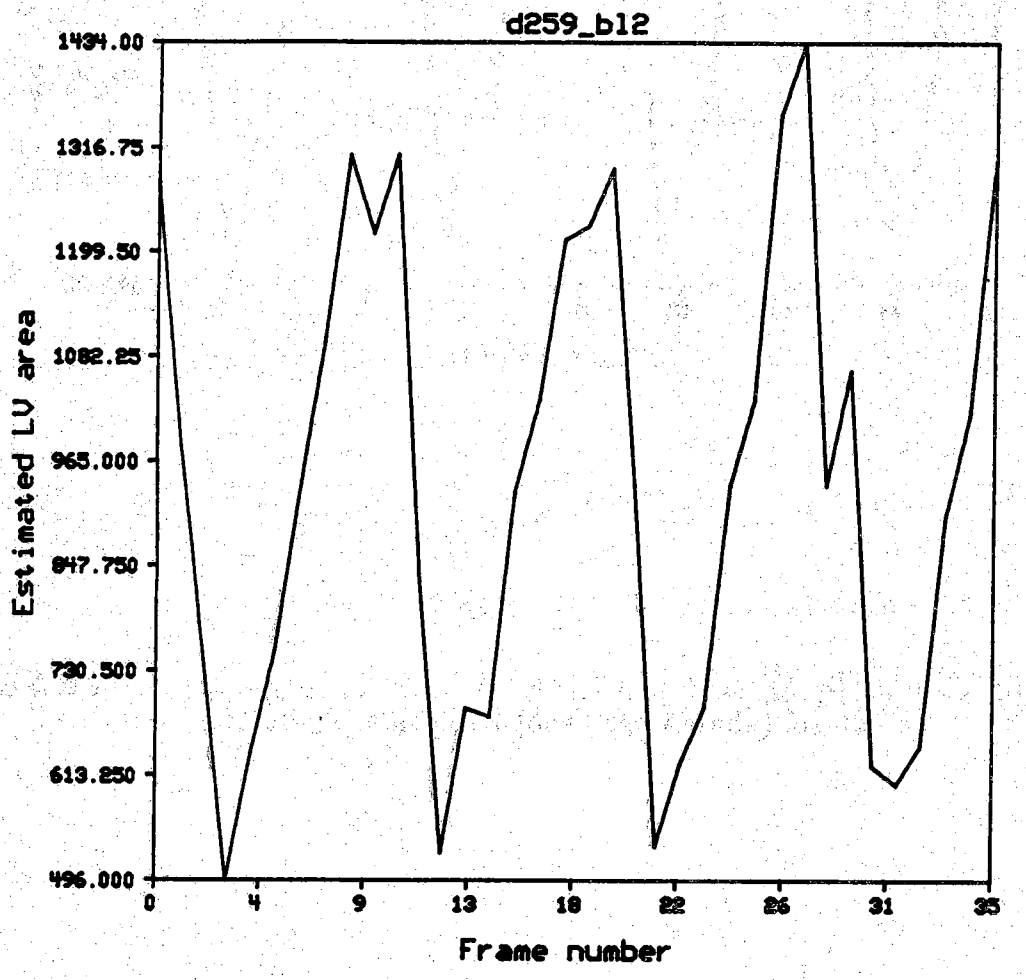

Figure 3.17 Estimate of the left ventricular area in pixel units for an infarcted canine heart (open chest study) for d259_bl2.

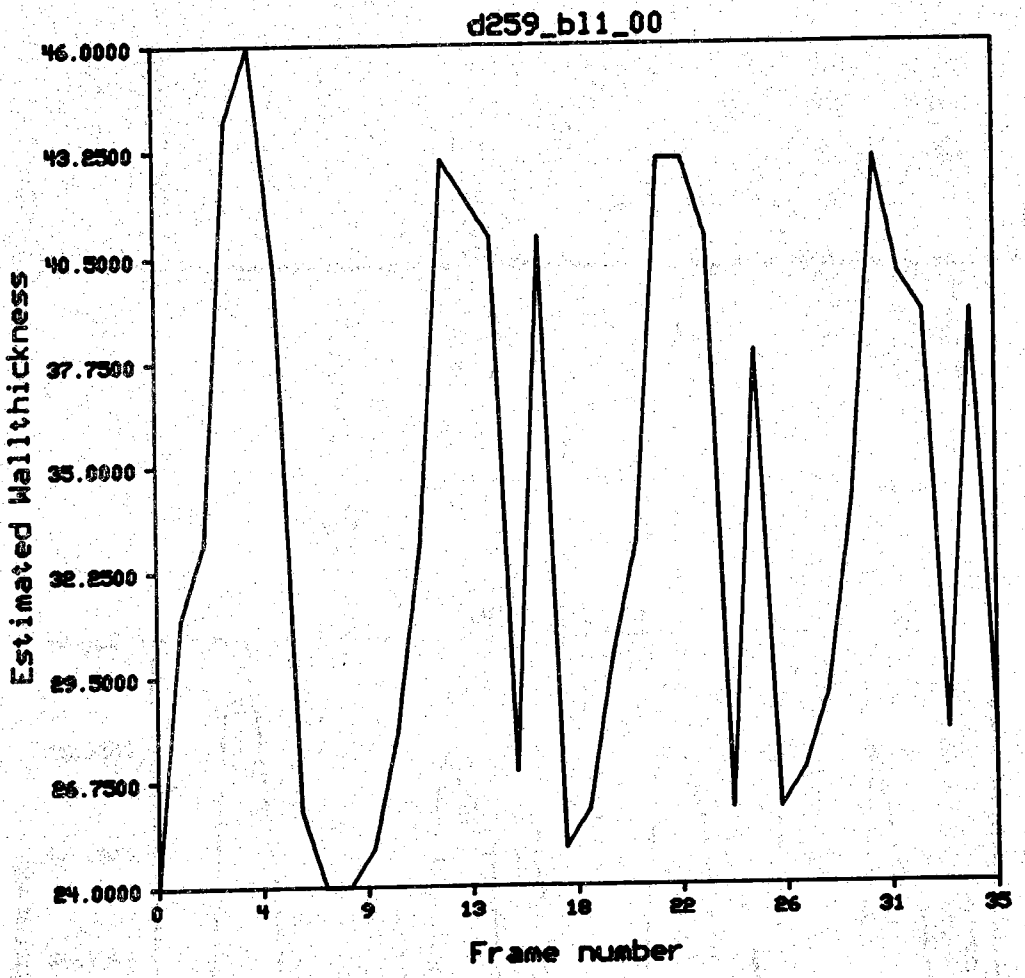

Figure 3.18 Wall thickness computed along the 0 degree radius for study d259_b11.

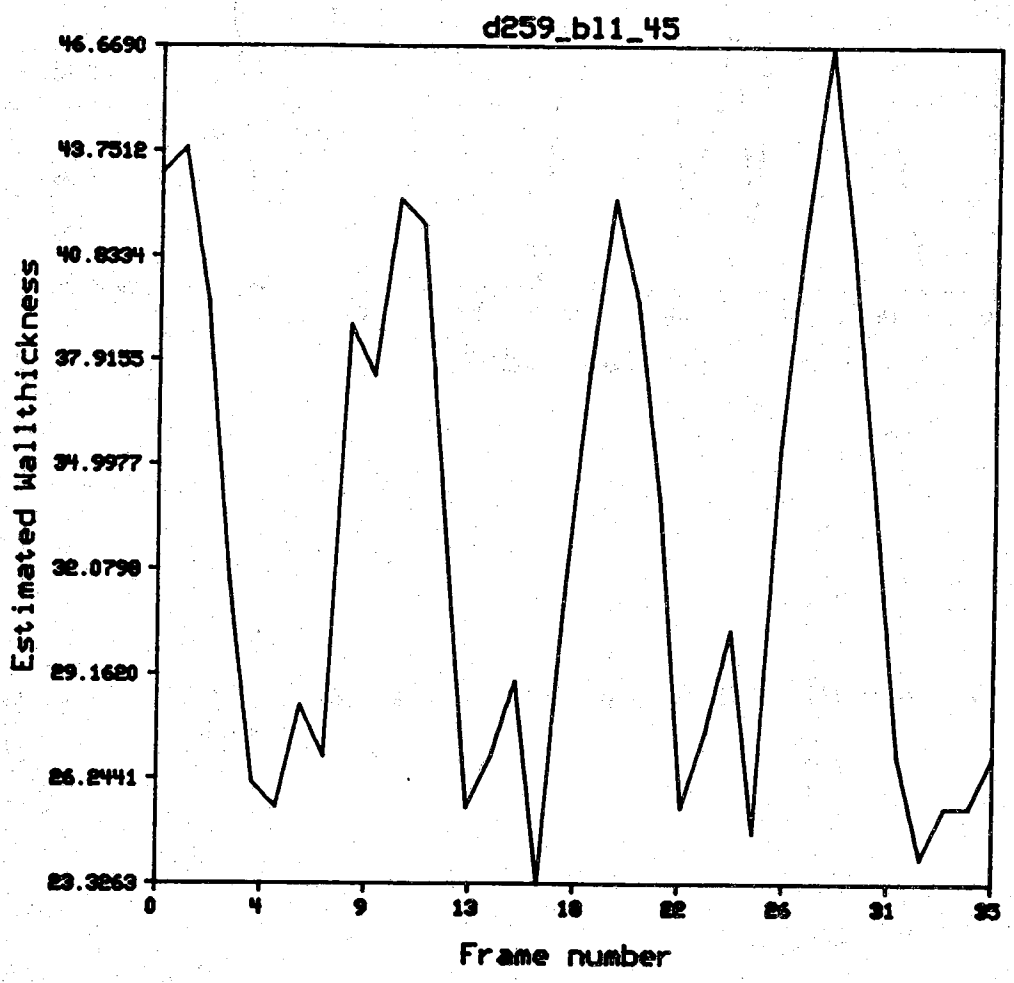

Figure 3.19 Wall thickness computed along the 45 degree radius for study d259_b11.

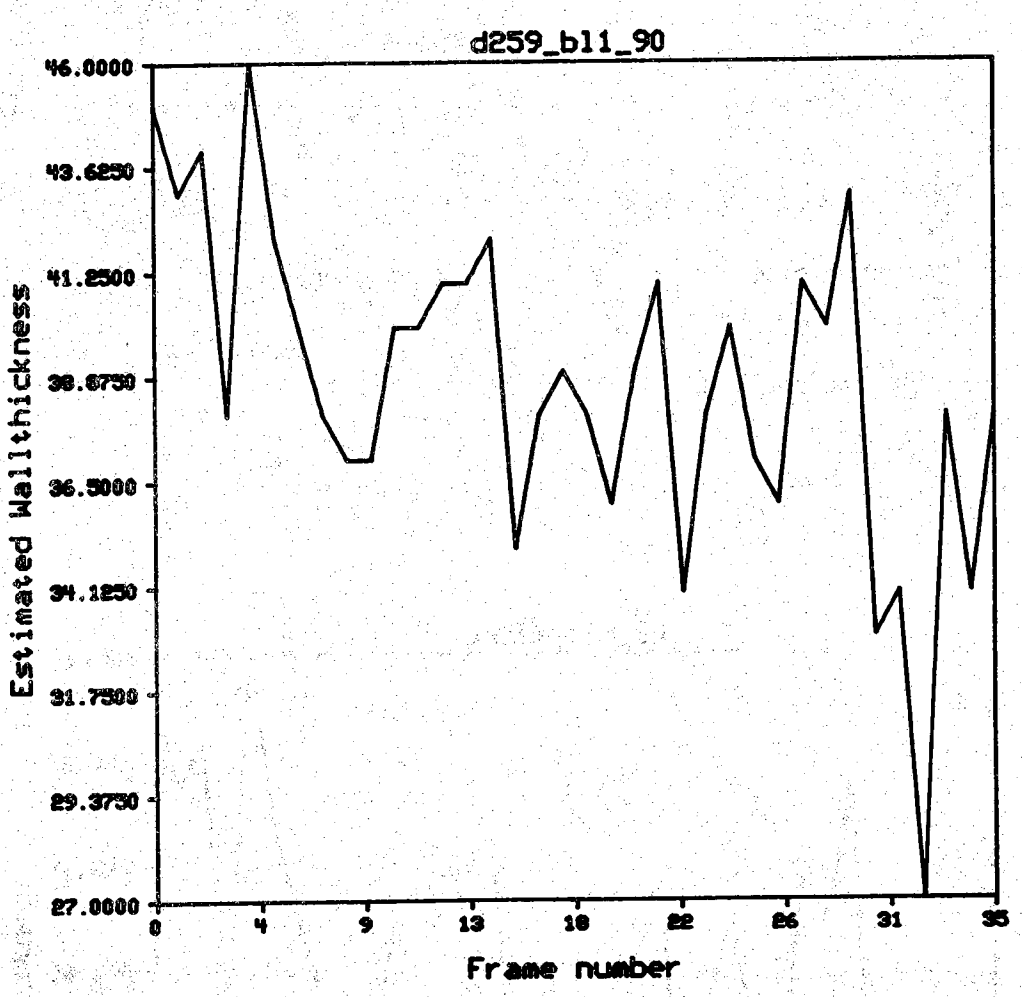

Figure 3.20 Wall thickness computed along the 90 degree radius for study d259_b11.

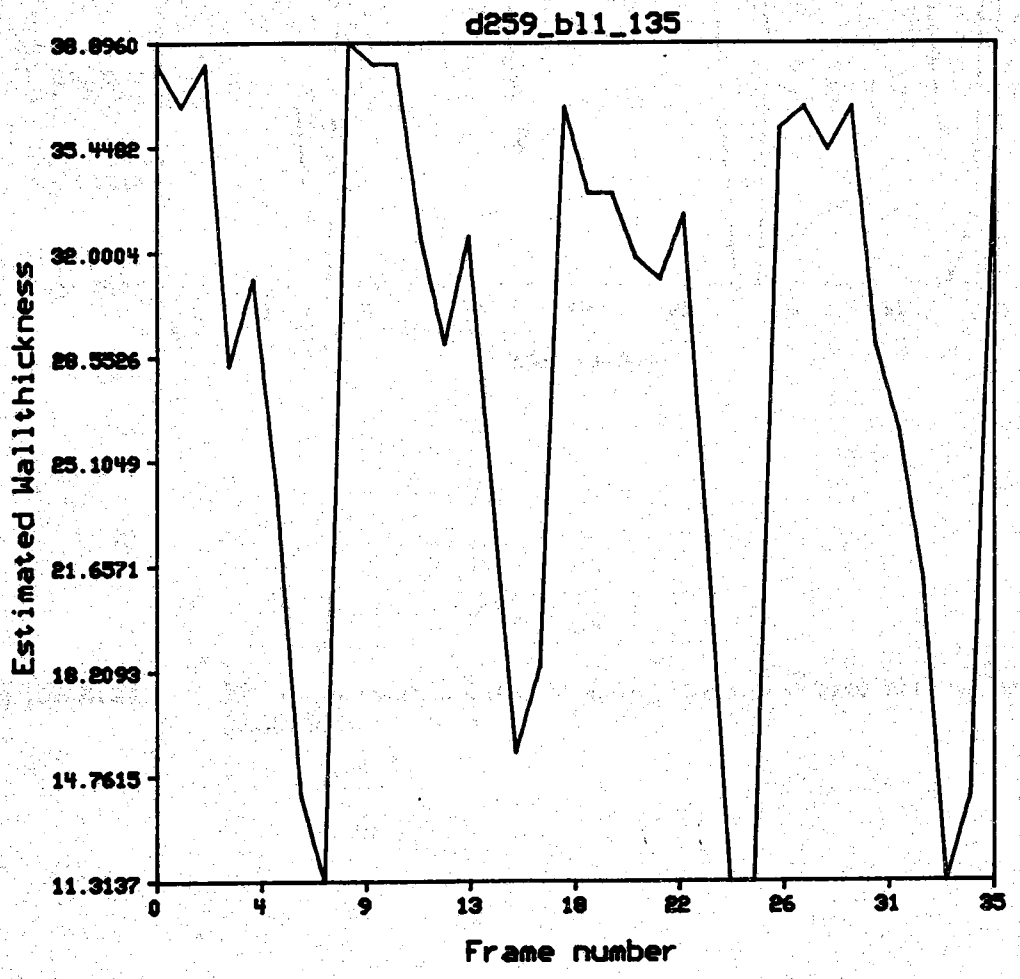

Figure 3.21 Wall thickness computed along the 135 degree radius for study d259_b11.

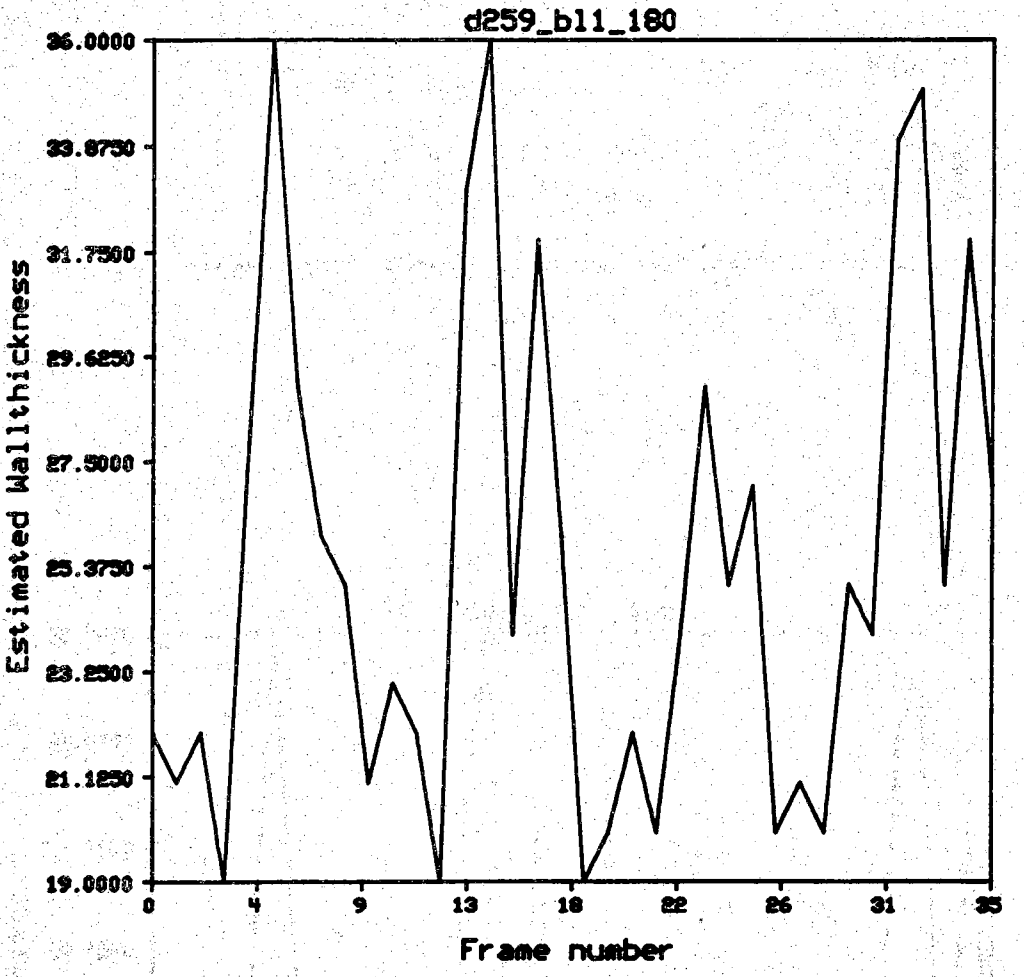

Figure 3.22 Wall thickness computed along the 180 degree radius for study d259_b11.

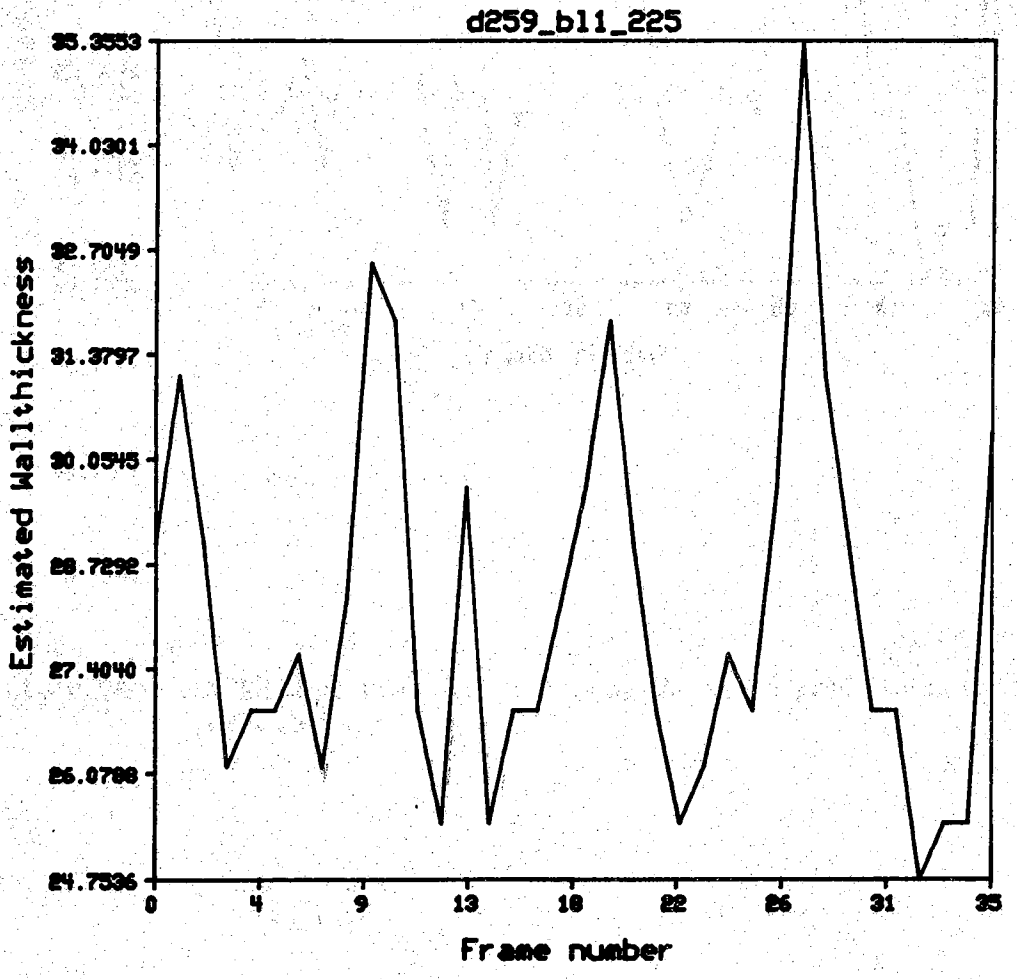

Figure 3.23 Wall thickness computed along the 225 degree radius for study d259_b11.

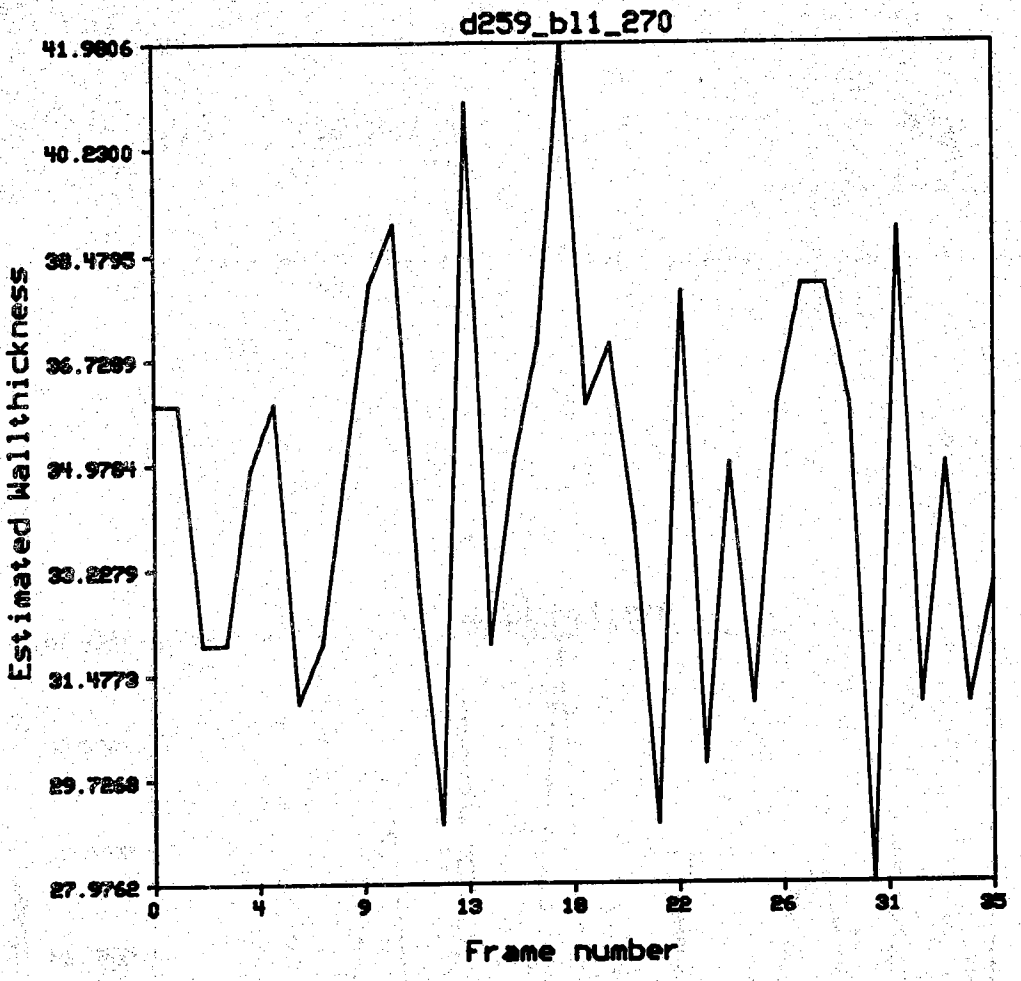

Figure 3.24 Wall thickness computed along the 270 degree radius for study d259_b11.

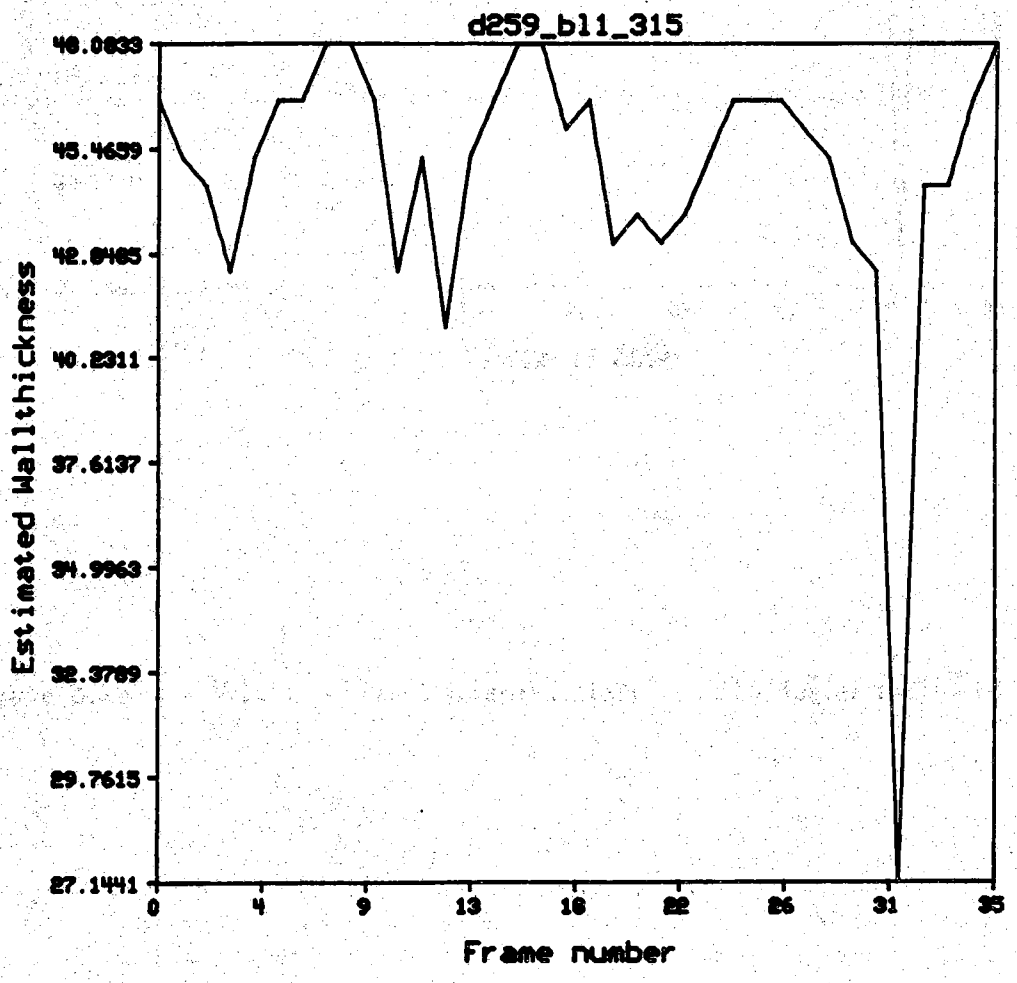

Figure 3.25 Wall thickness computed along the 315 degree radius for study d259_b11.

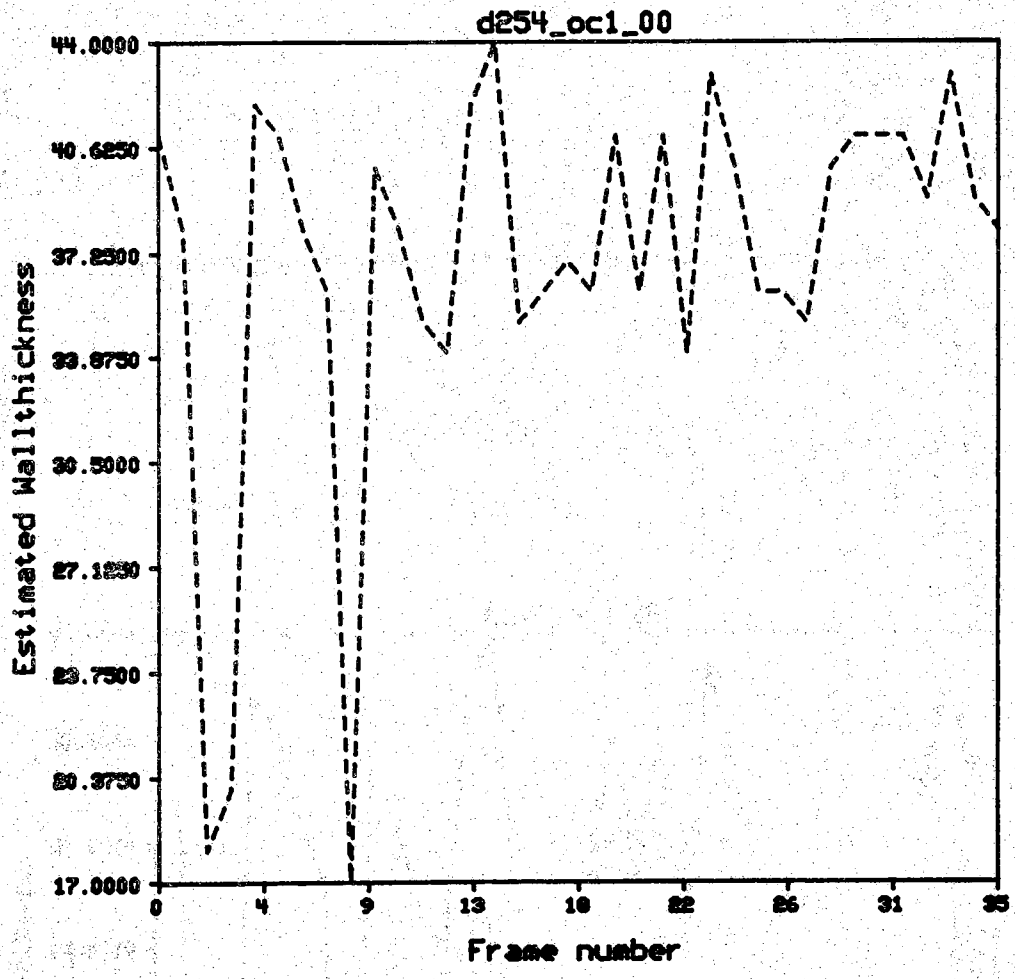

Figure 3.26 Wall thickness computed along the 0 degree radius for study d254_oc1.

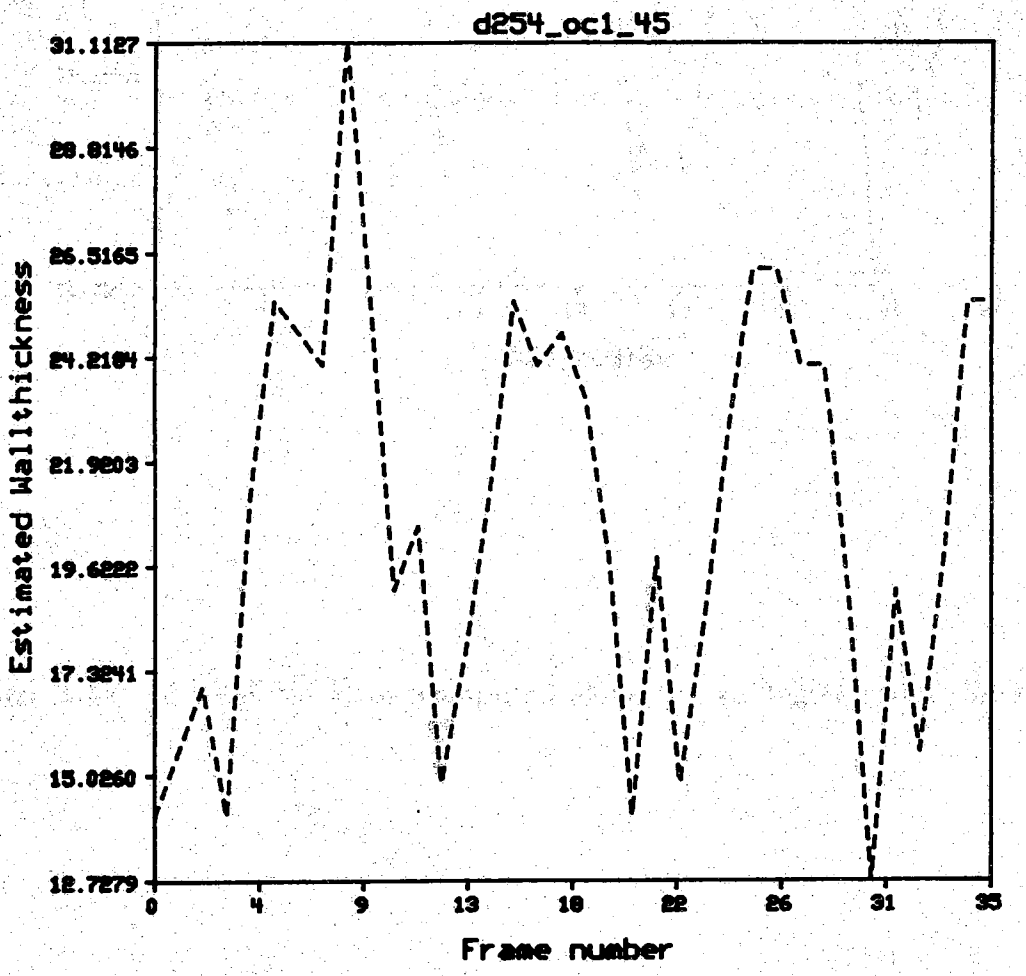

Figure 3.27 Wall thickness computed along the 45 degree radius for study d254_oc1.

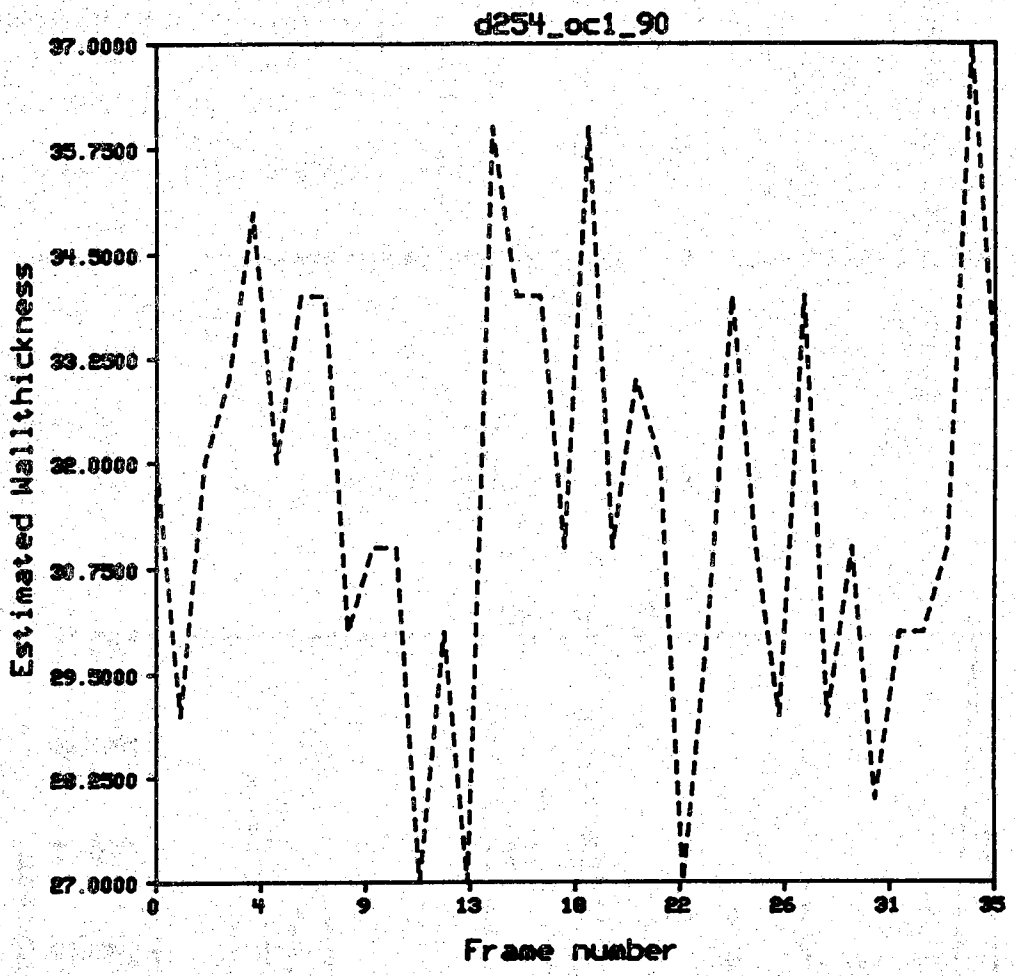

Figure 3.28 Wall thickness computed along the 90 degree radius for study d254_oc1.

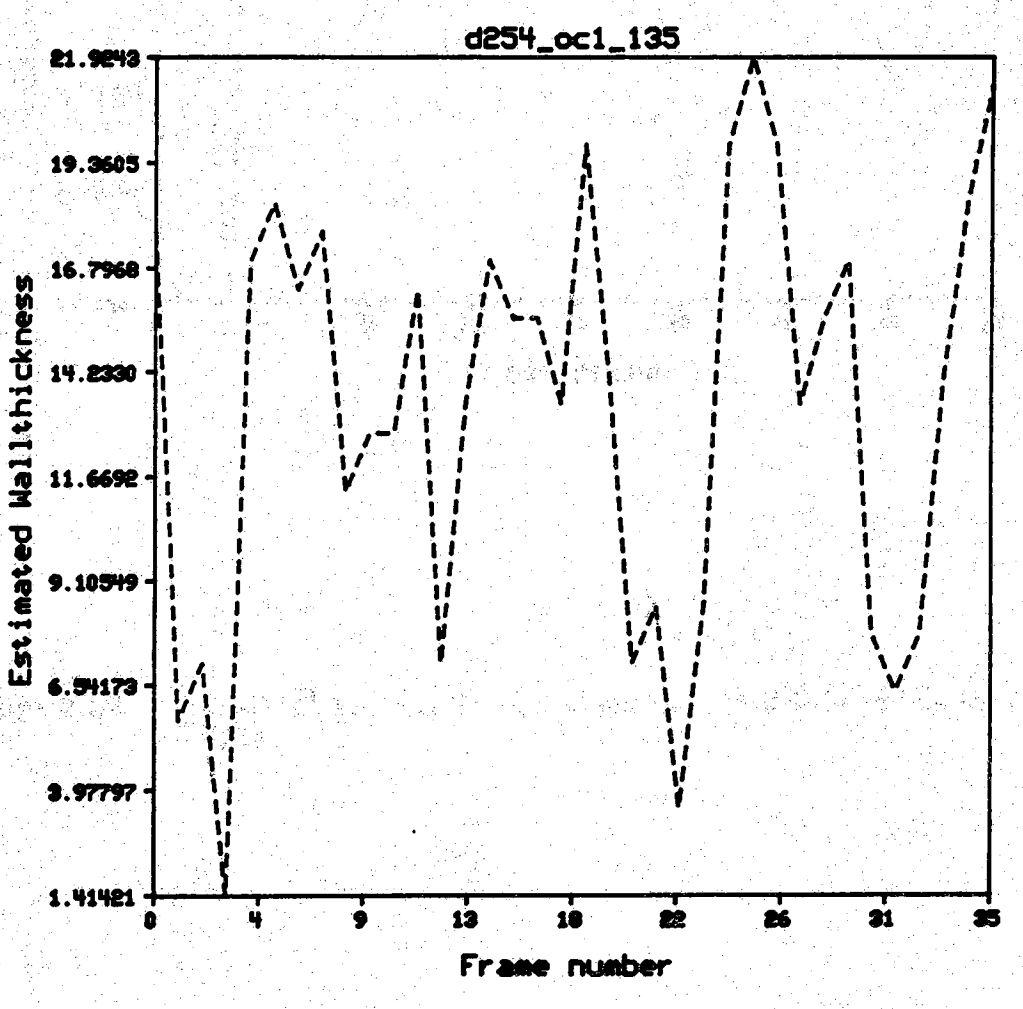

Figure 3.29 Wall thickness computed along the 135 degree radius for study d254_oc1.

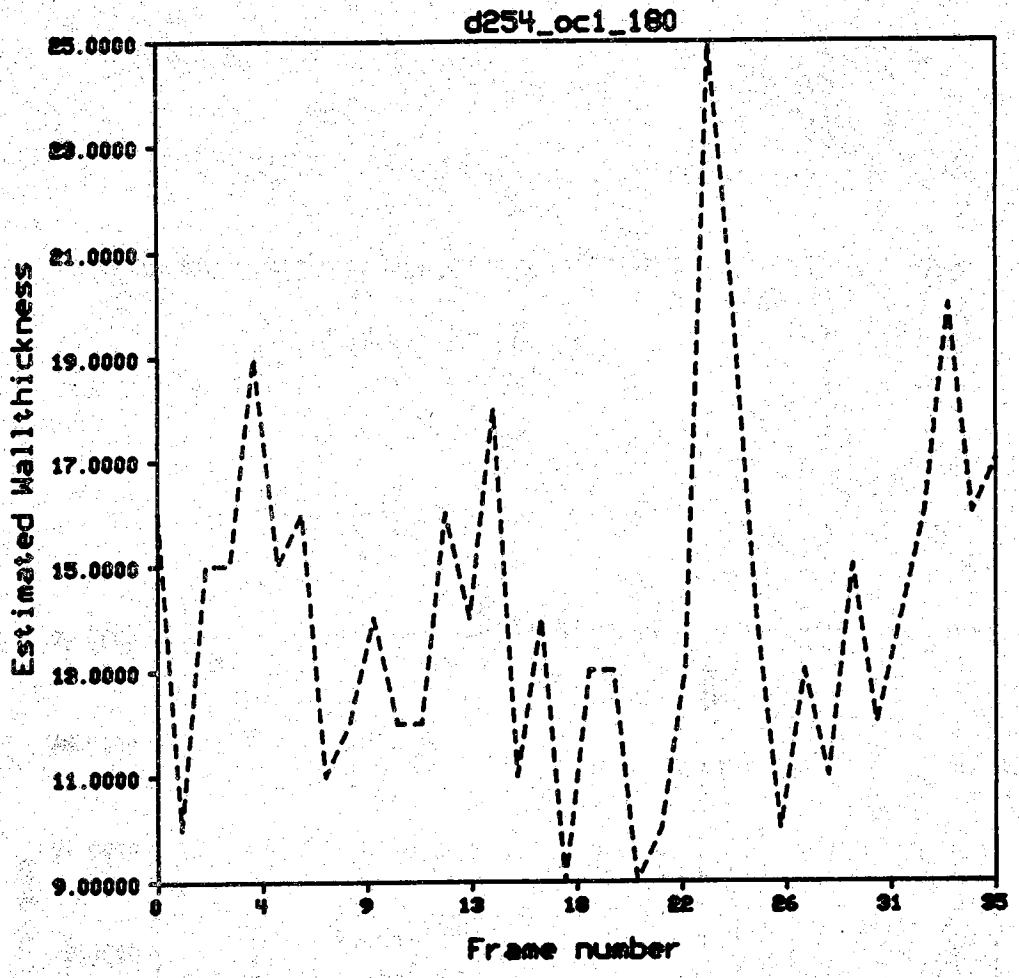

Figure 3.30 Wall thickness computed along the 180 degree radius for study d254_oc1.

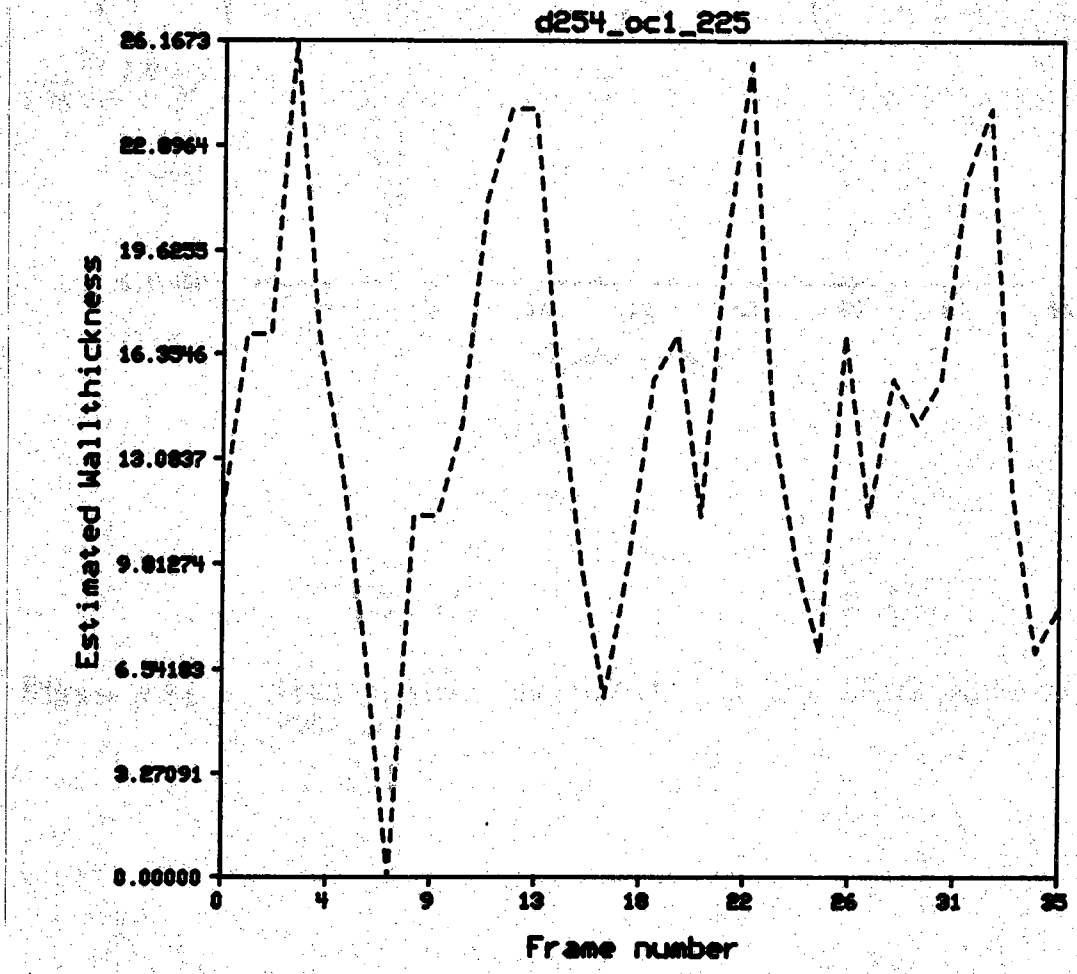

Figure 3.31 Wall thickness computed along the 225 degree radius for study d254_oc1.

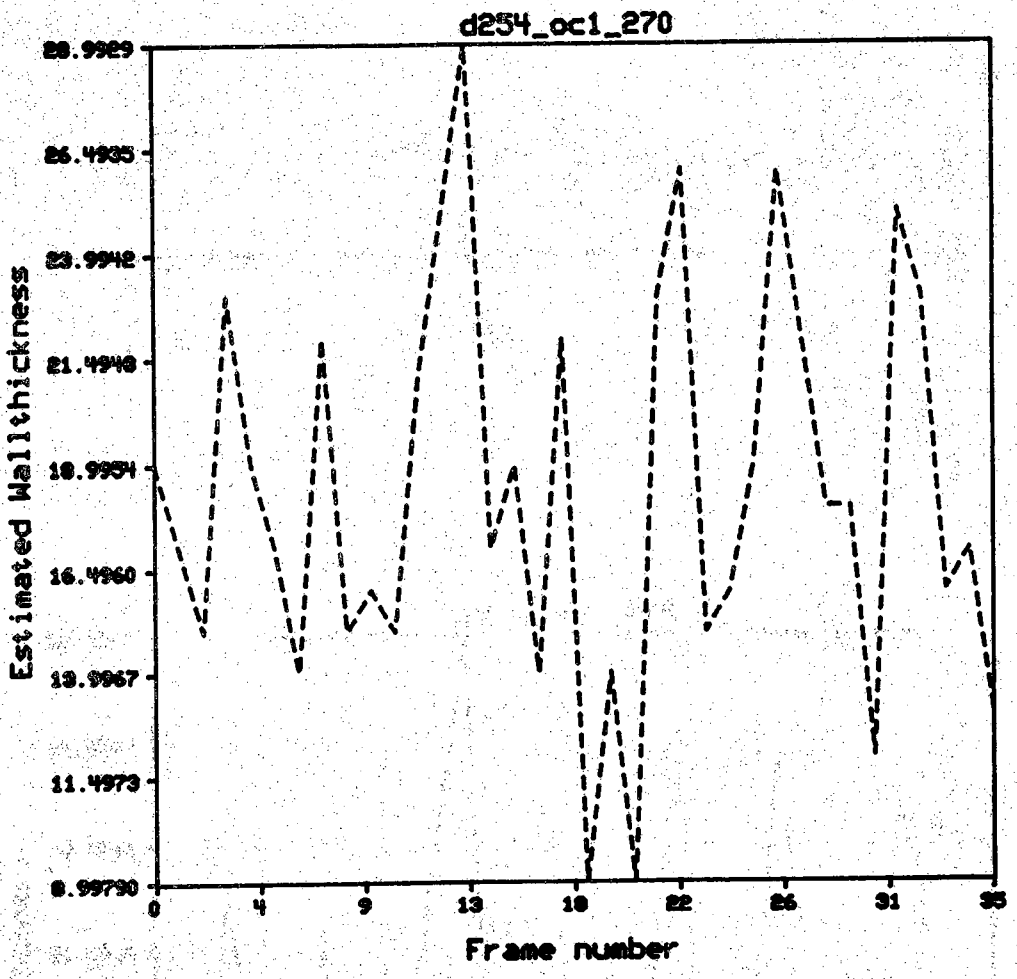

Figure 3.32 Wall thickness computed along the 270 degree radius for study d254_oc1.

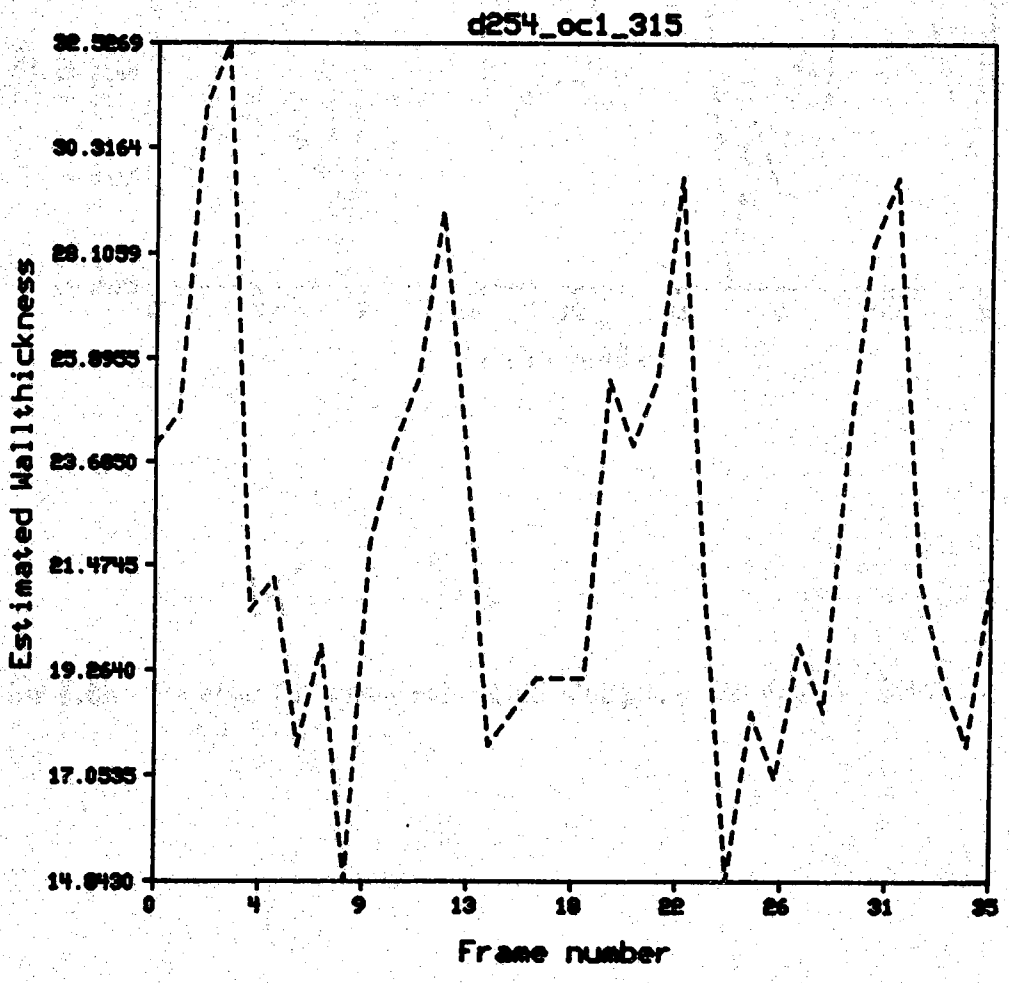

Figure 3.33 Wall thickness computed along the 315 degree radius for study d254_oc1.

CHAPTER 4
SHAPE ANALYSIS

4.1 Left Ventricular Shape Anlysis

Shape analysis of the left ventricle has largely been based on crude "low level" measurements of shape, e.g. regional or global measurements of wall thickness and area. Higher level shape measures would involve a more general description of shape or shape change. "Low level" techniques do not take into account the exact shape of the left ventricle (endocardial and epicardial boundaries), since area and wall thickness do not "really" represent shape.

Delp, et al. [12] have proposed the utilization of Fourier descriptors as a more general analysis tool for describing left ventricular shape. Linker and Pearlman [27] proposed the utilization of Fourier descriptors and invariant moments, discussing their properties such us computational complexity, uniqueness, physical meaning, etc. The problem with both these techniques is that they require a complete closed boundary which may not be available.

In this chapter, we discuss the use of curvature analysis in order to explore the characteristics of the endocardial boundaries of the left ventricle. Curvature analysis is justified by the assumption that the general shape of the endocardial borders has distinctive characteristics which make it different from any other "pattern" in an echocardiographic image. In addition, it allows the simulation of the movements of the endocardial boundaries.

4.2 Computation of Curvature and Detection of "Landmarks"

The curvature c of a planar curve f at a point Q (according to Mokhtorian and Mackworth [28]) is the instantaneous rate of change of the slope ψ of the tangent at that point Q with respect to the arc length s, and is equal to the inverse of the radius ρ of the circle of curvature at Q:

$$c = \frac{d\psi}{ds} = \frac{1}{\rho} \tag{4.1}$$

The circle of curvature at point Q is a circle tangent to the curve at point Q whose center P lies on the concave side of the curve and whose curvature is the same as that at point Q (see Figure 4.1).

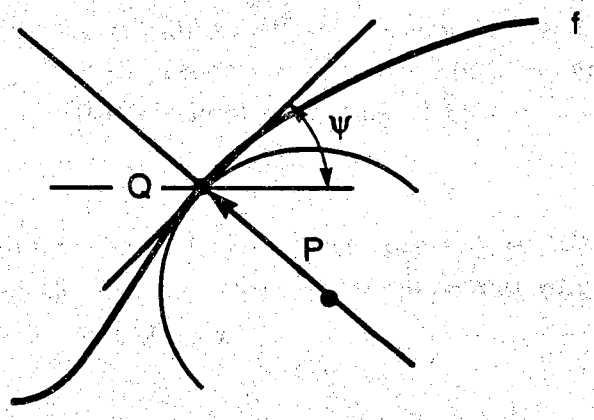

Figure 4.1 Geometry of the curvature function at point Q on curve f.

If we define $y' = dy/dx$ and $y'' = d^2y/dx^2$, then:

$$c = \frac{y''}{(1+(y'^2))^{3/2}} \tag{4.2}$$

An alternative form of computing c is expressing y' and y'' in terms of the derivatives of the parametric expressions of x and y as a function of the parameter t, where:

$$\dot{x} = \frac{dx}{dt};\ \ddot{x} = \frac{d^2x}{dt^2}; \tag{4.3.a}$$

$$\dot{y} = \frac{dy}{dt};\ \ddot{y} = \frac{d^2y}{dt^2}; \tag{4.3.b}$$

then

$$c = \frac{\dddot{x}\dot{y} - \dddot{y}\dot{x}}{(\dot{x}^2 + \dot{y}^2)^{3/2}} \tag{4.4}$$

After detecting the endocardial boundaries of the left ventricle, the x and y coordinates are computed. In order to compute the curvature it is necessary to smooth the contour due to the "ragged" nature of the functions x(t) and y(t). Since x(t) and y(t) are obtained from a digital image there are only four possible values of x(t) between two adjacent pixels (see Figure 4.2). A sliding 4 point window is centered about the point then a third degree polynomial is fitted to the points. The curvature is computed analytically given the coefficients of the polynomial.

An examination of the relative maxima and minima of the curvature points of the endocardial boundary suggests the presence of high curvature points. These points we call "landmarks".

Keeping track of the "significant" maxima and minima may provide information about how the heart moves. A significant maximum is defined as any relative maximum above the positive average value of the curvature function, a significant minimum is defined as any relative minimum above the negative average value. Keeping track of significant peaks involves curvature function matching. All the curvature functions are first sequentially sorted according to their temporal correspondence in the cardiac cycle. The curvature function is then matched.

The following function is computed between two curvature functions obtained from two successive frames:

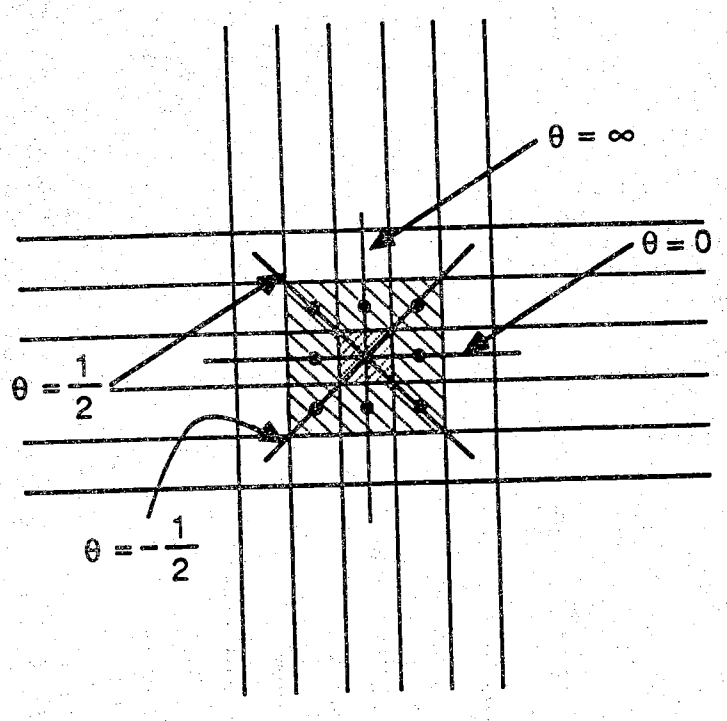

Figure 4.2 This shows the four possible slopes that can be obtained when dealing with two adjacent pixels. The four slopes are θ=0, θ=1/2, θ=∞, and θ=−1/2.

$$DR_k(n) = \frac{1}{N} \sum_{i=0}^{N-1} \left| c_k(i-n) - c_{k+1}(i) \right| \tag{4.5}$$

Where k denotes the k-th curvature function corresponding to the k-th frame and n is the lag value. $DR_k(n)$ is similar to a correlation function and describes the degree of likelihood between $c_k(n)$ and $c_{k+1}(n)$. Assuming that $c_k(n)$ and $c_{k+1}(n)$ are periodic, $DF_k(n)$ is zero for $n=n_0$ when $c_{k+1}(n)=c_k(n-n_0)$. Since the curvature functions are computed from the detected boundaries for the left ventricle, neither the length of the boundaries nor the starting points of the boundary may be equal. This makes necessary the utilization of some matching process, in this case formulated by $DR_k(n)$.

The algorithm for landmark tracking is the following: given two consecutive curvature functions $c_k(n)$ and $c_{k+1}(n)$, the length of both functions is normalized to one, then $DF_k(n)$ is computed assuming that $c_k(n)$ and $c_{k+1}(n)$ are periodic. Then the minimum of $DF_k(n)$ is obtained. The position of the minimum provides the delay between $c_k(n)$ and $c_{k+1}(n)$. Shifting $c_{k+1}(n)$ is performed in order to set the position of the minimum of $DR_k(n)$ to zero. In other words, we let $c'_{k+1}(n)=c_{k+1}(n+n_0)$ such that

$$DR'_k(n)=\frac{1}{N}\sum_{i=0}^{N-1}\left|c_k(i-n)-c'_{k+1}(i)\right| \tag{4.6}$$

has its minimum at n=0. Where $DR'_k(n)$ is $DR_k(n)$ using $c'(k)$.

Landmark tracking consists of identifying the positive and negative peaks of two consecutive curvature functions which remain at the same place in the cycle. In order to do this, all the maxima and minima of $c_k(n)$ are identified. Then the algorithm takes $c'_{k+1}(n)$ and again locates the peak values. Finally the algorithm finds which peaks in both functions are at similar positions. A "similar position" means that if a peak is at n_p in $c_k(n)$, there is another peak at position $n_p \pm \Delta n$ in $c_{k+1}(n)$.

Obviously, the larger Δn, the more true peak correspondences will be missing. Empirical evidence indicated that Δn should be between 20 and 30. Figures 4.3 and 4.4 describe the algorithm. This tracking algorithm is very illustrative since it preserves the significant "corners" of the detected epicardium.

4.3 The Utilization of Landmarks

A whole host of studies can be performed making use of the landmarks. One obvious study is wall motion analysis.

To begin with, it is possible to visualize wall motion by substitution of the detected endocardial boundary with a simplified version of the boundaries where high curvature points are linked using straight lines. For instance, a set of consecutives frames corresponding to an open chest study performed on a dog's heart covering were analyzed. A single frame of this study is shown in Figure 4.5.

The visualization of these simplified "heart walls" in the form of a motion picture reveals the area of myocardial infarction. Identification of the portion of the left ventricle which shows almost no wall motion, can be easily seen. These

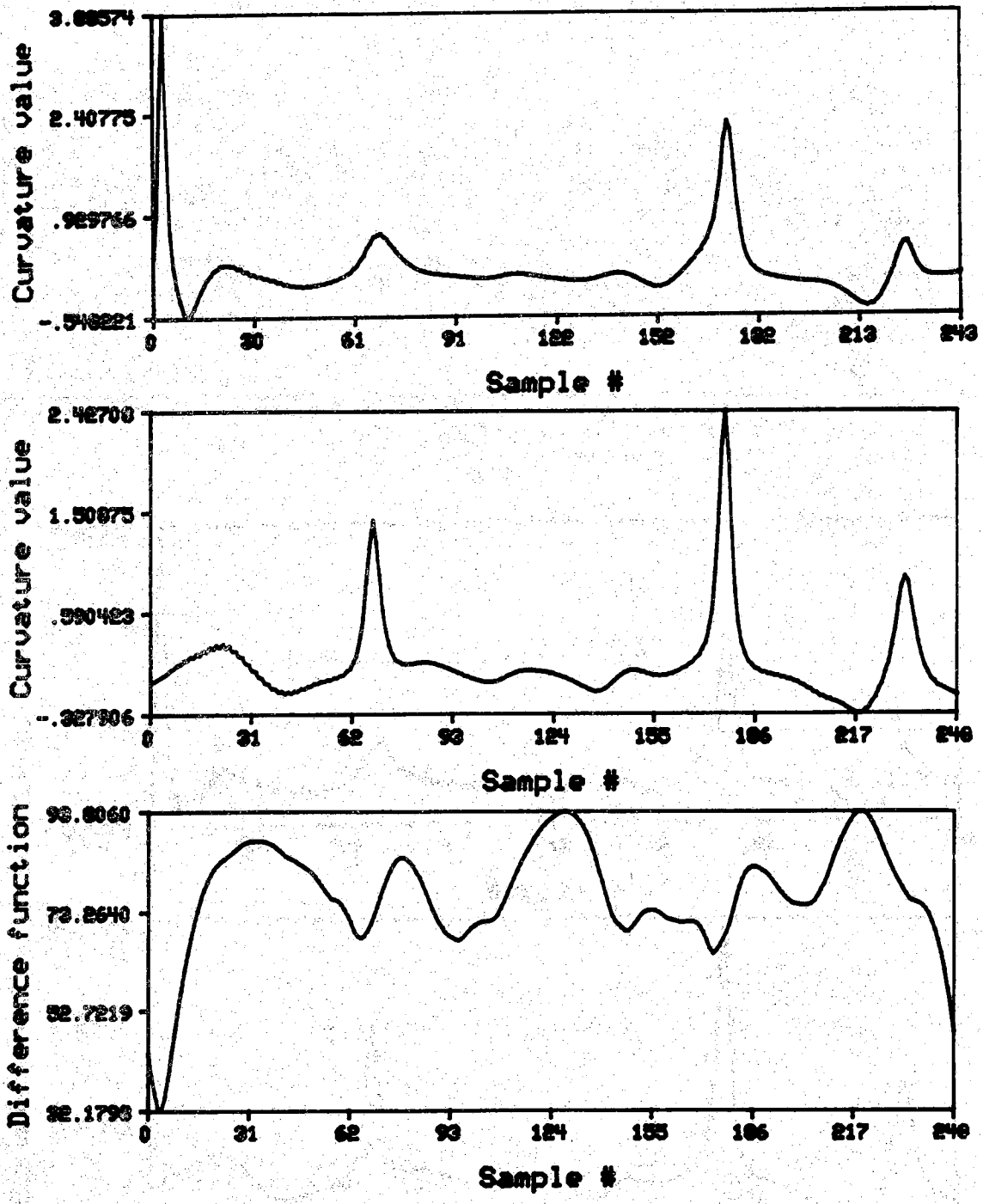

Figure 4.3 Two curvature functions extracted from two consecutive frames are shown along with their associated difference function $DF_k(n)$.

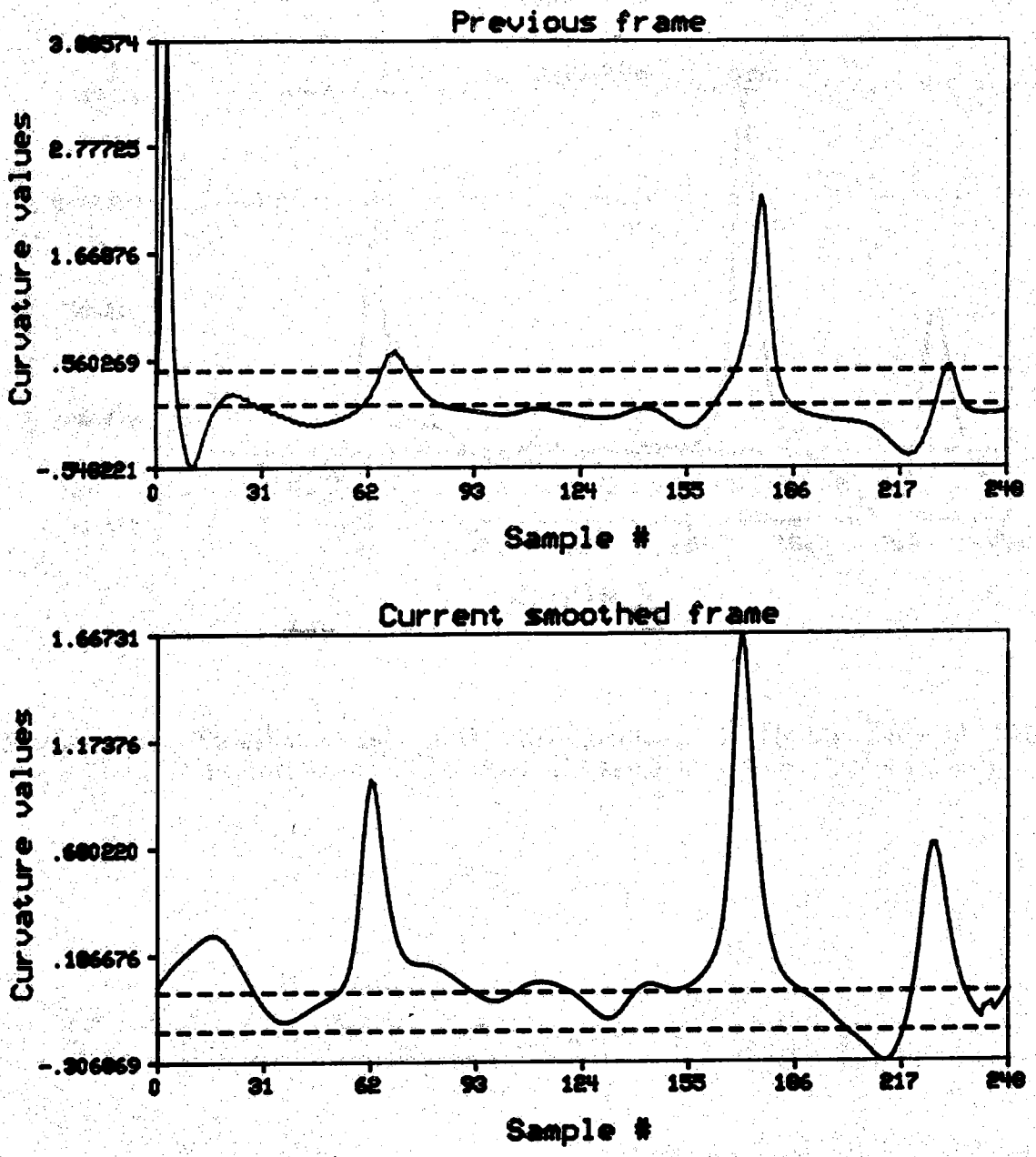

Figure 4.4 Thresholds and peak correspondence is shown between two consecutive matched frames (the same ones shown in Figure 4.3).

simplified borders are constructed as follows. Endocardial borders of the left ventricle are identified and landmark detection is performed. Then landmarks ("corners") are linked using straight lines. Diastole and systole frames are picked by examining the area plots (diastole is supposed to correspond to the highest cross section left ventricular area), and the frames in between are computed by interpolating linearly the position of the landmark. The result was made into an image sequence. It was noted how easy it was to recognize the infarcted area, since it hardly moved. Other studies that might be performed are landmark position tracking from frame to frame in order to assess how risky the assumptions of radial and linear movement are.

Curves of wall velocity should also help in assessing cardiac status after performing a comprehensive collection of data from normal and abnormal hearts. Finally, curvature functions can be the starting point for high level analysis in performing border detection.

4.4 Summary

It is obvious that a high level description of echocardiographic images is needed to assess cardiac status.

One such descriptor is curvature analysis. Since the curvature of the endocardial boundary has distinctive characteristics, it is reasonable to assume that it might be useful for high level description.

Basically, the high curvature points of the endocardium are detected and tracked throughout the cardiac cycle. These high curvature points are called *landmarks*. The first important application of landmarks is wall motion visualization. Since the movement of the heart wall is very complex, this complexity can be diminished by studying the movement of the position of the landmarks. This simplification of the heart beating process seems to be a potential tool for the identification of infarcted areas of the heart muscle.

Curvature analysis may be also used for characterizing the endocardial boundary. After detecting the boundaries in the first frame of a sequence of images, and the points of high curvature are determined, then it would be possible in consecutive frames to use this curvature information for the detection

of the endocardial boundary. For example, the endocardial boundary detected in the following frame should not have curvature points that are very different from the previously detected points.

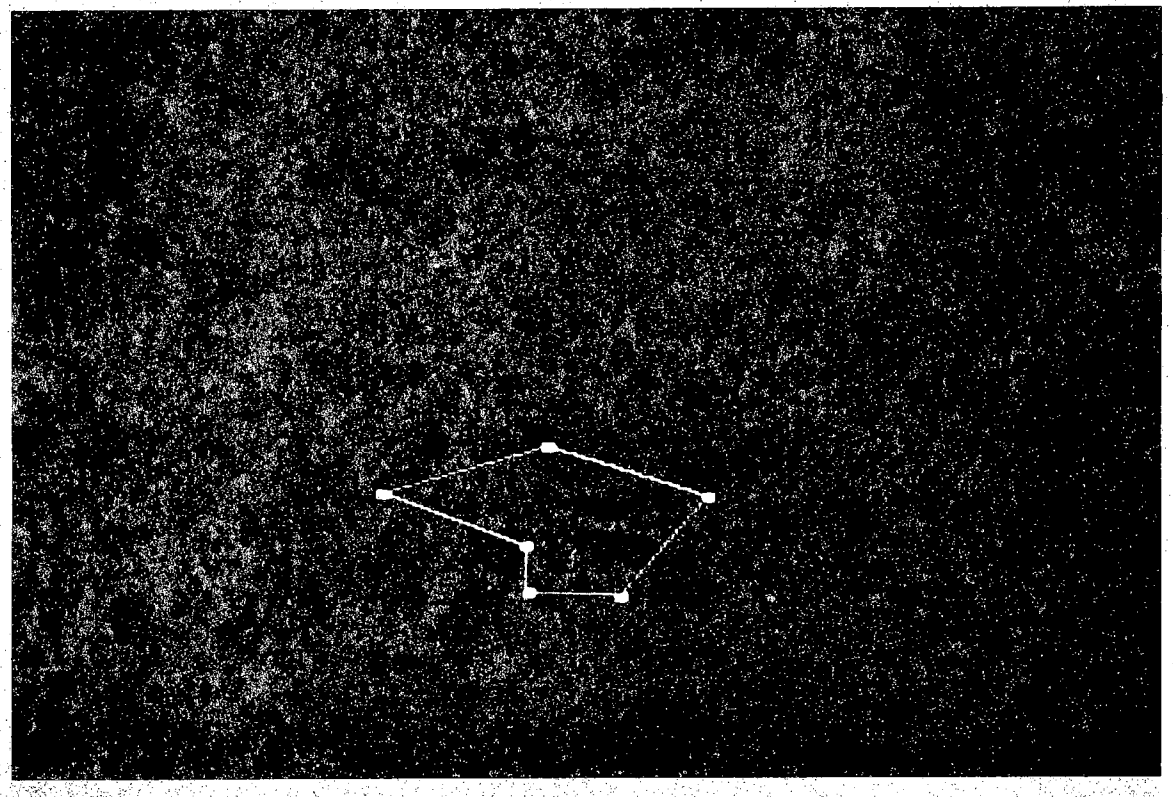

Figure 4.5 Simplified version of the endocardial boundary. High curvature points were linked using straight lines.

CHAPTER 5
CONCLUSIONS AND FURTHER RESEARCH

One of the main goals in the analysis of echocardiographic images has been automatic analysis. Most of the efforts have been concentrated on the automatic estimation of the endocardial and epicardial boundaries of the left ventricle by analyzing cross sectional views. In general most of the algorithms developed for boundary estimation need to work interatively with a human operator. This is because image processing techniques work on a pixel basis instead of using a higher level description. An initial use of higher level knowledge is the use of curvature analysis for wall motion.

Identification of landmarks on the endocardial boundary provides a simplified but valid description that allows visualization of wall motion. This simplification of the heart beating process seems to be a potential tool for the identification of infarcted areas of the heart muscle.

An area of further research would be the measurament of velocity and position of the landmarks. Measuraments of velocity and position might determine how the landmarks move and allow to distinguish between normal landmark behaviour and abnormal behaviour due to myocardial infarction.

We feel that landmark detection and tracking may help the boundary estimation process. As pointed out in Chapter 4, if the analysis is made on a sequential frame basis, the endocardial boundary detected in the following frame should not have curvature points that are very different from the previous detected ones. This additional "supervision" during boundary estimation could be used to trigger further action in the system if there is no agreement between landmarks of two consecutive frames, or simplify the analysis of the next frame by predicting the landmark positions based on the information obtained from previous frames.

Finally, further reasearch using experts systems could address the use of other types of knowledge available about cardiac dynamics and the modes of interpretation used by phisycians.

BIBLIOGRAPHY

BIBLIOGRAPHY

[1] S. W. Jacob, C. A. Francone, and W. J. Lossow, *Structure and Function in Man*, Philadelphia: W. B. Saunders Company, 1967.

[2] S. M. Collins and D. J. Skorton, *Cardiac Imaging and Image Processing*, New York: McGraw Hill Book Company, 1986.

[3] D. N. Smith, A. J. Buda, E. J. Delp, J. M. Jenkins, C. R. Meyer, and F. H. Splittberg, "Mitral valve tracking of directly digitized 2D echocardiograms," *Proceedings of Computers in Cardiology*, pp. 329-332, Seattle, Washington, 1982.

[4] E. Garcia, P. Gueret, M. Benett, E. Corday, W. Zwehl, S. Meerbaum, S. Corday, H. J. C. Swan, and D. Berman, "Real time computerization of two-dimensional echocardiography," *American Heart Journal*, Vol. 101, no. 6, pp. 783-792, June 1981.

[5] A. J. Buda and E. J. Delp, *Digital Cardiac Imaging*, Boston: Martinus Nijhoff, 1985.

[6] C. H. Chu, E. J. Delp, and A. J. Buda, "Detecting left ventricular endocardial and epicardial boundaries by digital two-dimensional echocardiography," *IEEE Transactions on Medical Imaging*, vol. MI-4, no. 7, pp. 81-90, June 1988.

[7] D. J. Skorton, C. A. McNary, J. S. Child, F. C. Newton, and R. M. Shah, "Digital image processing of two dimensional echocardiograms: identification of the endocardium," *The American Journal of Cardiology*, Vol. 48, pp. 479-486, September 1981.

[8] W. Zweh, R. Levy, E. Garcia, R. V. Haendchen, W. Childs, S. R. Corday, S. Meerbaum, and E. Corday, "Validation of a computerized edge detection algorithm for quantitative two-dimensional echocardiography," *Circulation*, Vol. 68, No. 5, pp. 1127-1135, November 1983.

[9] S. M. Collins, D. J. Skorton, E. A. Geiser, J. A. Nichols, D. A. Conetta, N. A. Pandian, and R. E. Kerber, "Computer assisted edge detection in two-dimensional echocardiography: comparison with anatomic data," *The American Journal of Cardiology*, Vol. 53, pp. 1380-1387, May 1984.

[10] A. Ezekiel, E. V. Garcia, J. S. Areeda, and S. R. Corday, "Automatic and intelligent left ventricular contour detection from two-dimensional echocardiograms," *Proceedings of Computers in Cardiology*, Linkoping, Sweden, September 1985.

[11] E. Garcia, A. Ezekiel, R. Levy, W. Zwehl, K. Ong, E. Corday, J. Areeda, S. Meerbaum, and S. Corday, "Automated computer enhacement and analysis of left ventricular two-dimensional echocardiograms," *Proceedings of Computers in Cardiology*, pp. 399-402, Seattle, Washington, 1982.

[12] E. J. Delp, A. J. Buda, M. R. Swastek, D. N. Smith, J. M. Jenkins, C. R. Meyer, and B. Pitt, "The analysis of two-dimensional echocardiograms using a time-varying approach," *Proceedings of Computers in Cardiology*, pp. 391-394, Seattle, Washington, 1982.

[13] D. T. Linker, A. S. Pearlman, T. K. Lewellen, L. H. Muntsman, and W. E. Moritz, "Automated endocardial definition of 2-D echocardiograms: a comparison of four standard edge detectors and improved thresholding techniques," *Proceedings of Computers in Cardiology*, pp. 395-398, Seattle, Washington, 1982.

[14] A. Rosenfeld and A. C. Kak, *Digital Picture Processing*, Vol. 1 and 2, London: Academic Press, Second Editional, 1982.

[15] L.-F. Zhang and E. A. Geiser, "An effective algorithm for extracting serial endocardial borders from 2-dimensional echocardiograms," *IEEE Transactions on Biomedical Engineering*, Vol. BME-31, no. 6, pp. 441-447, June 1984.

[16] L.-F. Zhang and E. A. Geiser, "An approach to optimal threshold selection on a sequence of two-dimensional echocardiograms," *IEEE Transactions on Biomedical Engineering*, Vol. BME-29, no. 8, pp. 577-581, August 1982.

[17] B. Bhanu and O. D. Faugeras, "Segmentation of images having unimodal distribution," *IEEE Transactions on Pattern Analysis and Machine Intelligence*, Vol. PAMI-4, no. 4, pp. 408-419, July 1982.

[18] A. Rosenfeld and R. C. Smith, "Thresholding using relaxation," *IEEE Transactions on Pattern Analysis and Machine Intelligence*, Vol. PAMI-3, no. 5, pp. 598-606. September 1981.

[19] G. T. Herman and H. K. Liu, "Dynamic boundary surface detection," *Computer Graphics and Image Processing*, Vol. 7, pp. 130-138, 1978.

[20] S. Sasayama, K. P. Gallagher, W. S. Kemper, D. Franklin, and J. Ross Jr., "Regional left ventricular wall thickness early and late after coronary occlusion in the concious dog," *American Journal of Physiology*, Vol. 240, pp. H293-H299, 1981.

[21] E. Garcia, G. Maurer, R. Levy, W. Zwehl, S. R. Corday, W. Childs, and E. Corday, "Recent advances in 2D echocardiography," *Diagnostic Imaging*, pp. 18-24, January 1982.

[22] H. L. Falsetti, M. L. Marcus, R. E. Kerber, D. J. Skorton, "Editorial: quantification of myocardial ischemia and infarction by left ventricular imaging," *Circulation*, Vol. 63, no. 4, pp. 747-751, 1981.

[23] A. N. Lieberman, J. L. Weiss, B. I. Jugdutt, L. C. Becker, B. H. Bulbkley, J. G. Garrison, G. M. Hutchins, C. A. Kallman, and M. L. Weisfeldt, "Two-dimensional echocardiography and infarct size: relationship of regional wall motion and thickening to the extent of myocardial infarction in the dog," *Circulation*, Vol. 63, no. 4, pp. 739-746, 1981.

[24] P. F. Moynihan, A. F. Parisi, and C. L. Feldman, "Quantitative detection of regional left ventricular contraction abnormalities by two-dimensional echocardiography: I.Analysis of methods," *Circulation*, Vol. 63, no. 4, pp. 752-760, 1981.

[25] A. F. Parisi, P. F. Moynihan, E. D. Folland, and C. L. Feldman, "Quantitative detection of regional left ventricular contraction abnormalities by two-dimensional echocardiography: II.Accuracy in coronary artery disease," *Circulation*, Vol. 63, no. 4, pp. 761-767, 1981.

[26] N. G. Pandian, D. J. Skorton, S. M. Collins, H. L. Falsetti, E. R. Burke, and R. E. Kerber, "Hetereogeneity of left ventricular segmental wall thickening and excursion in 2-dimensional echocardiograms of normal human subjects," *The American Journal of Cardiology*, Vol. 51, pp. 1667-1673, June 1983.

[27] D. T. Linker and A. S. Pearlman, "A mathematical basis for the quantitative comparison of cardiac borders: criteria for selection of descriptors and an analysis of two methods," *Proceedings of Computers in Cardiology*, pp. 169-172, Aachen, W. Germany, 1983.

[28] F. Mokhtarian and A. Mackworth, "Scale-based description and recognition of planar curves and two-dimensional shapes," *IEEE Transactions on Pattern Analysis and Machine Intelligence*, Vol. PAMI-8, no. 1, pp. 34-43, January 1986.

[29] G. E. Mailloux, A. Bleau, M. Bertrand, and R. Petitclerc, "Computer analysis of heart motion from two-dimensional echocardiograms," *IEEE Transactions on Biomedical Engineering*, Vol. BME-34, no. 5, pp.356-364, May 1987.